UNIVERSITÀ DEGLI STUDI FIRENZE

DOTTORATO DI RICERCA IN

SCIENZE CHIMICHE

CICLO XXIX

COORDINATORE Prof. PIERO BAGLIONI

Physico-Chemical characterization of innovative natural materials for the consolidation of aged flax fibres

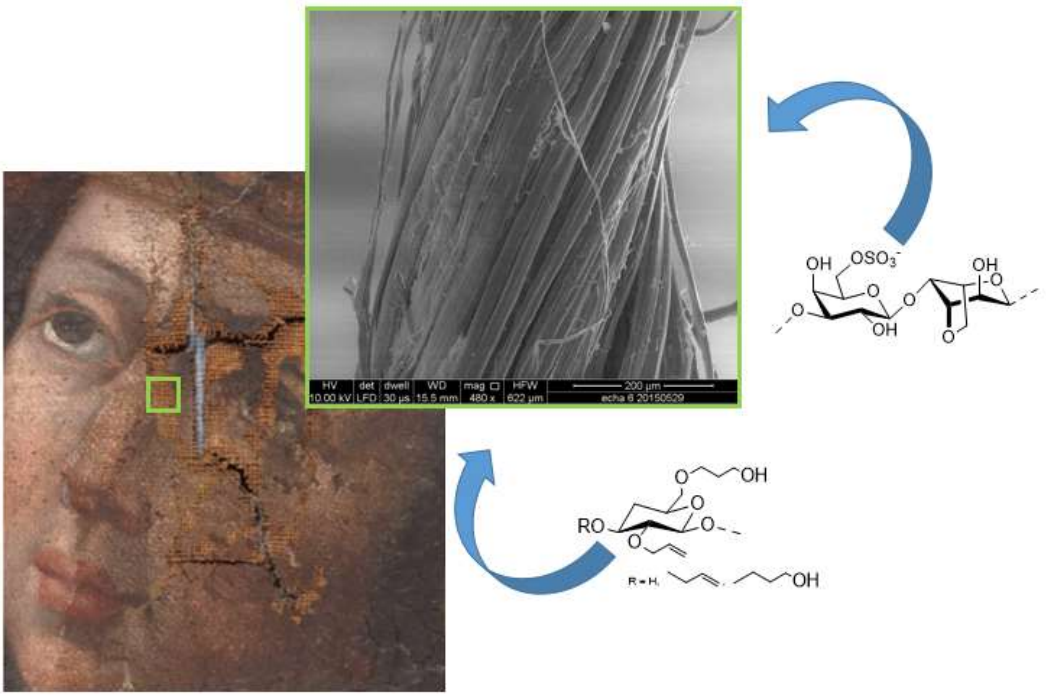

Dottorando	Tutore	Co-Tutore
Dott. Elisabetta Andrina	Dott. Emiliano Carretti	Prof. Luigi Dei

UNIVERSITÀ
DEGLI STUDI
FIRENZE

DOTTORATO DI RICERCA IN

SCIENZE CHIMICHE

CICLO XXIX

COORDINATORE Prof. PIERO BAGLIONI

Physico-Chemical characterization of innovative natural materials for the consolidation of aged flax fibres

Settore Scientifico Disciplinare CHIM/12

Dottorando	**Tutore**	**Co-Tutore**
Dott. Elisabetta Andrina	Dott. Emiliano Carretti	Prof. Luigi Dei

_____ _____ _____

Coordinatore

Prof. Piero Baglioni

_____

Anni 2013/2016

INDEX

Introduction

Canvas has begun the favourite painting's support of the modern age. Its extensive use as an independent support of paintings goes back to the XVI century. According to the tradition, in this period in Venice the problem of preserving frescoes against lagoon weather was mainly unsolved and so canvas represented an ideal alternative: it was cheaper than wood and gave the possibility to produce oversize supports, required to substitute frescoes in fulfilling the didactic role of large decorative cycles.

Natural fibres most used in the centuries to realise these supports were flax, hemp and later cotton. All these three types are mainly constituted by cellulosic fibers. One of the main conservative problems that affects them is the depolymerisation of cellulose chains. This degradation process involves a decrease of the molecular weight of cellulose chains that, in turns, causes a drastic fall of mechanical resistance of the fibre as a whole and so the structural failures of the fabric.

The restoration procedure more used in the centuries to overlap the structural failure of painting supports due to depolymerisation and degradation of fibres is the lining technique. This procedure came into general use in the 18th century[1]. It is a controversial method, because of the irreversible modifications of the original painting matter that involves, due to the high temperature and pressure conditions requested by the procedure. Traditional methods, namely glue-paste and wax-resin linings, involved a total impregnation of the painting with the adhesive, necessary to obtain a good adhesion with a stiff lining support. In the case of glue-paste, the adhesive is an aqueous mixture of animal glue, flour, resin and Venice turpentine. The adhesion was then achieved by the combined application of heat, pressure and moisture that inevitably results in a plasticising effect on the paint and ground layer. Moreover, the consistent moisture intake may cause shrinkage of canvases, with the subsequent loss of paint and ground[2]. Beeswax resin mixtures have been introduced as lining adhesives since the

[1] A. Conti, Storia del restauro e della conservazione delle opera d'arte, Electa, 1988.

[2] Carmen F. Bria Jr, The history of the use of synthetic consolidants and lining adhesives, WAAC Newsletter, Volume 8, Number 1, Jan. 1986, pp.7-11.

19th century[3]. It is a hot-melt lining. In this case, the adhesion was obtained with the use of hand irons to press the two canvases together. This variable heating condition and pressure involved damages in paint layers. The improvement of the method in 1950 with the introduction of the vacuum hot table let achieving more uniform conditions of heat and pressure, but the long period of high pressure and heat at which painting were undergone involved textural changes due to the weave imprinting of the textile support[4].

At the Greenwich Lining Conference, in 1974, traditional practices were seriously questioned for the first time. The keynote was the reconsideration of the so-called "lining cycle"[5]: the cycle of lining, de-lining and relining that represented the way of treating and retreating paintings throughout the previous decade and that has a cumulative effect on painting's deterioration. Indeed lining is not a treatment done ones and for all. Problems inherent in traditional methods are not only related with the initial moment of lining. Glue-paste adhesives, for example, became hard and brittle, risking to create damaging stresses on painting. On the other hand, wax-resin adhesive cause the darkening of the painting surface and so the progressive loss of legibility of the image. But the removal of lining adhesives often involve crude and laborious mechanical processes that can further weaken the original[6]. Therefore, what Percival-Prescott means is that when a painting is lined, it is automatically entered in that dangerous cycle.

From the Lining Conference to nowadays a number of new lining adhesives and consequently new procedures have been introduced. Among them the most important were heat-seal lining with BEVA 371 (Lascaux) and cold lining with Plextol B500 (Rhom & Haas). The first one is a combination of ethylene

[3] Ibidem.

[4] Paul Ackroyd, The structural conservation of canvas paintings: changes in attitude and practice since the early 1970s

[5] Percival-Prescott Westby, "The Lining Cycle," *Conference on Comparative Lining Techniques*, National Maritime Museum, 1974.

[6] Paul Ackroyd, The structural conservation of canvas paintings: changes in attitude and practices since the early 1970s.

vinyl acetate (EVA) resins with a variety of waxes and ketone resins[7] formulated by Gustav Berger. The second is an aqueous dispersion of an ethyl acrylate and methyl methacrylate based copolymer introduced by Vishwa Mehra. However, the lining remains a dangerous procedure that does not fit with the current restoration trend of minimal intervention. The aim of this research is to evaluate another less invasive way to solve the problem of the lack of mechanical resistance, which characterized depolymerized cellulosic fibres of aged textiles. To reach this goal two different products has been tested as consolidant materials: funori, an heterogeneous mixture extracted from a family of Japanese red seaweeds; Allyl n-hydroxy-propyl cellulose[8], a cellulose derivative synthesized by the research group of Prof. Antonella Salvini, associated professor of the "Ugo Schiff" Chemistry Department at the University of Florence;

Both the products chosen for the experimentation are characterized by a similar chemical nature with the flax fibre composing canvas supports. This characteristic not only guarantees the chemical compatibility of the two consolidants with the support they will be applied on, but it also allows to suppose the establishment of chemical interactions between the products and the support. Moreover, the combined treatment with calcium hydroxide nanoparticles dispersions has been tested. The aim was to add the preservative action of alkaline earth metal hydroxide nanoparticles against acidic hydrolysis of cellulose to the consolidating action of the two products chosen for the experiment.

[7] Lisa Kronthal, Judith Levinson, Carole Dignard, Esther Chao, & Jane Down, Beva 371 and its use as an adhesive for skin and leather repairs: background and a review of treatments, *Journal of the American Institute for Conservation*, Vol. 42, No. 2, Objects Issue (Summer, 2003), pp. 341-362.

[8] G.Cipriani, A. Salvini, P.Baglioni et al., Cellulose as a Renewable Resource for the Synthesis of Wood Consolidants, 2010.

CHAPTER 1

Funori: chemical characterization, applications and potentiality as a restoration material

In Japan seaweeds represent one of the most valuable of the aquatic resources. The abundance and variety of useful algae is due to many factors such as the great extent of the coastline and climate conditions. From thousands of years Japanese people were used to put different kinds of plants to the most appropriate uses, finding applications for many families of seaweeds, according to their characteristics. The general name referred to seaweeds in Japanese tradition is "nori", which often is used also to name the derivate products. Traditionally, a special attention is given to the preparation of kombu, amanori, kanten, iodine and funori [9]. The first and the second products, obtained from the genus *Laminaria, Alaria* and *Porphyra*, find various kinds of application in different dishes of Japanese tradition such as sushi or vegetable preparations. Kanten, obtained mainly from the genus *Gelidium*, is known in the scientific world under the name *agar-agar*. The manufacture of iodine from seaweeds, mostly from *Laminaria* and *Ecklonia*, is relatively recent in Japan, but the increase of demand for the chemical make this business one of the most important industries in the country. Funori is traditionally used as a glue to stiff fabrics, owing to its excellent sizing and adhesive properties[10]. The principal seaweeds from which funori is extracted are three types of red algae named *Gloiopeltis Furcata* (*fukuro-funori*), *G. Complanata* (*hana-funori*) and *G. Tenax* (*ma-funori*). The genus Gloiopeltis belongs to the family of Endocladiaceae. Red algae (Rodophyta) are generally grouped into three types: agars, carragenans and porphyrans. Funori is considered a subset of agars but, at the same time, its chemical and structural qualities are similar to those of carrageenans. One of the distinction between the two groups consists in stereochemistry. Both are

[9] Hugh M. Smith, *The seaweeds industries of Japan*, Bulletin of the bureau of fisheries, 1964.

[10] Ryo Takano, Hiroko Iwane-Sakata, Kaeko Hayashi, Saburo Hara, Susumu Hirase, *Concurrence of agaroid and carrageenan chain in funoran from the red seaweed Gloiopeltis furcate Post. Et Ruprecht (Cryptonemiales, Rhodophyta,* Carbohydrate Polymers 35, Elsevier Science, 1998, pp.81-87.

composed by polysaccharide chains based on two repeating forms of *β*-d-galactose and 3,6-anhydro-*α*-l or –d galactose, forming a double helix[11]. However, while in the carrageenan polysaccharide both the monomer galactose units are in the D-form, in the agar one the anhydride is in the L-form. Moreover, carrageenans are highly sulphated, whereas agars have traces at most. This characteristic involves substantial differences in physical properties: the lack of electrostatic and steric hindrance, due to the absence of sulphated groups, let agar polysaccharide chains pack tightly, causing its ready gelling ability at low temperature and at low concentrations. On the contrary, sulphate groups cause the helices to repel one another, make carrageenans solution viscous but not ready to gel.

Funori is usually obtained from the above mentioned raw material through an extraction in water that allows its separation from the water-insoluble fibrillose skeleton, that composes the cell wall[12]. It is a chemically heterogeneous polymeric mixture composed by a polysaccharide fraction and a protein one, which in addition to salts, lipids and colorants constitute the mucilaginous matrix of the seaweed's cells (Michel 2011). Recent studies confirmed also the presence of acetylated residues, uronic acids and xylose[13]. About the polysaccharide fraction, the main polysaccharides are based on the repetition of the *β*-d-galactose-6-sulfate – 3,6-anhydro-*α*-l-galactose units (Fig.1). The presence of the L-form of the anhydride make funori structure similar to the agar one. On the other hand, the sulphate groups make it close to carrageenan structure, giving the consolidant the low gelling ability characteristic of this group. Takano R.[14]assessed that while the main polysaccharide just described has a negative specific optical rotation, the other minor polysaccharide fractions have a rather largely positive

[11] Joseph R. Swider, Martha Smith, *Funori: overview of a 300-year-old consolidant*, JAIC 44, 2005,pp. 117-126.

[12] Francoise Michel, *Funori and JunFunori: two related consolidants with surprising properties*, Adhesives and Consolidants for conservation: research and application, Proceedings of Symposium 2011, Ottawa.

[13] Tuvikene R. et al., *Funoran from Gloiopeltis species. Part I. Extraction and structural characteristics*, Food hydrocolloids, 2014, pp.1-12.

[14] Ryo Takano, Hiroko Iwane-Sakata, Kaeko Hayashi, Saburo Hara, Susumu Hirase, *Concurrence of agaroid and carrageenan chain in funoran from the red seaweed Gloiopeltis furcate Post. Et Ruprecht (Cryptonemiales, Rhodophyta,* Carbohydrate Polymers 35, Elsevier Science, 1998, pp.81-87.

optical rotation, suggesting the presence of polysaccharide other than the sulphated agaroid. Moreover, an higher sulphate content distinguished minor fractions from the main reported above. Takano R. identified minor fraction with ion-exchange chromatography on the basis of the elution times and coelution with the authentic oligosaccharides. Among the ten disaccharides and trisaccharides isolated, some present an agaroid backbone, others a carrageenan backbone. Finally, the compresence of the agaroid chain and the carrageenan chain is assessed in funori by many studies and gives the consolidant its peculiar properties. Nevertheless, it has been already noticed in several red algal polysaccharides[15].

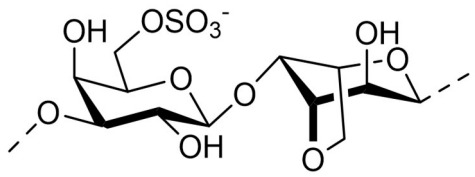

Fig.1 : major repetitive unit of funori polysaccharidic fraction

The preferential site for sulphate substitution is normally C-6. This specificity may be beneficial as protection against development of acidic environment on treated materials subjected to sulfuric acid production.

Its particular structure and composition gives funorans many other properties. In particular, funoran from *G. Furcata* have been reported to possess antitumor activity. This potentiality has been also recognized in another sulphated polysaccharide with an agarose sulphate structure, this time from *Gracilaria dominguensis*. Porphyran from *Porphyra yezoyensis*, another red algae characterized by an agarose type structure very close to funorans and polysaccharide composing the sulphated agar fractions of *Gracilaria verrculosa* seems to enhance activation and/or increment of

[15] Tuvikene R. et al., *Funoran from Gloiopeltis species. Part I. Extraction and structural characteristics*, Food hydrocolloids, 2014, pp.1-12

macrophage. Anti-HIV activity has been assessed for a kind of carrageenan[16]. Finally, funorans have shown an antimicrobiological activity[17]. Swider and Smith[18] reported that in their laboratory at the Freer Gallery of Art and Arthur M. Sackler Gallery by the Smithsonian Institution of Washington D.C., although funori has been used for decades for the conservation of the relevant collection of East Asian paintings and sculptures, there are no record of microbiological attack on funori-treated artifacts (Swider and Smith, 2005).

Gloiopeltis grows on rocks along the entire Japanese coast and is gathered at all seasons using long-handled hooks. The conversion of the raw seaweed in marketable product is quite simple and is practiced since about 1673. At first, dried algae are sorted and cleaned from sand, mud and other foreign substances. Than raw algae are soaked in fresh water and than placed in thin layers on large shallow trays with reed or bamboo bottom. They are pressed by hand to obtain a loose sheet. By inverting the trays, sheets are then turned out and are left to bleach and dry upon pieces of matting. Once obtained the desirable level of bleaching the drying is completed and funori sheets are gathered in bundles. Sheets obtained from this century-old preparation's tradition are loose meshed, thin flexible and of quite uniform thickness. Nowadays, after soaking many processes imply the use of potassium hydroxide or sodium peroxide as a bleaching agent, lightening the colour of the seaweed to an orange-yellow[19]. The glue is obtained from extraction in water.

The historical use of this product is mainly related with the starching and dyeing of fabrics, in particular of Kimono-Yuzen[20]. In Japan this material is traded since Heian period (794- 1185 A.D.) and its use begin hypothetically with the origin of the silk production. In the following centuries funori has

---

[16] Ryo Takano, Kaeko Hayashi, Saburo Hara & Susumu Hirase, *Funoran from the red seaweed, Gloiopeltis complanata: polysaccarides with sulphated agarose structure and their precursor structure*, Carbohydrated Polymers 27, Elsevier Science, 1995, 305-311.

[17] Satoru Inagaki, Yoji Saeki and Kazuyuki Ishihara, *Funoran- Containing Xylitol Gum and Tablets Inhibit adherence of oral streptococci*, J. Oral Bioscience 53, 2011, pp. 82-86.

[18] Joseph R. Swider, Martha Smith, *Funori: overview of a 300-year-old consolidant*, JAIC 44, 2005,pag. 117-126.

[19] Ibidem.

[20] N. Hayakawa, T. Araki, S. Kainuma et al., *Characterization of funori extraction of red seaweed as a restoration material*, Science for conservation 48 , 2004, pag. 16-32.

been used as a starching material for fabric and paper and as a plaster additive (Swider, Smith 2005), but also for paper and fabric gilding, to stick paper on the mud walls of the tea ceremony room, to protect them from abrasions and to decorate porcelain. Japanese women use funori also to clean their hair.

With the birth of the artworks' restoration and conservation awareness, in Japan funori became one of the most used restoration material for japanese paper and textile artworks[21]. Its most common use in this field is related with restoration of *kakemono*, traditional paintings on paper. In particular it has been used as a weak adhesive, to temporary apply rice paper on the paintings face, with the aim to protect them while the restoration of the back side of the paint was carried out[22]. Moreover, funori is considered also a useful thickening agent for animal and starch glues. This is in accordance to the widespread principle that the maximum compatibility with artwork materials is given from the use of the same materials which compose them, also for their conservation, without the introduction of new products with different chemical nature and behaviour. According to this view, in Japan the use of funori as a restoration material is extensive and descends directly from its traditional centuries-old uses.

In the last decades, the peculiar physico-chemical properties of this material began to attract even the community of western restorers. The most appreciated capacity of funori consist in preserving the appearance of the surface on which it is applied together with its ecocompatibility and its non toxic nature (Swider and Smith, 2005). The former uncommon ability made it appropriate to consolidate powdering matt paint layers, like tempera ones, solving one of the most challenging aspects in conservation (Swider and Smith, 2005). The matt appearance is due to the high pigment volume concentration of the paint layer with reference to the binder. Pigment particles, not completely surrounded by the binder matrix, make the paint surface rough and irregular in the micro scale. The light is scattered from the rough surface giving the paint layer its matt aspect. The poorness in binder often turn in less cohesive and adhesive properties and therefore less

[21] Other important restoration adhesives from the japanese tradition are: the shin-nori (jin-nori) and the furu-nori, both obtained from wheat starch; ox glue;

[22] This operation is commonly called “facing”.

stability against mechanical stress. Furthermore, the aging of the binder often imply the decrease of the adhesive strength between pigment particles. Gelatine, sturgeon glue and the cellulose ethers, often used for this conservation purpose, usually alter the aesthetic issue of the object by producing undesired glossy effect, darkening or tide lines[23] .The use of Funori, on the other hand, minimize the risk of optical changes. One possible explanation has been found in the capacity of the polysaccharide chains to bind a large amount of water. If no free water molecules are present, the transportation of dirt and microparticles does not occur and so no tide lines appear on the surface[24].

The adhesive strength of funori is weak and so it is generally used when a low-strength adhesive is required. Indeed, it find extensive application in the fields of paper and textile conservation. However, it can be reinforced by adding sturgeon glue for the consolidation of flaking paint layers. Funori has found applications also as a cleaning agent for the removal of water stains and as a medium for matt retouching (Michel, 2011). Other uses reporting in literature are: to repair silver and gold leaf and mica; for backing paintings when mixed with animal glue and to repair the structure of wooden object;

Like every new restoration substance, initially the use of funori has been imported without having awareness of its chemistry and its best method of preparation, only basing on its successful application verified with empirical evidences. About the extraction procedure there wasn't, and still there isn't, an unique trend. Literature reports a lot of different methods (Swider and Smith, 2005) unless giving information about advantages and disadvantages of each one in terms of extracted materials and chemical characteristics of the product obtained. About concentration, it varies from 1g to 10g in 100ml. Temperature of extraction varies between 40°C and 100°C (Michel, 2011). Table 1 reports the main extraction procedures collected by Swider and Smith in their review of 2005. In recent years, the study of this natural consolidant grows up, also due to the growing importance of ecocompatibility of restoration products and the development of the

[23] T. Geiger, F. Michel, *Studies on the polysaccharide JunFunori used to consolidate matt paint*, Studies in Conservation, vol. 50, 2005, pag. 193-204.

[24] Francoise Michel, *Funori and JunFunori: two related consolidants with surprising properties*, Adhesives and Consolidants for conservation: research and application, Proceedings of Symposium 2011, Ottawa.

minimal intervention trend. Conservation scientists began to investigate it to understand its chemical structure and properties and to define completely its potentiality, also predicting its behaviour upon aging. The algae-based consolidant aging behaviour has been thoroughly investigated in 2002 in a research project of the Institute for the Preservation of Historical Monuments and Buildings (ETH Zurich) in collaboration with the Swiss Federal Laboratories for Materials Science and Technology (EMPA) and the Center for Conservation of the Swiss National Museum (SNM)[25]. Comparing with the other most used aqueous consolidants, such as gelatin, sturgeon glue, hydroxypropylcellulose (Klucel E®) and methylcellulose (Methocel MC®), funori shows a very well performance both in terms of film flexibility and optical properties after ageing. In addition, the susceptibility to microorganism seems to be no higher or lower than the other consolidants[26]. In occasion of the same project, the possibility to obtain a consolidant poured from salts and substances responsible for the colour and the odour of funori solution has been improved. The aim was to reduce the heterogeneity and the fluctuation in quality characteristic of all natural products mainly due to different places of cultivation and variable treatment procedures undertaken by different producers. The purifying process was composed by different steps. First of all only *Gloiopeltis Furcata* was used as row material. It seems that its rate of yield is higher than the product obtained from the other two species. In addition, the seaweeds used in this process haven't been bleached with sodium peroxide. As a first step, a simple washing under deionized water was improved, to remove the main salts founded in the seaweed: sodium chloride, potassium chloride and calcium carbonate. However, it must be specified that negative impacts caused by these salts has not been observed yet and as a consequence of that washing some soluble materials are lost. In the second step the soaked seaweed is finely chopped and the funoran is extracted in deionized water at 40°C for 3.5 hours, under intensive stirring. Than, the addition of charcoal let to eliminate impurities responsible for colour and odour. After a

[25]Francoise Michel, *Funori and JunFunori: two related consolidants with surprising properties*, Adhesives and Consolidants for conservation: research and application, Proceedings of Symposium 2011, Ottawa.

[26] Ibidem.

centrifugation at 5000 rpm for 30 minutes in order to remove all the insoluble components, the process foresee the filtration under pressure of the warm solution through a fibreglass filter (mesh size <1 µm) at 8 bar. The solution is then dried at 60°C and over two days it forms a thin film. The product obtained, purified from salts, colorants and protein is called *Jun Funori*, where "jun" in Japanese language correspond to "pure". Jun funori solution is prepared dissolving 1g of the thin film in 100 ml of deionized water. To obtain the complete dissolution of the dry film, the solution has to be warmed at 50°C -60°C under stirring for several hours. The result is a colourless, transparent and odourless consolidant, with a viscosity of 90-125 mPa.

However, in recent years this product registered considerable fluctuation in quality. In 2006 a new producer bought the rights of *Jun Funori*, and the characteristics of the product changed, no more corresponding to that of the first generation (2003- 2006).

In 2011, a thorough study was carried on by the Historic Scotland Conservation Group[27] to compare all the most used adhesives in the field of restoration to established which one can be appropriately considered a facing material and an adhesive for tempera painted wood. The aim of facing is to temporary protect the painted surface preventing damage during treatment, storage or transport. Adhesive strength was tested by pasting two strips of 200g/m2 watercolour paper. The strips were 7cm x 1.5mm x 0.3mm, the joined surface 3mm x 1.5mm x 0.6mm. The ends of the strips were than clamped ad pulled them apart vertically with a tensile machine. Considering as a benchmark the tensile strength of the chalk ground, representing the paint layer, Funori solutions (prepared at different concentrations) show more than 20N less tensile strength, meaning that these consolidants would fail earlier than the paint layer. This must be considered a useful property because in such a way the paint layer couldn't be damaged by adhesive resistance. JunFunori shows an higher strength value compared to its natural source.

About stiffness and reversible flexibility, the Emod, Funori and Jun Funori performed well: they are more flexible than the chalk ground reference.

[27] Chantal-Helen Thuer, *Scottish Renaissance Interiors: facings and adhesives for size-tempera painted wood*, Historic Scotland Technical paper 11, 2011.

After artificial aging, samples have been tested again and comparing the results to the corresponding preliminary test ones, both Funori and Jun Funori appear more plastic than before the ageing, supporting the findings by Geiger and Michel (Geiger and Michel 2005). Colorimetry, Glossimetry and PH tests have been performed before and after the aging on Whatman filter paper samples, on standardized structural replicas of ceiling panels and on some original ceiling panels. No gloss, discolouration or darkening was noticed. The original paint layer became slightly lighter but it is probably related to a cleaning effect. Despite in pure form both show a tendency towards alkalinity with about 8 after aging, this seemed to have no influence on the original paint layer, which stayed between pH6 and pH7. Further tests verified the Funori and Jun Funori performance as facing material on structural replicas of ceiling panels and on original ceiling panels. Funori (1.5% / 2%) and JunFunori 1.5% perform exceptionally well, maintaining the adhesion between the painted surface and the rice paper on all test substrates also after ageing despite all other consolidants tested. Moreover they are readily removable after accelerated ageing and after the removal of the japanese paper there are no tide lines on the painted surface. Jun Funori performed as well as Funori in the former tests, but some difficulties in the product application related to its higher viscosity and lower penetration have been noticed. The final consideration of the authors is that Funori and JunFunori showed the best overall performance of all adhesives tested along with the volatile ones.

In 2013, in collaboration with the scientific laboratories of CCR "La Venaria Reale", a master thesis' case study represented the starting point to open a branch of research about the potentiality of Funori to restore physical breaks of deteriorated cellulosic fibers[28]. The case study is a canvas painting that is the altarpiece of the parish church of Rondissone, a small city near Turin in Piedmont (Italy). The fibres which compose the canvas support were overviewed with the Scanning Electron Microscope (fig. 1). They seemed very damaged in their micro-structure and, as a consequence, the lack of mechanical resistance of the fibres.

[28] E. Andrina, *Potentiality of funori to restore physical breaks of deteriorated cellulosic fibers*, Ceroart online, 2014.

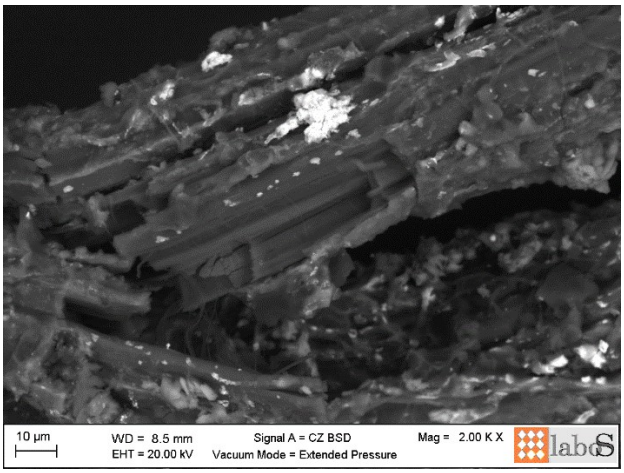

Figure 1: SEM image of depolymerized canvas wire, captured by SEM-EDX microscope of Scientific laboratories at Conservation and Restoration Centre "La Venaria Reale"[29].

Three different funori in water solutions have been prepared at different concentration: 0,5%; 1%; 1,5%. In order to help the penetration in the structural breaks of fibres, low pressure table was used during the drying.
The samples were placed to the low pressure table between a blotting paper and Melinex®. Then the low pressure was started. After five minutes the blotting paper was replaced by a new one and the samples were again put under pressure for ten minutes to dry them completely, an essential condition not to have any problems during the SEM overview.
Observing samples with the Scanning Electron Microscope before and after the treatment it was possible to observe the different ways in which Funori settles on the wire surface according to the solution concentration. The sample treated with funori at 0,5% didn't shown the presence of the consolidant at the morphological observation. Probably the low concentration of the solution combined with the high porosity of the yarn caused the completely penetration of the solution, that in that way disappear from the surface. In the second sample, treated with the solution at 1%, the overview by SEM has shown two different deposition ways. Funori fills structural breaks of the damaged fibres. Moreover some parts of the fibre are covered by a thin film of consolidant which follows the trend of the

[29] SEM Zeiss EVO60 equipped with micro-probe EDX Oxford PentaFET.

surface (fig.2). The third sample confirmed the behaviour overviewed in the second one (fig.3).

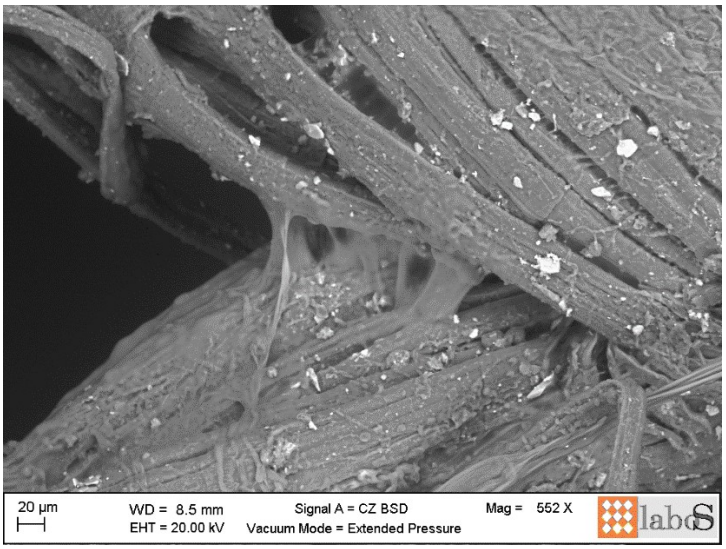

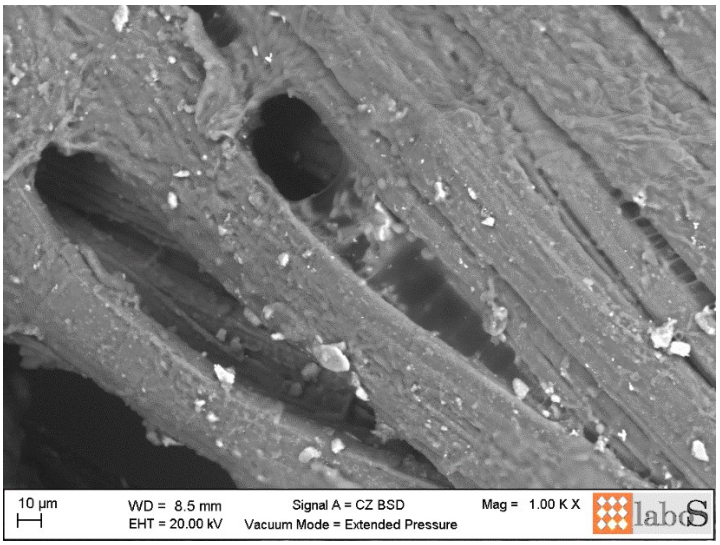

Figure 2: SEM images of depolymerized wire treated with funori water solution at 1%, captured by SEM-EDX microscope of Scientific Laboratories at Conservation and Restoration Centre "La Venaria Reale".

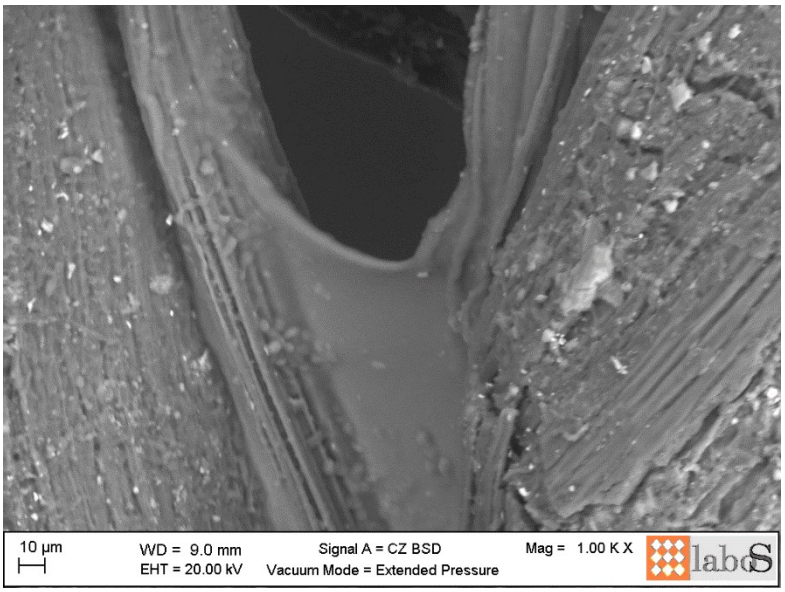

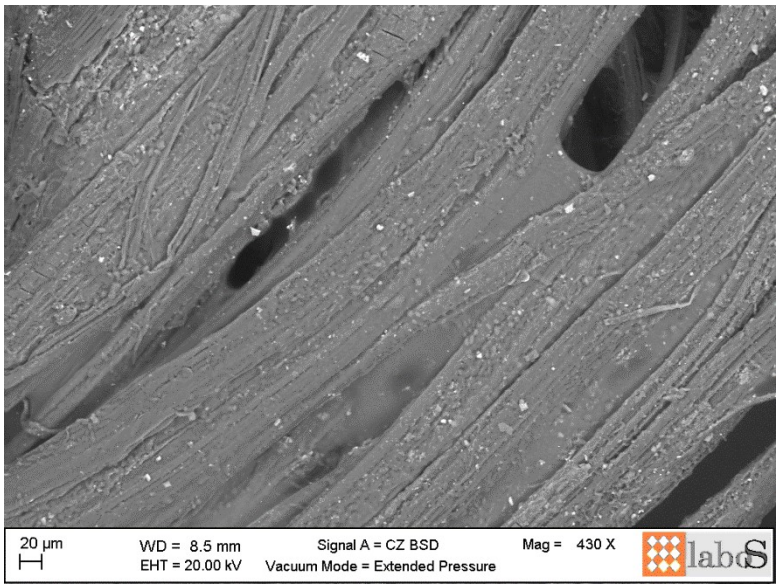

Figure 3: SEM images of depolymerized wire treated with funori water solution at 1.5 %, captured by SEM-EDX microscope of Scientific laboratories at Conservation and Restoration Centre "La Venaria Reale".

Allil- n-hydroxy-propyl cellulose: synthesis[30]

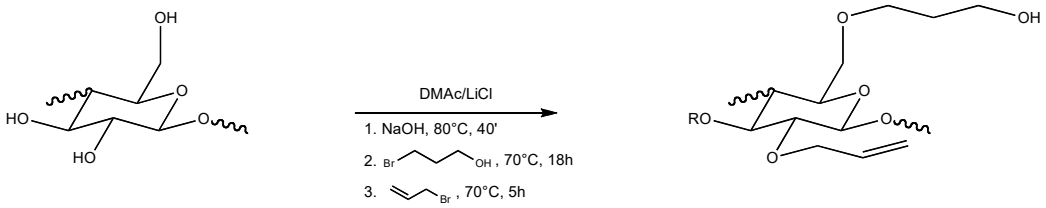

Figure 4: Synthesis of Allyl n-hydroxypropyl cellulose.

Into a dry 100-mL, two-necked flask equipped with a vacuum/nitrogen inlet/outlet and a reflux condenser, powdered sodium hydroxide (0.64 g, 16 mmol) was added under continuous stirring to 20 mL of a LiCl/DMAc (6% w/w) cellulose solution under a nitrogen atmosphere, and the mixture was heated at 80_C for 40 min. After cooling at room temperature, a solution of 3-bromo-1-propanol (0.72 mL, 8 mmol) in DMAc (15 mL) was added, and the mixture was allowed to react at 70_C for 18 h. Powdered sodium hydroxide (0.36 g, 9 mmol) was added, and the mixture was heated at 80_C for 40 min. After cooling at room temperature, a solution of allyl bromide (0.39 mL, 4.5 mmol) in DMAc (15 mL) was added, and the mixture was allowed to react at 70 C° for 5 h. The reaction mixture was then added to 250 mL of ethanol, and the precipitate obtained was filtered through a Gooch Funnel, washed with ethanol, and dried in vacuo (1.2 g). The white solid was added to 100mL of ethanol and kept under continuous stirring at room temperature for 3 h. After filtration, the solid was dried in vacuo (0.62g, DS n-hydroxypropyl= 0.6, 98.0% yield).

[30] G.Cipriani, A. Salvini, P.Baglioni et al., Cellulose as a Renewable Resource for the Synthesis of Wood Consolidants, 2010.

1H-NMR (D2O, 400 MHz, ppm): 1.87 (m, 2H,-O-CH2-CH2-CH2-OH); 3.23 (m, 1H, H2 cellulose

backbone); 3.68 (m, 4H, -O-CH2-CH2-CH2-OH); 3.83, 3.96, 3.98, 4.01 (m, 4H, H3AH6 cellulose

backbone); 4.12 (m, 2H, -CH2-O-allyl); 4.54 (m, 1H, H1 cellulose backbone); 5.33 (m, 2H,

CH2=CH-CH2-); 5.99 (m, 1H, CH2=CH-CH2-).

CHAPTER 2

Funori preparation

The attention has been first focused on the optimization of the extraction protocol. At this purpose, a series of extraction tests have been performed at different temperature and extraction time in order to evaluate the influence of these parameters on the extraction yield and the chemical composition (Table 1).
Different funori extracts have been prepared by soaking 0.2 g of dry seaweed in 19.8 g of Millipore water. An extended range of extraction temperatures are experimented to enhance potential differences between the products obtained. The aim is firstly to evaluate differences in terms of chemical composition and yield of the products obtained.

Product	Amount of dried seaweed (g)	Dried product (g)	Solution concentration (%)	Yield (%)
Room temperature 2,5h	0.25	0.13	0.52	52
Room temperature 24h	0.25	0.14	0.56	56
60°C 2,5h	0.25	0.23	0.92	92
30°C 2,5h	0.25	0.15	0.6	60
30°C 24h	0.25	0.17	0.68	68

Table 1: extractions tested and yields.

In order to separate the insoluble fraction, the samples were purified filtering them by the use of a wire stirner (mesh size 1 mm), followed by centrifugation with IEC CL31R multispeed centrifuge (Thermo Electron Corporation, USA) at 8000 rpm, 25°C for 5 min. Supernatants and residues

were then freeze dried with a Virtis benchtop freeze dryer (SP Scientific, USA) for 48 hours.

FTIR characterization of the extracts

FTIR spectra shown that the procedure tested gave similar results about relative concentration of polysaccharide fraction and the protein one in the solution, regardless of variation in temperature and time of extraction. Elemental analysis confirmed that result.

All the spectra (fig. 5-6-7-8-9-10) of the extracted materials show several similar features: a broad band at 3260 cm^{-1} due to the –OH stretching vibration; the absorption bands between 1200 cm^{-1} and 950 cm^{-1} due to the stretching of–CO and C-CH appertaining to the pyranoid ring, and to the C-O-C stretching of the glycosidic bonds. The peaks at 1219 cm^{-1} and 813 cm^{-1} can be attributed respectively to the adsorption band of asymmetric stretching of S=O and to the C-O-SO_3 on C6 of sulphated galactose. Furthermore, the bands at 1647 cm^{-1} and 1550 cm^{-1} are characteristics of the amide groups (stretching of –C=O and bending of N-H). Comparing the relative intensity of the protein and polysaccaridic peaks in different extracts, it is possible to assess the analogy of the procedures in terms of chemical composition of the products obtained.

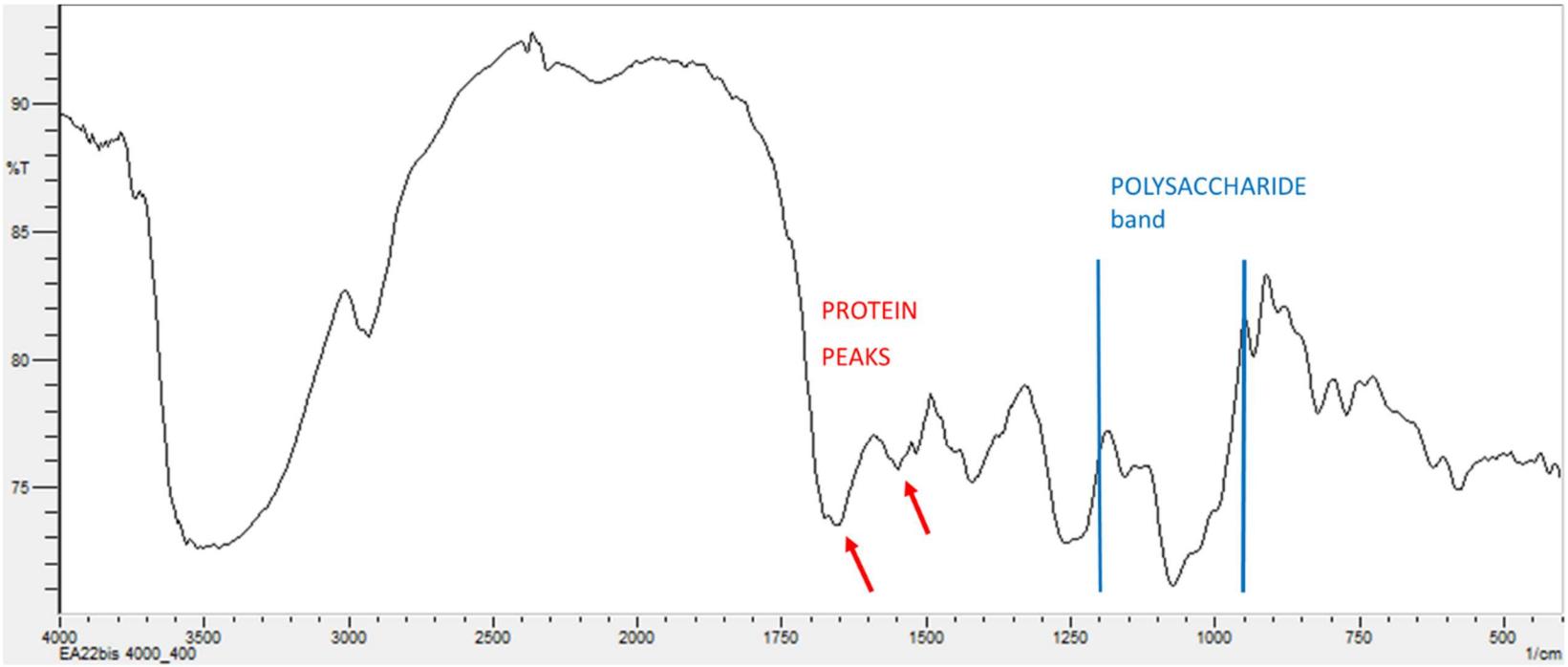

*Figure 5: FTIR spectra of the product obtained by the extraction at 30°C, 2.5 h (**F30**). The two peaks highlighted in red (1647 $cm^{-1}$and 1550 cm^{-1} respectively) are characteristics of the amide groups of the protein fraction. The broad band highlighted in blue is related to the pyranoid ring and to the the glycosidic bonds.*

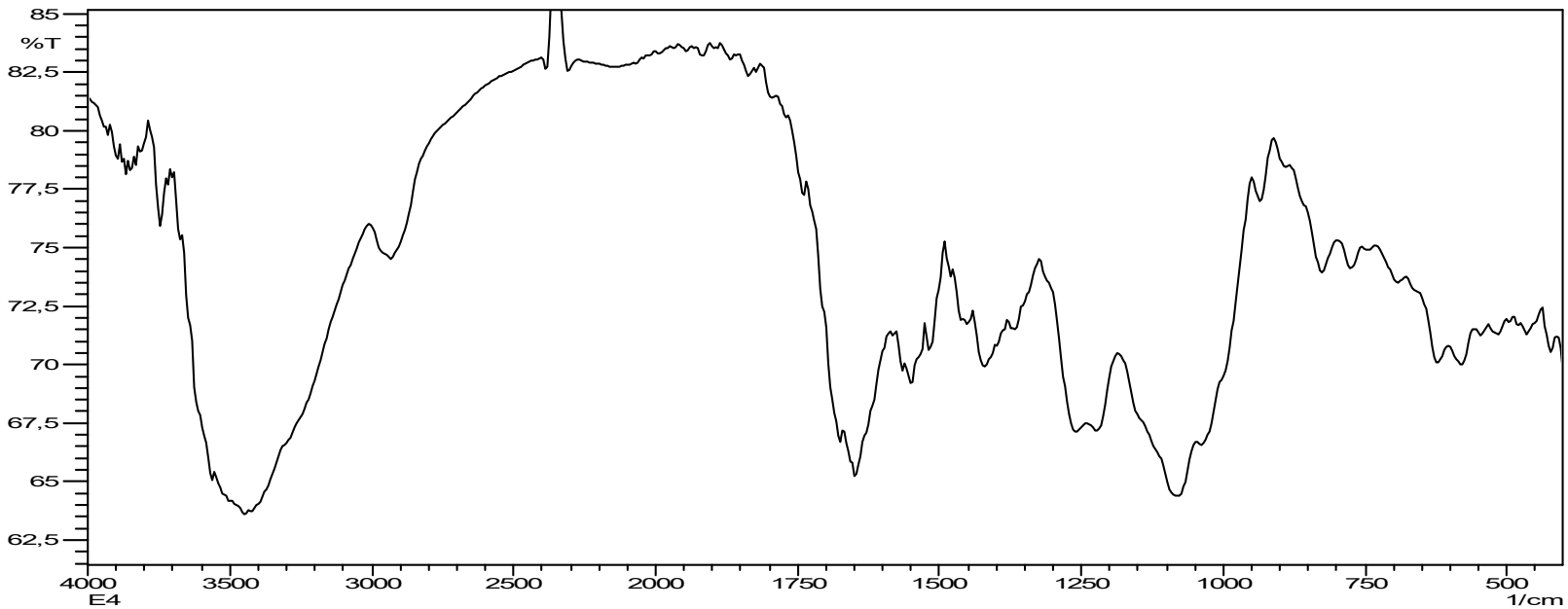

Figure 6: FTIR spectrum for EA26 extraction (room temperature for 24 hours).

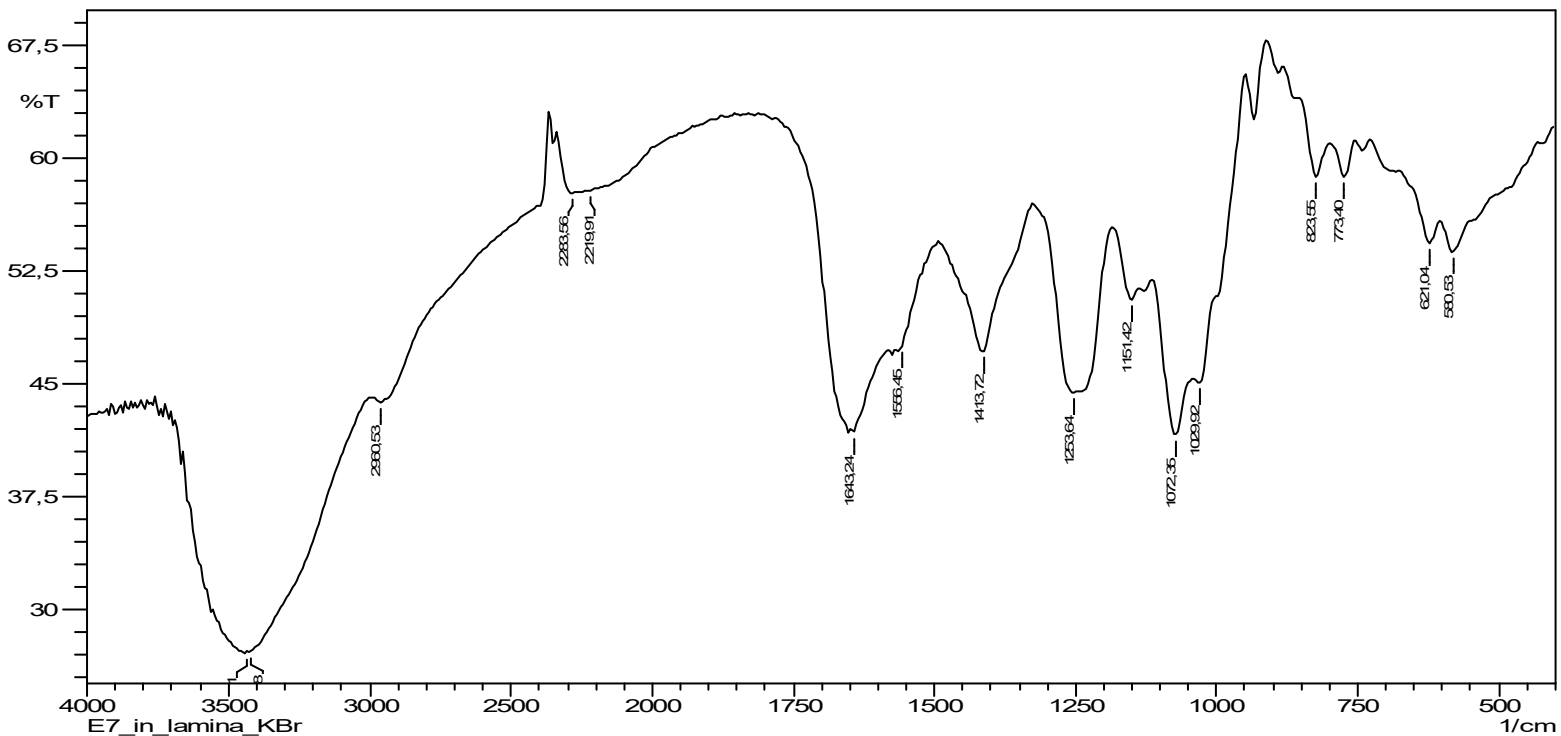

Figure 7: FTIR spectrum for EA20 extraction (room temperature for 2.5 hours).

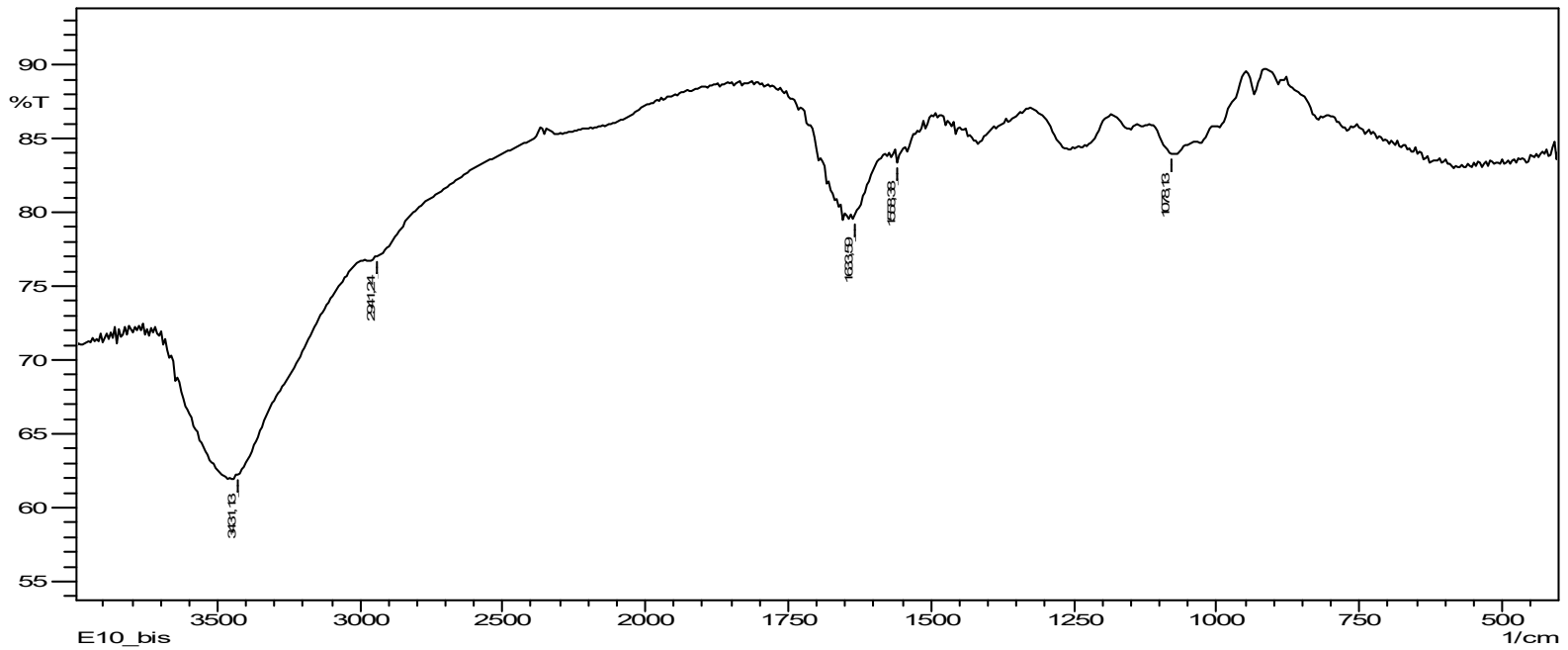

Figure 8: FTIR spectrum for EA24 extraction (60°C for 2.5 hours).

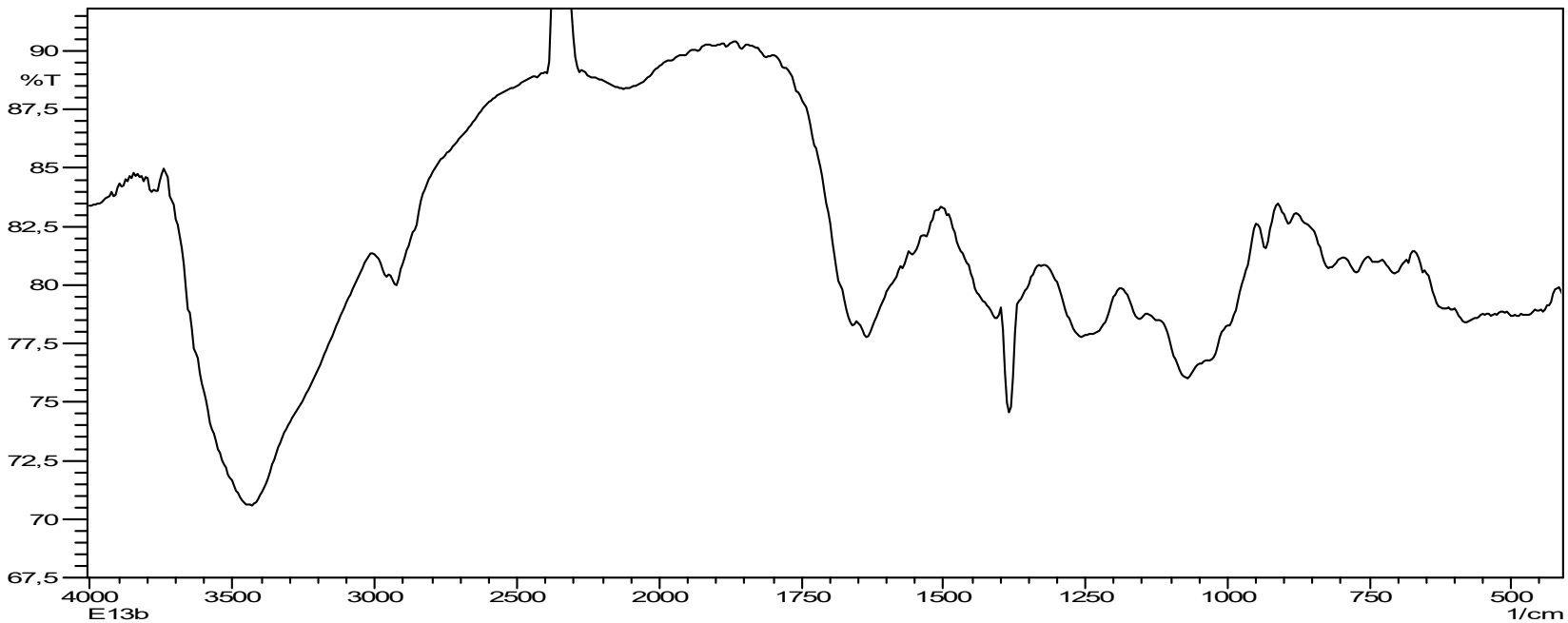

Figure 9: Figure 7: FTIR spectrum for EA22 extraction (30°C for 2.5 hours).

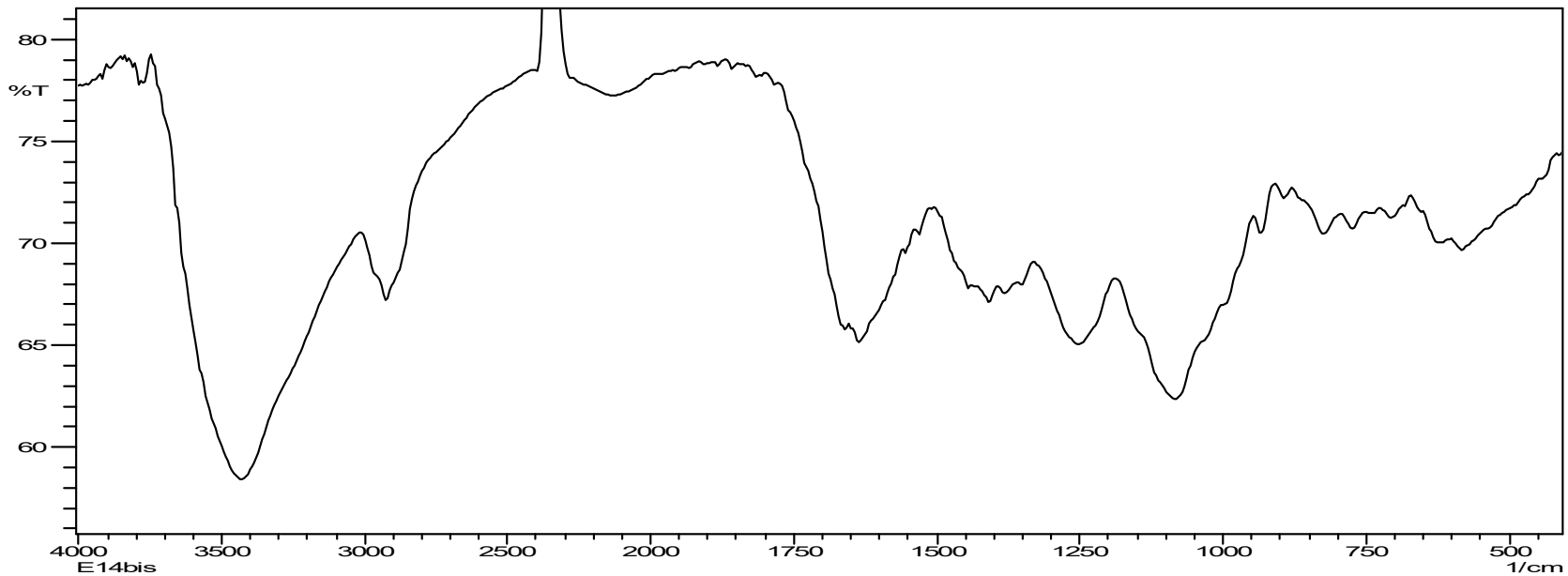

Figure 10: FTIR spectrum for EA27 extraction (30°C for 24 hours).

There are relevant differences between one procedure to another in terms of yields (Table 1). As expected, when the extraction temperature increased, the yield of extracted funori increased as well. However, the higher yields obtained increasing the temperature is not a real advantage in this case: in fact, a further increase of T up to 60°C favours a higher dispersion of swelled fragments of funori, more than a real increase of the amount of solubilised fraction. The removal of those residues by centrifugation had to be performed in the second step of the protocol to obtain the consolidant solution. With this last procedure, the effective yields of the extract obtained at 60°C is finally comparable with the others.

The extraction time influences a little the yield: by increasing the extraction time from 2.5 up to 24 hours, maintaining the temperature constant at 30°C, the yield increases by almost 13%. This increase is probably related to the fact that longer extraction time causes the swelling of a higher amount of longest polysaccharide chains.

Taking into account these results and the advantages of a reduced extraction time, extraction at 30°C in 2.5 hours has been chosen as standard procedure. The physico-chemical characterization has then been performed on that product (EA22).

Some further evaluations have been made taking into account the two products extracted at 30°C (EA22 and EA27). FTIR measures have been performed both on the supernatants and the precipitates (fig.11-12-13-14), to understand the nature of the insoluble fraction which results after the extractions, appearing as micro particles dispersed in the liquid (Table 2) .

Products	Products befor drying (g)	Dry products (g)	Yield (%)
EA22 supernatant	16,85	0,0613	0,36
EA22 precipitate	16,85	0,0208	0,123
EA27 supernatant	16,85	0,0637	0,37
EA27 precipitate	16,85	0,0043	0,02

Table 2: products obtained from the centrifugation of EA22 and EA27, for 15 minutes at 2790 R.P.M .

With the centrifugation has been not obtained a clear separation between polysaccharide fraction and the protein one. FTIR spectra show an enrichment in protein content in the precipitate fraction. So the lesser soluble substances are proteins, which tends to precipitate.

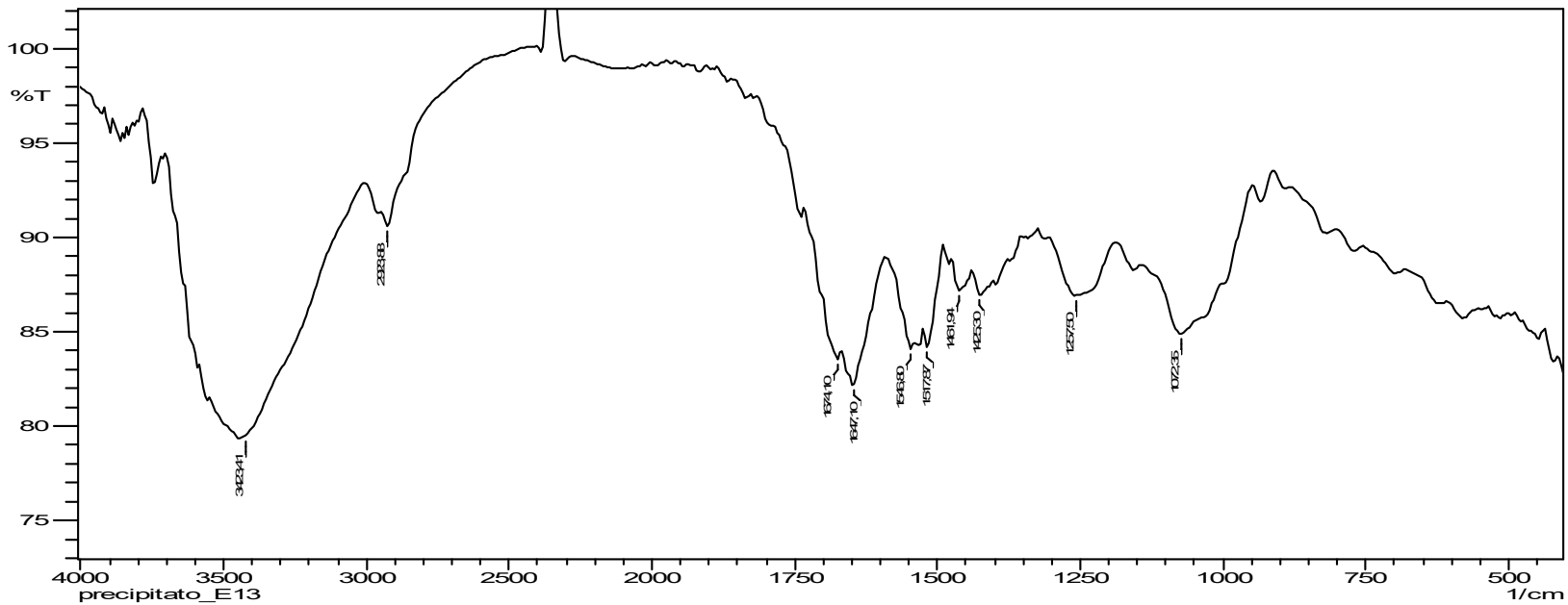

Figure 11: FTIR spectrum for EA22 precipitate.

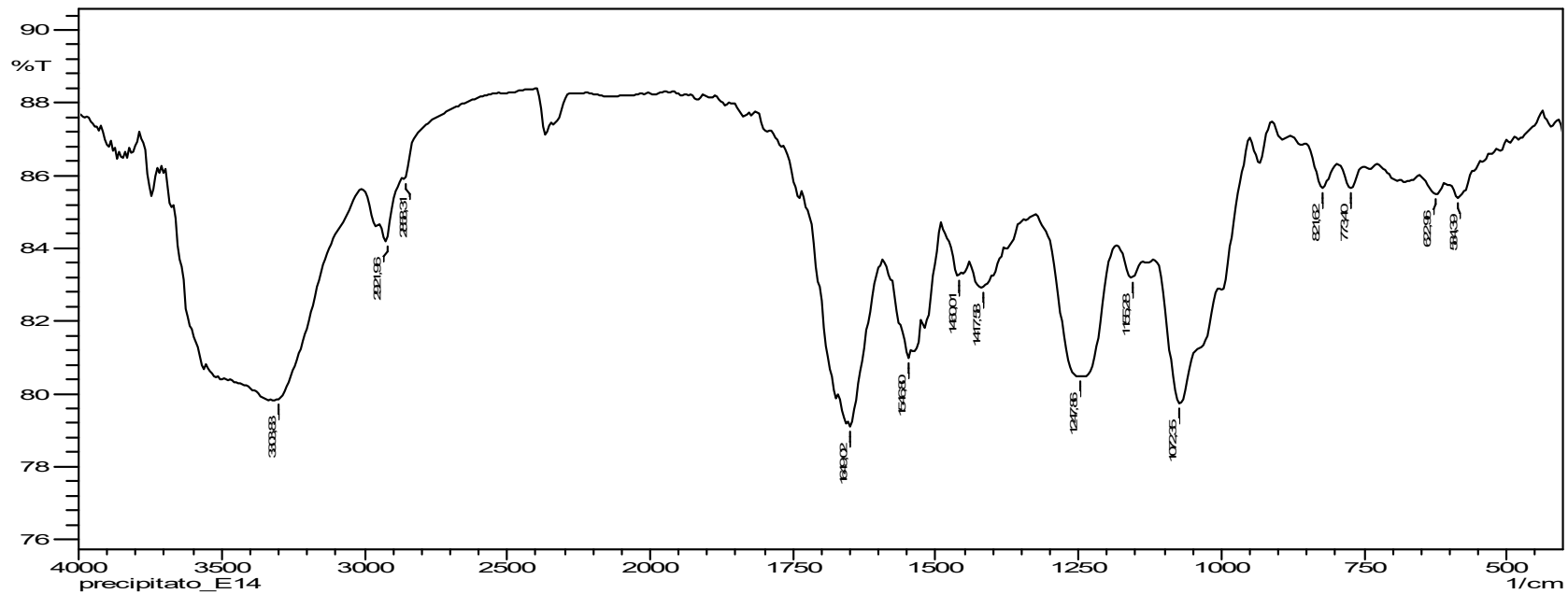

Figure 12: FTIR spectrum for EA27 precipitate.

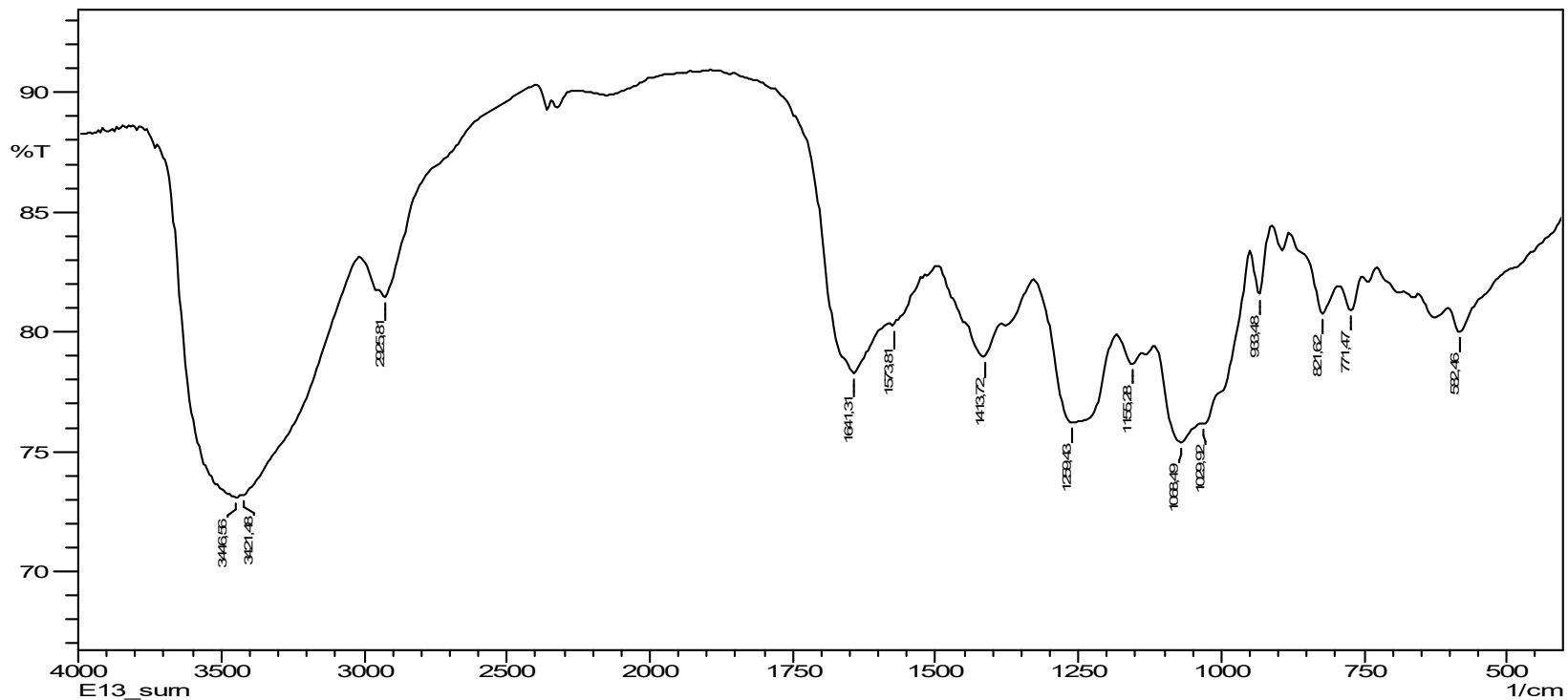

Figure 13: FTIR spectrum for EA22 supernatant.

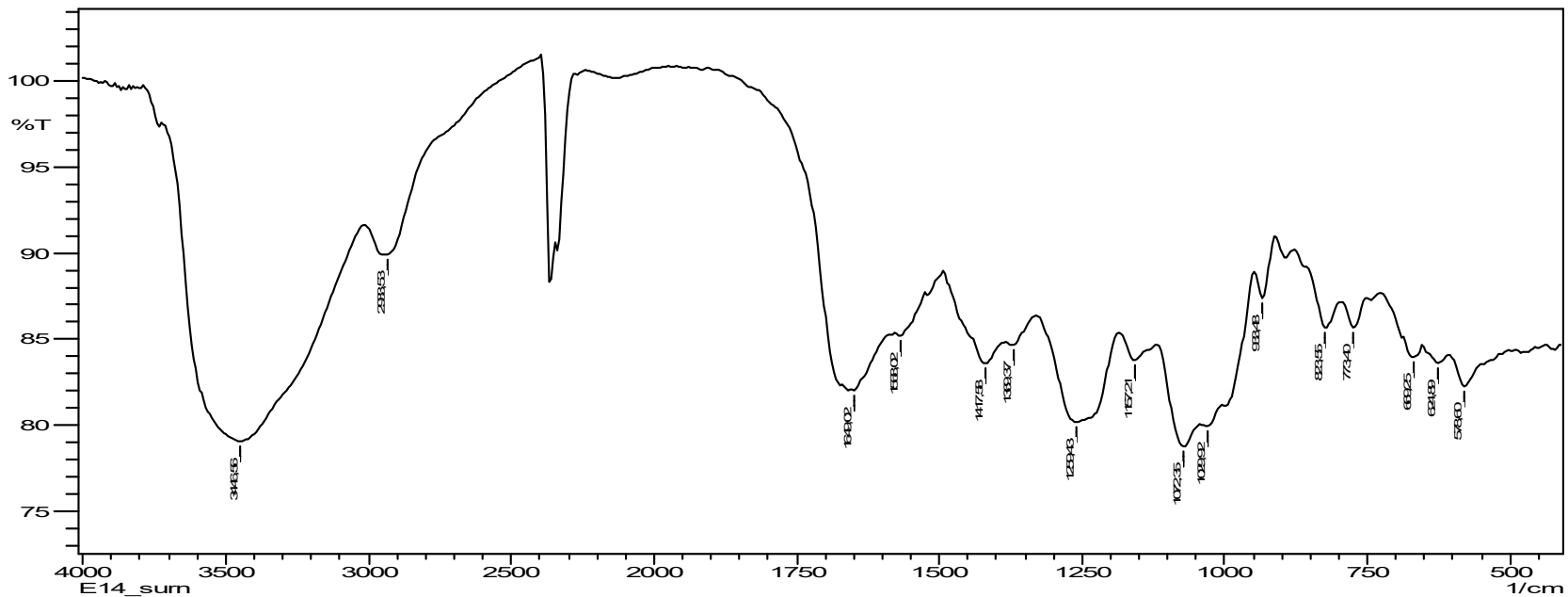

Figure 14: FTIR spectrum for EA27 supernatant.

The measure of solution viscosity and contact angle

Fig.15 shows the trend of the viscosity of the solution F30 in relation with the shear stress applied, at different temperatures tested. At the increasing of the shear stress, viscosity gradually decrease. Furthermore, viscosity decreases increasing temperature. This behaviour is typical of Newtonian liquid.

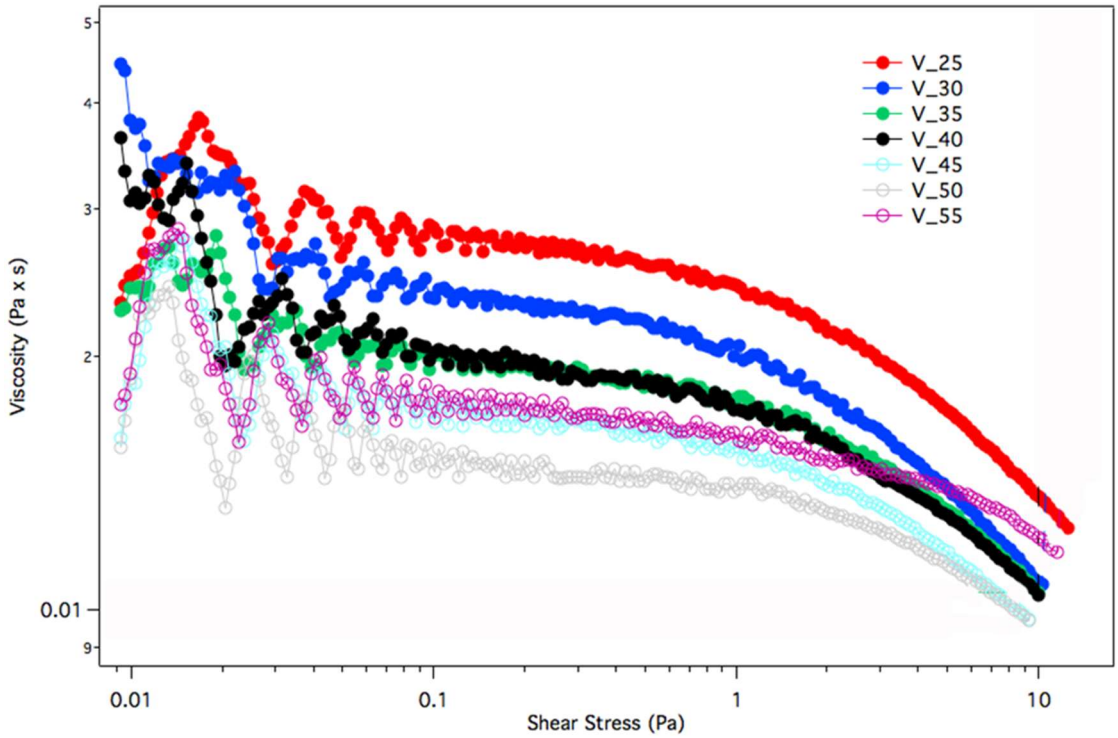

Figure 15: trend of viscosity of the funori solution in relation with the shear stress applyied, at different temperature.

The belonging of funori solution to this category is shared also from fig.16. The graph confirms an inversely proportional trend between viscosity and temperature. This relation follows the Arrhenius law:

$$\eta = \eta_0 \exp(\mathrm{E}_{act}/RT)$$

η : viscosity;

η_0 : a constant value related to molecular weight and molar volume of the fluid;

E_{act} : activation energy necessary to start flux molecules;

RT: gas constant multiplied by absolute temperature;

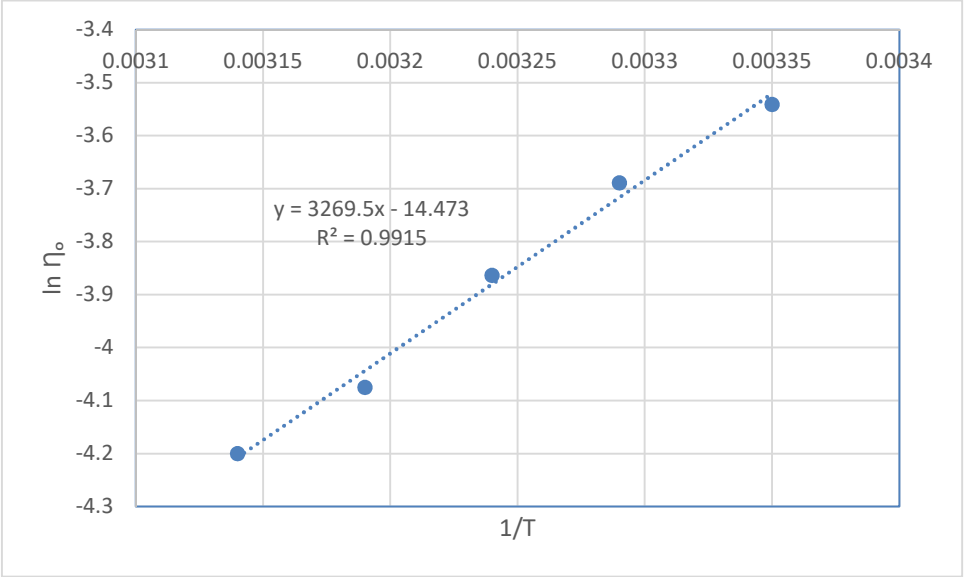

Figure 16: inversely proportional trend between viscosity and temperature.

From the Arrhenius relation has been finally obtained the value of the activation energy.

$$E_{act} = 27.18 \frac{kJ}{mol}$$

The analysis of this results gives important indications also for the practical use of the product, such as the temperature of application. Thanks to the inversely proportional relationship between temperature and viscosity assessed above, a slight warming is suggested. Indeed, a low viscosity is preferred when the aim is the consolidation of a surface. Low viscosity imply

a better and more homogeneous coating and distribution of the product on the substratum.
About the measure of the contact angle, this measure allowed to express in a number the interaction between funori film and water. Dropping water on funori films, the contact angle is calculated with a specific software on images acquired by a microscope connected to the system.

$$Contact\ angle: 86.3 \pm 6.2$$

According to the general rule that a material is considered wettable if its contact angle is included in the rate from 0°to 90°, funori can be considered a hydrophilic material.

Determination of water content in extracted funori.

Being that water plays a primary role in most of the degradation processes (such as hydrolysis and development of fungi and bacteria of funori films), the distribution of water molecules inside some samples exposed and equilibrated to an atmosphere at controlled temperature and RH has been investigated. In that way it is possible to understand which are the best conditions, in terms of conservation atmosphere (and extraction conditions), that minimize the uptake of water vapour from the atmosphere. The extracts have been maintained at controlled Relative Humidity (RH) and Temperature to study their tendency in absorbing water from the external environment, through Differential Scanning Calorimetry (DSC) and Thermogravimetric Analysis (TGA).
It is well known that in an aqueous solution of a hydrophilic polymer, three different populations of water molecules interacting with the polymer chains by different strengths can be found.
In particular three different populations of water molecules are usually present:

- Free water or unbound water (FW): in this case melting and crystallization temperature are the same of bulk water, because molecules aren't bounded with the polymer nowise.

- Interfacial water or freezable bound water (FBW): it is the one end fixed hydrated water. This weak interaction with the polymer allow water molecules to partially retain their mobility. This implies a shift of the phase-transition temperature, that become lower than that of bulk water[4];
- Non-freezable bound water or bound water (BW): in this case, both the hydrogen atoms of the water molecule are strongly bound to the hydrophilic groups of the polymer by hydrogen bonding. This situation compromises a lot the mobility of such water molecules. As a consequence, such water is not able to crystallize when cooled down[5]. Then, if water is strongly associated to funori, this relation makes its molecules inactive, resulting in the inhibition of degradation processes.

DSC is commonly used to determine the distribution of the water molecules in hydrate polymers. During a change in temperature, samples analysed radiates or absorbs a heat quantity that is measured by DSC, by calculating the difference between the sample and the reference material.
In particular, about the quantification of different classes of water there are some general rules for the interpretation of the curves.

Materials and methods

H_2SO_4 were purchased from Carlo Erba Reagents. KCl (99.5%), KI (≥ 99.00 %), NaCl (99.80%) and 2-s-propanol (≥ 99.81%, GC grade) were purchased from Sigma- Aldrich. 5g/L of $Ca(OH)_2$ nanoparticles in 2-propanol was prepared by CSGI, University of Florence. All the chemicals were used as received. The Whatman paper no.1 (Scheicher & Schuell, 99% of cellulose) was used to achieve paper ageing samples. Higly pure water, purified by Millipore water purification (Elix®, Millipore Corporation, France) was used during the experiments.
The DTGA curves of funori extracts samples were recorded in dynamic, not isothermal conditions, using SDT Q600 from TA Instrument, USA. The experimental conditions were as follows: temperature range 25-500 °C; sample weight, 1-5 mg; heating rate, 10 °C/min. The tests were performed under a nitrogen atmosphere with a flow rate of 100 mL/min.

DSC experiments were carried out with a Q1000 TA Instruments apparatus using Tzero hermetic aluminium pans under nitrogen atmosphere (flow rate equal to 50 mL/min) with the following temperature cycle: from room temperature down to -90 °C at 60 °C min-1, isotherm at - 90 °C for 4 min, from -90 °C up to 30 °C at 0.5 °C min-1.
An empty sealed aluminum pan was employed as a reference. The enthalpy of fusion of the water was calculated by integrating the heat flow curves.
The Free Water Index (FWI), a parameter that represents the percent of free and freezing bound water contained in the samples, was calculated using the following formula:

$$FWI = \Delta H_{samp}/\Delta H_{purewater\_} x\ 100$$

where ΔH_{samp} is the enthalpy change due to the fusion of the ice contained in the HVPD sample (J g_{water}^{-1}), experimentally determined from the DSC curve; $\Delta H_{freewater}$ (= 333.6 J g^{-1}) is the theoretical value of the specific fusion enthalpy of pure ice at 0°C.
Thus, the fraction of bound not freezable water (BWI, bound water index) was obtained as follows:

$$BWI = 1 - (FWI + FBWI)$$

where FBWI is the fraction of freezable bound water.

Samples preparation

First, all film samples were dried for 48 hours at 50°C in an oven (ISCO NSV 9000) under vacuum (pressure 1 bar), then they were arranged into three sealed big glass jars containing saturated aqueous solutions of KI, KCl and water, in order to maintain the Relative Humidity (RH) constantly equal to 68%, 84% and 99% respectively, keeping the temperature constantly equal to 22°C for 14 days. The values of RH and temperature were measured before starting the experiments by means of RS 1365 humidity-temperature meter. Each sample was weighed before and after equilibration. The amount of water uptaken (WU) expressed as wt%, has been calculated as follows:

$$WU = \frac{a-b}{b} \times 100$$

where, *a* and *b* are is the weigh (in mg) of the sample after and before the equilibration respectively.

Film samples were subjected to two different aging procedures. The first was subjected to a hydrothermal ageing, the second to a combined acid and hydrothermal ageing. In the first case the samples were held in a sealed glass jar containing a saturated aqueous solution of NaCl and put in an oven at 80°C (in these conditions the RH was equal to 76%). The second group of samples was maintained at the same temperature and RH, but in this case the relative humidity inside the glass jar was maintained by the use of saturated solution of NaCl in 1M of HCl, generating an acidic atmosphere. All the samples were maintained in a Memmert (Schwabach) oven, model 400.

Results and discussion

Figure 17 shows DSC heating curves of funori extracts at 22°C for 2.5 hours, equilibrated at three different RH conditions and at environmental conditions. The funori sample equilibrated in an atmosphere at 68% RH do not show any endothermic peak in the heating phase. This means that, in these conditions, only bound water strongly associated to funori skeleton is present. Considering that RH standard value established for museum's rooms must be maintained around 50- 60%, the results confirm that the extractions performed at room temperature (at that RH values, the trend of the curve of product extracted at 30°C is the same observed for the one extracted at 22°C) are suitable for treating works allocated to museums.
No melting peaks of free water appeared at 0°C on the heating scan, hence free water is missing. The FBW index has been evaluated from the integration areas of endothermic peaks. In non-equilibrated samples and equilibrated samples at 68%RH only the presence of bound water has been assessed.
At higher relative humidity, 84%RH and 99%RH, the FBWI will be determined taking into account the influence of extraction temperature and time to the FBWI. This can be important to evaluate for different types of applications of funori. In the last years it has been taken into account also for the

consoildation of stones or frescoes, that is to say for artworks often positioned in an outside environment. In these case UR values are subjected to an extreme variability and could reach also very high values. For these of applications the best temperature of extraction seems to be 20°C, because it guarantees the minor FBW contents.

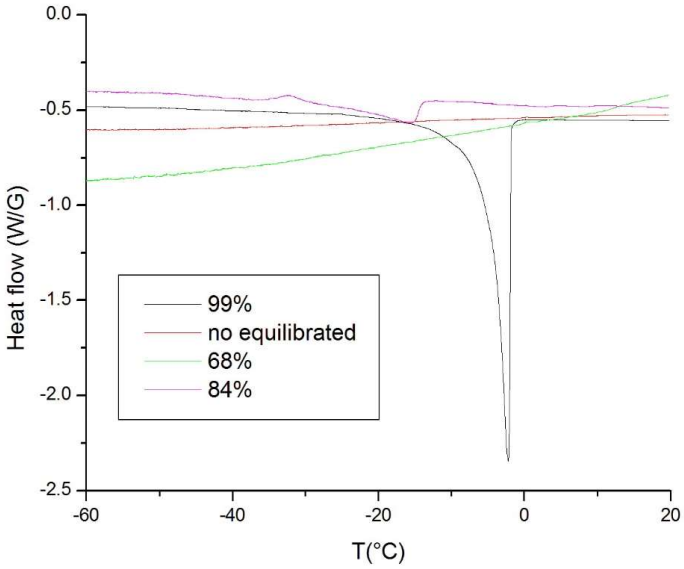

Figure 17: DSC heating curves of funori extracted at 22°C for 2.5 hours.

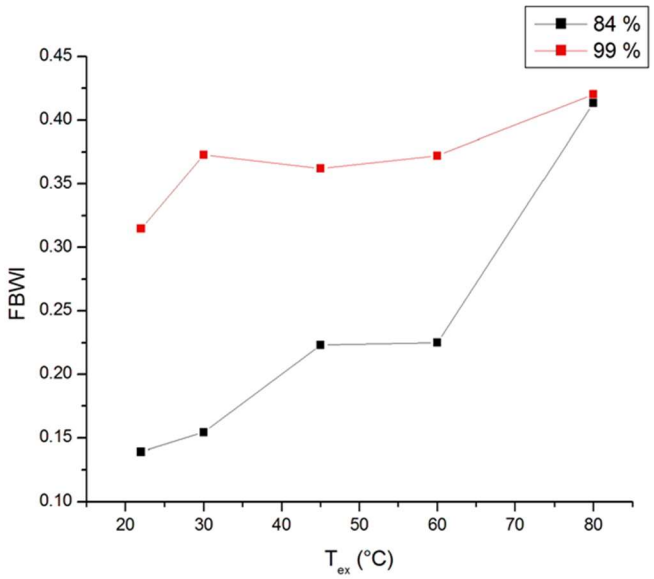

Figure 18: the effect of extraction temperature on the FBWI of funori extracts determined by DSC.

Figure 18 presents the trend of FBWI as a function of the estraction temperature for samples equilibrated at 22°C and 84% RH and 99% RH. In comparison with 84% RH, the FBWI of equilibrated samples at 99% RH is higher, indicating an higher amount of loosely bound water present in the samples. But in both cases low temperature extractions involved a lower content of FBW.

About the influence of extraction time, considering samples equilibrated at 84%RH, FBWI values are almost the same in both the extraction times tested (2.5 and 24 hours). On the other hand, samples conditioned at 99%RH show a considerable increase in FBWI value: from 0.30 at 2.5 hours to almost 0.60 at 24 hours. Therefore, the 2.5 hours extraction time must be preferred.

In conclusion, there is an inversely proportional relationship between total amount of water adsorbed by funori and extraction temperature. Indeed, the total amount of water adsorbed by funori decreases by increasing the extraction temperature. On the contrary, the FBWI increases by increasing the extraction temperature. It means that the extraction at low temperature allow to obtain a product that has an higher total amount of water adsorbed

in its polymer structure but all these water molecules are tightly bound with the chains. This strong association makes water inactive about degradation processes. Increasing temperature of extraction, the total amount of water adsorbed by the polymer decrease but the amount of partially bound water (FBW) drastically increases. This type of water is weakly bounded with funori, so could be involved in degradation mechanisms. For this reason, the extraction at low temperature (30°C) has been evaluated as the best one and has been chosen also to prepare nanocomposite.

Preparation of stable nanocomposite

Several blends of extracted funori and calcium hydroxide nanoparticles have been developed in order to obtain efficient formulations for the inhibition of degradation processes related to acidic hydrolysis and strengthening of cellulose-based artefacts. $Ca(OH)_2$ nanoparticles are stable in alcohol, but funori is soluble only in water. Therefore, the decision is to avoid as much as possible the use of water to avoid the agglomeration and sedimentation of $Ca(OH)_2$ nanoparticles. In order to solubilize funori, which is insoluble in 2-propanol, a 50:50 mixture of water and 2-propanol was used as dispersing medium for $Ca(OH)_2$ nanoparticles.

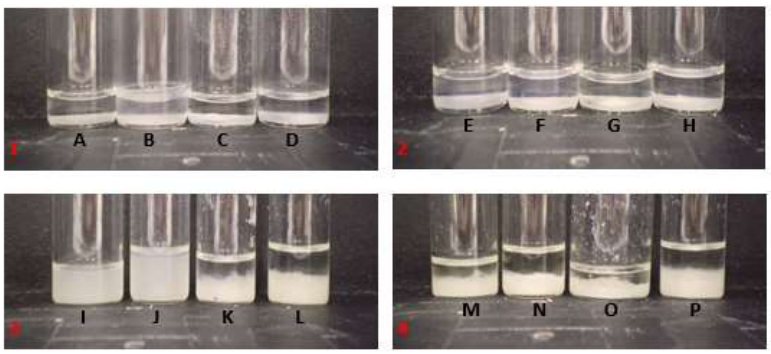

Figure 19: the appearance of mixed nanoparticles-funori dispersion; series 1) 0.1% w/w of funori extract 2) series 2: 0.2% w/w of funori extract 3) series 3: 0.5 w/w of funori extract 4) series 4: 1.0% w/w of funori extract.

In order to be applied for conservation purposes, nanocomposite must be stable for a certain period of time. Therefore, the kinetic stability of

nanocomposites I and J was determined by preliminary visual examination and turbidity measurements. The preliminary examination consisted in the observation nanocomposites at different periods of time and comparing each one with the dispersion of $Ca(OH)_2$ nanoparticles without the addition of funori extract.

Within 15 minutes all the dispersions were stable and no settling was observed. The dispersions of nanoparticles without funori used as comparison exhibited a slight separation of the two phases above 30 min, due to the settling of $Ca(OH)_2$ nanoparticles. As shown in figure 19, nanocomposites I and J are the most stable ones. They didn't show any phase separation, being stable for more than one hour. Nanocomposite I contains the extracted funori and $Ca(OH)_2$ nanoparticles in the same concentration, that is 0.5% w/w. Nanocomposite J contains 0.5% w/w of funori extract and 0.10% w/w of $Ca(OH)_2$ nanoparticles. Increasing the concentration above 0.5% w/w, the amount of funori is too high to be dissolved in water/2-propanol 50:50, resulting in the formation of aggregates formed by $Ca(OH)_2$ nanoparticles and funori. Below 0.5% w/w the sedimentation of $Ca(OH)_2$ occurs just after 15 min.

However, the preliminary visual examination didn't allow to notice differences in stability between the two nanocomposites identified. Nevertheless the concentration of $Ca(OH)_2$ nanoparticles in nanocomposite J was two times higher than that in nanocomposite I. Thus, the dispersion J was characterized via turbidimetric analysis. The absorbance of samples was measured at 640 nm as a function of time. The absorbance at 640 nm is proportional to the turbidity of samples; it means the decline of absorbance as a function of time manifested the agglomeration and settling of samples.

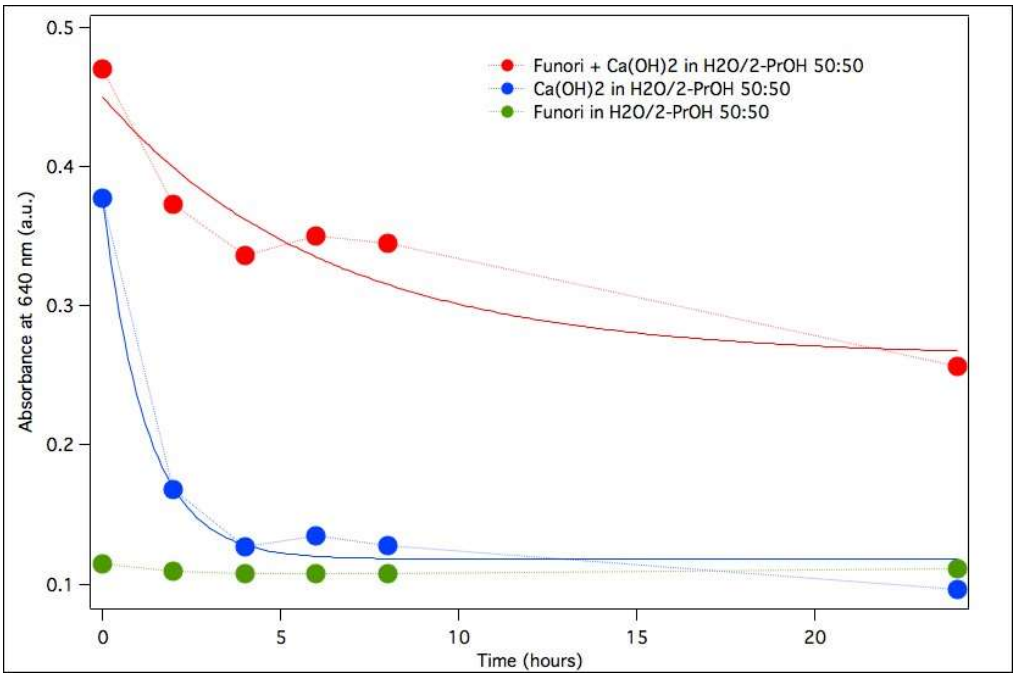

Figure 20: the kinetic stability of nanocomposite observed by turbidimetric measurements via absorbance at 640 nm.

Figure 20 shows the trend of the absorbance at 640 nm as a function of time. It is worth noting that no absorption is shown at this wavelength. The dispersion of 0.50% w/w extracted funori mixed with 0.10% $Ca(OH)_2$ nanoparticles (fig.20, red curve) is much more stable than the one with 0.10% w/w $Ca(OH)_2$ nanoparticles without extracted funori (fig.20, blue curve). The first case exhibits a slow decrease of absorbance (from almost 0.5 at t=0 to around 0.35 at t=3 hours). In the second case, the graph shows a steep decrease of absorbance from almost 0.4 to 0.1 absorbance value.

Both the decay curves are well fitted (R^2= 0.9642 and 0.9784, respectively) by a monoexponential function (see equation 1); the output fitting parameters are reported in table 10.

$$Abs = A_1 \, exp(\frac{-t}{\tau}) + Abs_\infty \quad (1)$$

Where τ is the relaxation time, A_1 is a pre-exponential factor and Abs_∞ is the asymptotic value of the absorbance.

Sample	A1	τ(S)	$Abs_{\infty\infty}$
A	0.13	4536	0.34
B	0.25	3818	0.13

Table 3: Output parameter obtained by the fitting curve A and B (fig.20).

Nanocomposite relaxation time is a parameter indicating the rate of nanoparticles deposition. Its value (fig.20, red curve) is quite higher (almost 16%) than the one of the dispersion (fig.20, blue curve) meaning that the settling rate of the mixed system is lower than the one of nanoparticles in absence of funori. Therefore, the extracted funori apparently have a stabilizer effect, preventing the agglomeration of $Ca(OH)_2$ nanoparticles.

Characterization and ageing of thin films

Thin films were prepared from the mixture of 0.1% w/w $Ca(OH)_2$ nanoparticle and 0.5% w/w extracted funori. Figure 21 shows SEM images of the surface structure of films obtained from funori extracted at three different temperatures (A= 30°C; B= 60°C; C= 80°C). Surface structures of the films seem influenced by the extraction temperature. Indeed the pattern effect of the aligned microscopic structures formed by polysaccharide molecules seems slightly more pronounced for the samples obtained through an extraction carried out at 30°C and 60°C. For funori extracted at 80°C (fig. 21 C) the film appears a little less regular.

Figure 22 illustrates the appearance of nanocomposite films, showing the aggregation of $Ca(OH)_2$ nanoparticles into clusters sedimented on the surface. The difference with the aspect of funori films is remarkable. The typical texture due to the aligned microscopic structures noticed in the first

series of films was completely lost in the second one. Moreover, as just said above, the presence of micron-sized agglomerates of nanoparticles is also evident.

Both the films series were then characterized using ATR-FTIR analysis in absorbance mode. The aim is to highlight possible changes of funori molecular structure induced by $Ca(OH)_2$ nanoparticles. Figure 23 compares the spectra of both systems. The broad band at 3337 cm^{-1} is assigned to –OH stretching of water molecules associated to the OH groups of polysaccharide glycoside rings or other water molecules through hydrogen bonds. The weak band at 2898 cm^{-1} is assigned to –CH stretching. The medium intense bands at 1653 cm^{-1} and 1558 cm^{-1} are assigned to the amide groups (stretching of –C=O and ending of N-H) due to the protein content of funori[7]. Moreover, the absorption bands between 1219 cm^{-1} and 766 cm^{-1} are attributable to C-C, C-O stretching and C-O-C bending of glycoside ring. Funori also contains sulphate groups substituted on C6 in galactose equatorial position. This substitution explains the presence of 1219 cm^{-1} and 813 cm^{-1} peaks. The first can be attributed to the absorption band of asymmetric stretching of S=O, while the second one is assigned to C-O-SO_3 on C6 of galactose. The spectrum of nanocomposite differs only for the additional band at 871 cm^{-1}, related to the characteristic band of $CaCO_3$, due to the carbonation reaction of $Ca(OH)_2$. In general, the characteristic bands of $CaCO_3$ are at 1797, 1427, 876 and 712 cm^{-1}. Moreover, the peaks at 1653 cm^{-1} and 1558 cm^{-1} correspond respectively to the –C=O stretching and N-H bending of amide groups. In the nanocomposite spectrum these peaks disappear, probably due to the degradation of protein provoked by the alkalinity of $Ca(OH)_2$.

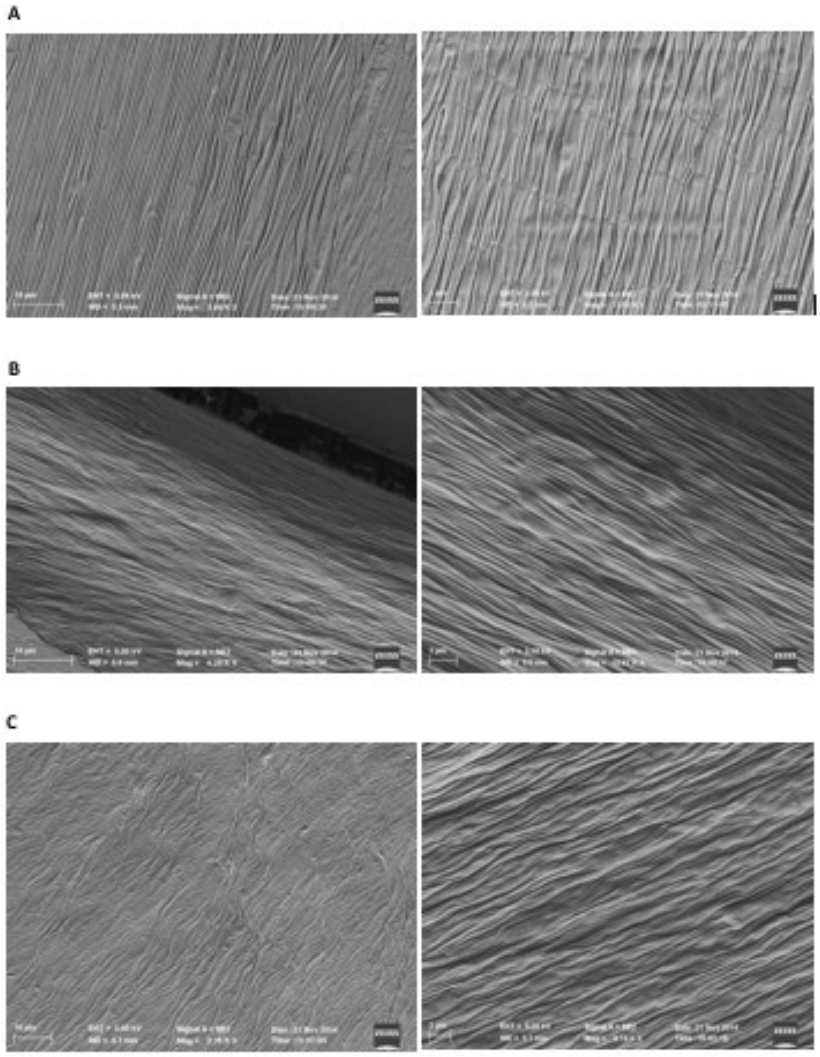

Figure 21: SEM images of extracted funori films; A)funori extracted at 30°C; B) funori extracted at 60°C; C) funori extracted at 80°C; each film is analysed at two different magnifications;

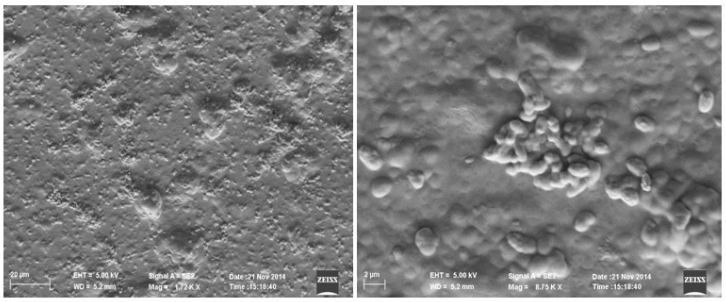

Figure 22: SEM images of nanocomposite film formed by Ca(OH)2 nanoparticles and funori extract.

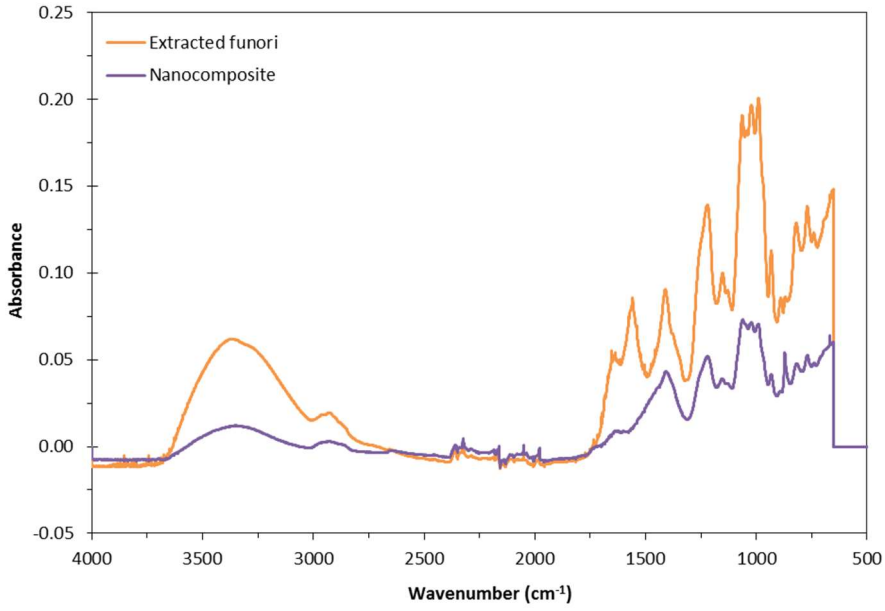

Figure 23: ATR-FTIR spectra of extracted funori and nanocomposite films.

Funori and nanocomposite films were then undergone to accelerated ageing to study the stability of materials and the degradation behaviour in long-term service. High relative humidity and temperature were used to speed up degradation reactions. As just said above, film samples undergone aging

treatments have been divided in two groups. The first was subjected to a hydrothermal ageing, the second to a combined acid and hydrothermal ageing. These ageing treatments lasted seven weeks. ATR-FTIR and thermal analysis were performed weekly, in order to investigate how the funori molecular structure changed upon time and consequently how changed the interaction and association between funori and water.

About films undergone hydrothermal ageing condition, DSC analysis shows no endothermic peaks associated to funori aged films. This result suggests the exclusive presence of bound water. To evaluate the degradation of the funori films, also TG measurements were performed week by week. Those measures underline a slight decrease in water loss and in weight loss. The weight loss starts at 35% and ends at 32%, while the water loss starts at 16% and ends at 12%. These percentages suggest that hydrothermal ageing does not affect the capability of funori to bond water strongly. This result is in line with those of DSC analysis. Since the thermal behaviour is almost the same of the unaged, funori seems only slightly degraded after seven weeks of hydrothermal ageing. Figure 24 shows ATR-FTIR spectra of funori films monitored weekly. The only appreciable difference between the eight spectra can be observed in the merging of the two peaks at 1653 cm^{-1} and 1558 cm^{-1} into a single peak. These signals are attributed to the amide groups, so this changing is probably due to the denaturation of protein at high temperature.

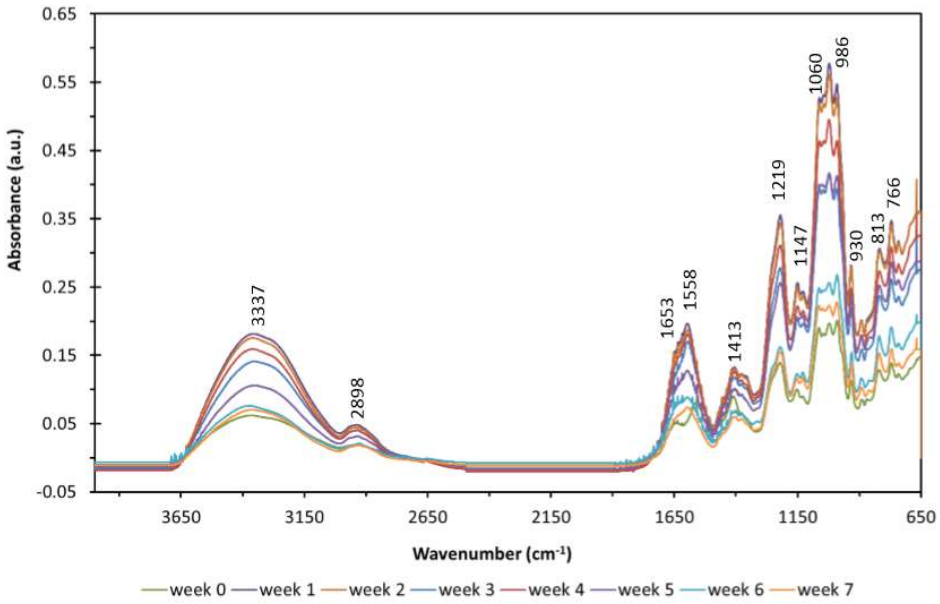

Figure 24: ATR-FTIR spectra of funori films undergone hydrothermal ageing monitored weekly.

Nanocomposite films exposed at the same ageing conditions shown the same behaviour. The only difference could be detected in ATR-FTIR spectra. The main characteristic peaks of $CaCO_3$ at 871 cm^{-1} could be seen just after one week, confirming the complete carbonation of calcium hydroxide and the formation of an alkaline buffer.

About films exposed to a combined acid and hydrothermal ageing, DSC analysis on funori films provides the same results already described for samples aged in not acidic environment. No endothermic peaks are present, suggesting the presence of bound water only. The thermograms in figure 25 show the peak's shift to the lower temperature in the temperature range of 200°C to 380°C. The peak disappears after 3 weeks of ageing. This behaviour suggests that funori films were severely degraded in that acid conditions: A very acidic environment acts in polysaccharides as a catalyst to speed up degradation process via acid-catalyzed hydrolysis. However, at least within three weeks of ageing, the funori capability to bind water seems to be not influenced. ATR-FTIR spectra confirm that degradation (figure 26).

Characteristic funori bands positioned in the range between 1219 cm^{-1} and 766 cm^{-1} show some changes through the exposure time. As expected, the absorption band at 1653 cm^{-1} and 1558 cm^{-1} shift and merge into a single peak due to the denaturation of protein. About nanocomposite films, the behaviour is the same just described regarding funori films. The characteristic $CaCO_3$ peak at 871 cm^{-1} disappears after one week of ageing (figure 26). The meaning is that the amount of $Ca(OH)_2$ was not enough to act as an alkaline buffer for the neutralization of acidity and so to completely inhibit the degradation.

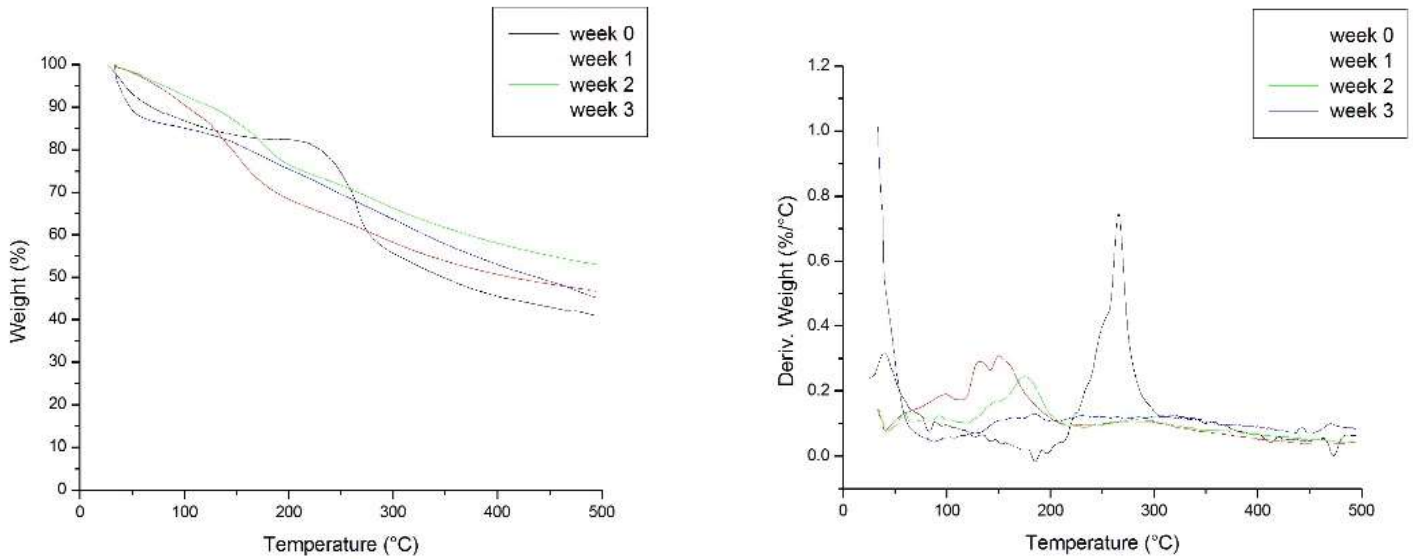

Figure 25: thermogram of funori films undergone acidified- hydrothermal ageing monitored weekly.

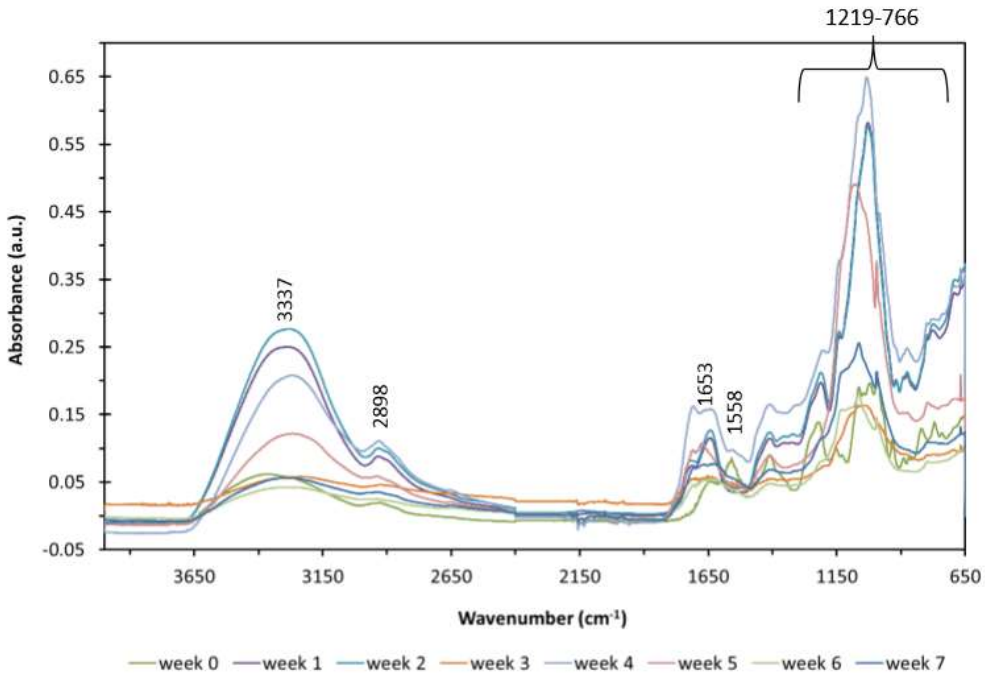

Figure 26: ATR-FTIR spectra of funori films undergone acidified-hydrothermal ageing monitored weekly

CHAPTER 3

Structure of flax fibres

Cellulose is the main component of all natural fibres obtained from plants. The major or minor presence of other substances allow to distinguished from cotton, made by almost pure cellulose, and linen or hemp, where the presence of lignin, pectin and hemicellulose is relevant.

Considering flax fibres, they are obtained from the stems of *Linum usitatissimum*, an 80 cm high plant. Flax elementary fibres are multinucleate cells without septum or partition, long between 2 and 5 cm and thick between 10 and 25 µm, with a polyhedron section, useful to improve the packing in the technical fibre. Indeed, they are arranged in bundles of 10 to 40, disposed all along the stem and along the periphery of a stem cross-section[31], forming the phloem system of the plants, surrounding the central void. Cellulose is the major component of flax fibre. According to the variety, it represents between 65% and 75% of the total weight of the dry mass[32]. Apart from cellulose there are other polymers often designated as "encrusting components". These non cellulosic polymers (NCPs) contain hemicelluloses and pectins. Depending on the variety and the extraction method, NCPs constitute from 5 to 15% of the dry mass of flax fibres[33].The main of them has been clearly identified in long chains of β1-4-D-galactan[34], which account for 3% to 7% of the mass. Its chain has a DP varying from 8 to 30 and are linked to O-4 of 2-linked rhamnogalacturonan as side chains. Together with the last one and polygalacturonic acid, β1-4-D-galactan represents the most abundant NCPs, confirming the pectic nature of the main NCPs composing flax fibres[35]. On the other hand, glucommannan,

[31] Tensile deformation of flax fibres, K. Charlet, S.Eve, J.P. Jernot, M.Gomina, J.Breard, 2009, Procedia Engineering 1.
[32] Influence of drying on the mechanical behaviour of flax fibres and their unidirectional composites, C. Baley, A.Le Duigou et al., 2012, Elsevier.
[33] Ibidem.
[34] Building flax fibres: more than one brick in the walls, C.Morvan et al., Plant Physiology and Biochemistry 41, 2003.
[35] Ibidem.

xyloglucan and xylan represent hemicellulosic polysaccharides components. Glucomannans are the principal hemicelluloses and is composed by alternating blocks of β-1,4 glucan and β-1,4 mannan.

About the presence of lignin, literature is contradictory. There are different positions about its amount, its location and its molecular composition. According to most authors lignin present in cell fibres is mainly composed by guaiacyl units, while in the xylem cells occurs the mixed guaiacyl-syringil lignin type. According to this position, lignin content may vary between 0.9 and 5%[36].

Glicine-rich proteins (GRPs) constitute about 0.1-0.4% of the mass fibre. The high flexibility attributed in literature to GRPs, makes them good to play a role at the interface between plasmalemma and cell wall, in conjunction with other proteins and macromolecules[37]. Arabinogalactan-proteins (AGPs) account for less than 0.1% of the fibre mass.

Going through the microstructure of single flax fibres it is possible recognized a concentric structure made up of composite layers reinforced by cellulose fibrils[38]. During its growth, each fibre, that is the elementary cell of the plant, develops two main layers named primary and secondary cell walls. The primary cell wall constitutes the outer layer (0.1-0.5 μm thick) and is flexible enough to allow wall expansion during the plant growth. It contains a large amount of pectins, hemicelluloses and crosslinked lignins. As just said above, the most common pectins in flax fibres are homogalacturonanes (HGA) and rhamnogalacturonanes (RG-I). HGA is an α-1,4 homopolymer of D-galacturonic acid. RG-I has a backbone composed by alternated galacturonic acid and L-rhamnose (α-1,2 linked) on which long side chain of β-a,4 galactans are branched[39]. At this level their function is to ensure cohesion

[36] Ibidem.

[37] Building flax fibres: more than one brick in the walls, C.Morvan et al., Plant Physiology and Biochemistry 41, 2003.

[38] Influence of drying on the mechanical behaviour of flax fibres and their unidirectional composites, C. Baley, A.Le Duigou et al., 2012, Elsevier.

[39] Pectinase treatments on technical fibres of flax: effects on water sorption and mechanical properties, S.Alix et al., Carbohydrated Polymers 87, 2012.

between cells[40]. During the differentiation phase, these molecules accumulate in the external zones of fibre cell such as in the primary wall and in cell junctions. However, they are present also in the secondary cell wall. Also in this case they have an adhesive function but between cellulose fibrils. The secondary wall consists of ca. 70% of cellulose micro fibrils embedded in a pectins-hemicellulose-lignin matrix and represents 80% of the fibre cross-section, measuring from 6 to 13 µm[41]. In this layer, microfibrils have a helical arrangement[42], making an angle of about 10°C with the longitudinal axes of the fibre[43]. This spiral and highly oriented structure makes the secondary wall able to influence largely the mechanical behaviour of the fibre and essentially provides its high tensile strength. Flax fibre can be easily sketched as a complex composite multilayer structure, in which micro fibrils of cellulose work as reinforcement material, whereas pectin and hemicelluloses compose the polymeric matrix[44]. According to C. Baley, the hemicellulose, thanks to its branched structure, not only acts as a matrix but also as a coupling agent. Bonded to cellulose by hydrogen bonding, they acts as cross-linking molecules, forming a network between cellulose microfibrils which is considered the main structural component of the fibre cell[45]. Lignins, complex cross-linked phenolic polymers, increase even more the strength of that network,

An interesting model (fig.27) describing interconnections between the polymers in the secondary wall of flax fibres has been proposed by C. Morvan et al. (Moravan, 2003). According to this model cellulose microfibrils are tethered each other by cross-linking polymers and embedded in NC matrix. Part of glucans and glucomannans seems to be tightly bound to fibre walls and the authors suggests it plays a role as a cross-linking polymer in

---

[40] [40] Influence of drying on the mechanical behaviour of flax fibres and their unidirectional composites, C. Baley, A.Le Duigou et al., 2012, Elsevier.

[41] Ibidem.

[42] The fine structure of fibers and crystalline polymers. Interpretation of the mechanical properties of fibres, J.W.S. Hearle, Journal of applied polymer science vol.7, 1963.

[43] Influence of an Agatha flax fibre location in a stem on its mechanical, chemical and morphological properties, K.Charlet, J.P. Jernot et al., 2009, Composite Science and Technology.

[44] Ibidem.

[45] Effects of environmental conditions on mechanical and physical properties of flax fibres, A. Stamboulis et al.,2001, Composites: part A 32.

secondary wall. GRPs, on the other hand, may form an independent network, becoming cross-linked through ester linkages between glutamic acids and cellulose. According to the model, also the association between AGPs and pectins occurs through ester linkage between acidic amino acids and β-1-4-galactan or uronic acids of the pectic backbone and arabinogalactans II. However, authors suggest that AGPs are not directly associated to cellulose chains but this linkage is allowed thanks to cross-linking glucans or (galacto) glucomannan. Also binding of pectins with glucans and/or glucomannans through phenolic compounds is hypothesised by the authors.

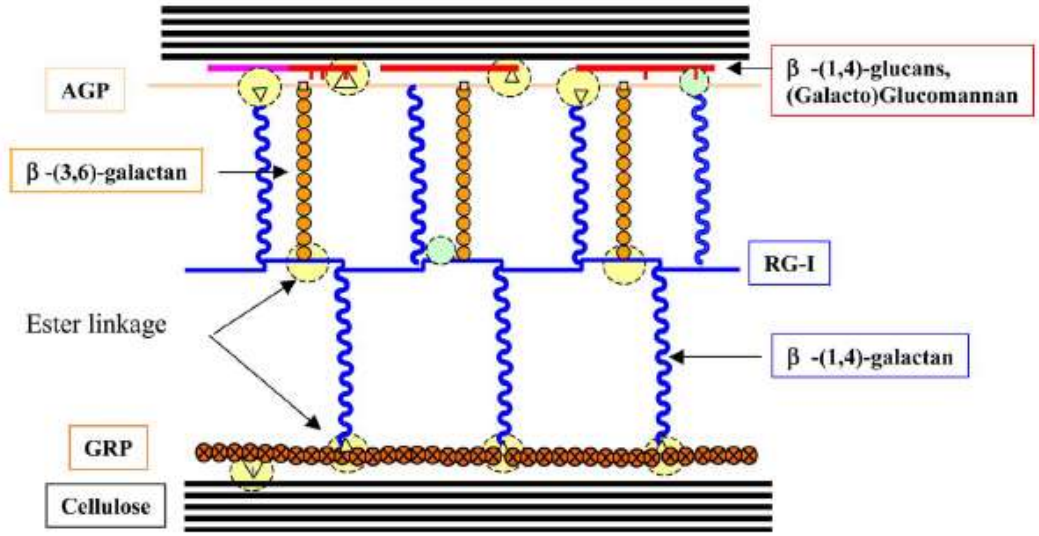

Fig. 3. Schematic representation of possible interactions between polymers within the secondary wall of flax fibres. Glucans ( ) and (galacto)glucomanan ( ) are hydrogen-bound to cellulose. GRPs ( ) rich in glutamic acid ( ) could directly bind to cellulose, via ester linkages ( ). Both GRPs and hemicellulosic glucans, might be the polymers coating cellulose microfibrils. β(1-4)-D-galactan chains ( ) linked to RG-I ( ) could be associated with AGPs ( ), GRPs and/or glucans. Pectins may also interact with type II galactan ( ) side chains of AGPs. Cross-linking might occur again via ester linkages, due to the presence of uronic acids of pectins as well as acidic amino acids of proteins, or involve phenolics via phenyl–phenyl or phenyl–ether linkages ( ). See text for detailed description.

Figure 27: model of interconnections between the polymers in secondary cell wall of flax fibres proposed by C.Morvan et al. (Morvan, 2003).

The described structure well explain the tensile strength and stiffness of flax fibres, reported being 1500 MPa and 90 GPa respectively. Only comparing these values with the ones of E-glass fibres (tensile strength 2500 MPa and stiffness 72 GPa) it's possible to understand why flax fibres are considered

promising candidates for the reinforcements of polymer matrix composites instead of synthetic E-glass fibres[46].

The strength of flax has been well explained also by taking in consideration the theory of composite material. Indeed, even though cellulose is the strongest component of flax, non-cellulosic polymers have an important role in the mechanic distribution of forces, allowing the strength of the cellulose to be effectively utilised[47]. A composite is stronger than the fibrous component alone if occur some conditions. The matrix have to be weaker than the fibres, to be able to deflect cracks into a longitudinal direction, but at the same time it have to be strong enough to transmit stresses from one fibre to the next. According to the theory, the longer and thinner the fibres, the more is the available surface to transmit the stresses and the weaker the non-cellulosic polymer matrix can afford to be, unless fibres sliding apart. The length/diameter ratio in flax fibre cells is high and it is still higher in the nano scale, regarding cellulose microfibrils present in secondary walls. In the micro scale, the corresponding role in connecting together the secondary cell-walls in flax is played by the middle lamella and the primary cell wall, both weaker than the secondary cell wall because of the lack of longitudinally oriented microfibrils.

However, the natural origin of flax fibre results in the spread of its properties. It has been shown that mechanical properties are affected both by the variety and the location of the fibres along the stem. K. Charlet[48] demonstrated that fibres obtained from the middle region of the plant stem present the higher values of Young's modulus and failure stress then the fibres issued from the upper and lower regions. This result can be explained taking in consideration the growth process of the plant. The growing cycle lasts only 100 days between sowing in March and harvesting in July. In this time frame, the only fibres that are able to complete their development are those taken from the middle of the stem. On the contrary, fibres from the top interrupt their differentiation process when the maturation of the seed begins. Likewise, the ones from the bottom are unable to develop

[46] Tensile deformation of flax fibre, K. Charlet, S.Eve, J.P.jernot, M.Gomina, J.Brerard, 2009, Procedia Engineering 1.

[47] Galactans and cellulose in flax fibres: potative contributions to the tensile strenght, R. Girault et al., International Journal of Biological Macromolecules 21, 1997.

[48] Cfr. 40.

completely the secondary wall owing to low temperature condition and lack of daylight. It results in a secondary wall thicker than the one of fibres from the middle stem[49].

Another element that can affect mechanical resistance and contribute to the scattering of strength values is the inevitable presence of defects. They are created during the growth of the plant but also during the extraction processes, and are randomly displaced along the stem[50]. The current methods of extraction of flax fibres from the plant consist in retting them, in order to free the bundles from the surrounding cortical cells. Then bundles are scotched to separate fibres from the woody central cylinder. The fibres obtained are then hackled, to remove definitely any other non-fibrous material, degummed and finally bleached. Only after all these processes, fibres are ready to be spun into yarns. Unfortunately during this processing cycle just describe, fibres loss part of their mechanical resistance. An inevitable consequence, considering the nature of the treatments they have to be undergone. Retting and other chemical treatments cause an uncontrolled solubilisation of fibres and microfibrils matrix, able to reduce the breaking strength of dry fibres from 5.0 to 1.4 N mm^2. On the other hand, scotching, hackling, combing and spinning cause folds and cracks in the fibres, which have to be added to the ones just naturally present on the surface of flax fibres. The result is the shattering of the matrix that, as just said above, plays an essential role in the correct distribution of forces along the fibre. Being no more fixed in the cross-linked structure, fibre cells can slide apart, determining less resistance to mechanical stresses. “Kink band” (fig. 28) is a term used to describe the peculiar morphology assumed by the surface of flax fibre cell when occurred a structural failure: the primary cell wall buckles outwards along all the diameter in response to a damage occurs in the secondary cell wall. This type of damage is so peculiar in flax fibre that it is often reported as a sign for the microscopic identification of linen, together with the flute morphology of the fibre tails.

[49] Ibidem.

[50] Scattering of morphological and mechanical properties of flax fibres, K. Charlet et al., 2010, Industrial Crops and Products.

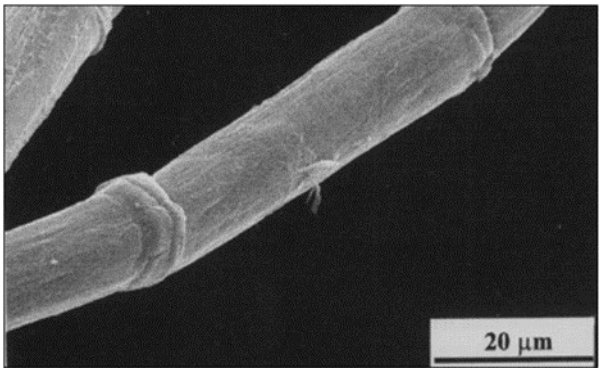

Figure 28: kink band on a flax fibre cell.

Tensile behaviour of flax fibers

The comprehension of the micro and nano structure of the fibre cell is essential to understand the tensile behaviour of flax yarns. The complex composite multilayers structure and the high orientation of cellulose microfibrils compared to the fibre axis in the second wall cell, strongly affect the mechanical response of fibre cells and consequently of spun yarns.

The known mechanism of the yarn longitudinal deformation during a tensile test can be described as follows[51]:

A. Firstly non-linear load- extension response due to a combination of low decrimping and yarn extension;

B. A linear elastic region, reached as the tension increases. The reason is the predominate of the yarn extension when decrimping is complete. In this second region a direct yarn straightening is recorded;

The stiffness increasing with strain is related with two factors involving the nano scale: firstly, the reorientation of cellulose fibrils and reduction in the microfibril angle during tensile test[52]; secondly, the crystallization of the amorphous part of the micro- fibrils[53] induced by the strain;

Some studies[54] suggested that the sequence of events at the nano-scale could be the following:

A. Increase in length of microfibrils and non-crystalline regions (NCPs matrix);
B. Once exceeded a certain value of shear stress, the breaks of hydrogen bonds and slippage of the matrix occurs[55], allowing the spiral spring extension by flection and torsion of micro fibrils, initially

[51] S. Fontaine, "Fabric thickness dynamic measurement during a classical uniaxial tensile test".
[52] Influence of drying on the mechanical behaviour of flax fibres and their unidirectional composites, C. Baley, Composites: Part A 43, 2012, pp. 1229.
[53] "The tensile deformation of flax fibre sas studied by X-ray scattering".
[54] Influence of drying on the mechanical behaviour of flax fibres and their unidirectional composites, C.Baley, A. Le Duigou et al., Composites Part A 43, 2012, pp. 1226-1233.
[55] Elementary flax fibre tensile properties: correlation between stress-strain behaviour and fibre composition, A. Lefeuvre et al., Industrial Crops and Products 52, 2014, pp. 762-769.

making an angle of about 10° with the fibre axis, until reaching a partial alignment with the fibre axis. This process is accompanied by a reduction in volume of fibre cells. Such a reorganizations implies an elasto-visco-plastic deformation;

C. Removing of shear stress induces the formation of new hydrogen bonds which lock microfibrils into the new position. This mechanism is called "stick- slip" is the result of the conformation of xyloglucanes and galactanes linked to cellulose microfibrils and their capacity to entangle and disentangle with the pectin matrix. The rearrangement of the network allows the loads to be transferred from NCPs matrix to cellulose microfibrils[56];
D. Then, considering the polymer scale, some authors suggest that the fibre stiffening could be the effect of a partial crystallization of the amorphous regions of cellulose chains as an effect of the exceeding of a certain value of strain[57], that in this phase affect specially microfibrils;

Take in consideration the micro scale, the scale of the fibre cell, all the mechanisms just described above result in a typical tensile behaviour like the one showed in figure 29. Relating the cell-wall composition with the analysis of stress- strain behaviour it is possible to better understand the tensile trend of the curve: the alignment of cellulose microfibrils, described above is led to the rearrangements in the surrounding amorphous matrix (mainly made of pectins and hemicelluloses), implying an elasto-visco-plastic deformation that explain the initial non-linear trend of the curve[58]. The second linear region correspond to the elastic response of the aligned microfibrils[59] and corresponds with a Hookean behaviour. Young's Modulus of fibre is determined taking in consideration the slope of this linear part of

[56] Influence of drying on the mechanical behaviour of flax fibres and their unidirectional composites, C. Baley et al., Composites: Part A 43, 2012, pp. 1230.
[57] Elementary flax fibre tensile properties: correlation between stress-strain behaviour and fibre composition, A. Lefeuvre et al., Industrial Crops and Products 52, 2014, pp. 762-769.
[58] Flax fibre and its composites- A review, Libo Yan, Nawawi Chouw, Krishnan Jayaraman, Composites Part B 56, 2014, 296-317.
[59] Effect of chemical treatments on water sorption and mechanical properties of flax fibres, S.Alix, E.Philippe et al., Bioresource Tecnology 100, 2009.

the stress-strain curve. Deformation is entirely elastic until fracture and no plastic region occurred again.

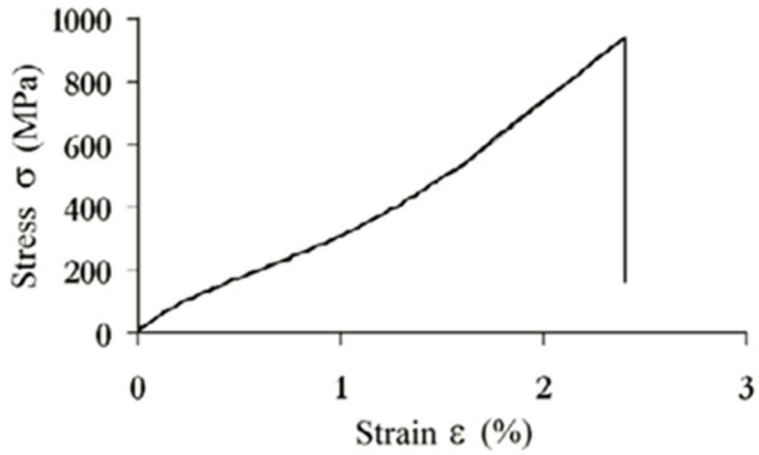

Figure 29: example of a stress-strain curve of an elementary flax fibre[60]

Once reached the failure threshold, rupture firstly involved the primary cell wall, which breaks in a brittle manner. Then the separation between primary and secondary cell walls occurs. Fibrils composing secondary cell wall extended themselves in an elastic manner, until to the completion of failure. The breakage of secondary wall reflect its fibrillar nature. ESEM observation reveals that in this case a coarse crack occurs[61].

As just said above, in recent years the use of flax fibres to reinforce composites is expanding. These fibres are able to provide significant reinforcement due to their excellent mechanical properties, reducing at the same time environmental impact if compared to glass fibres, which traditionally represented the most used reinforcing materials in the composite industries. Together with their low, easy availability and the lower healthy and safety problems involved by flax fibres during handling of fibre products, these fibres have been accepted in engineering markets like the automotive and construction industry[62]. As a consequence, flax fibres

[60] Flax fibre and its composites- A review, Libo Yan, Nawawi Chouw, Krishnan Jayaraman, Composites Part B 56, 2014, 296-317.
[61] Ibidem.
[62] Effects of environmental conditions on mechanical and physical properties of flax fibres, A. Stamboulis, C.A. Baillie, T. Peijs, Composites Part A, 2001.

mechanical behaviour has been thoroughly studied in the last decade. The major studies finding in literature have been performed on elementary fibres (Table 4), taking in consideration the fibre cell mechanical behaviour by evaluating parameters like Tensile strength (MPa), Young's Modulus (GPa) and Failure Strain (%).

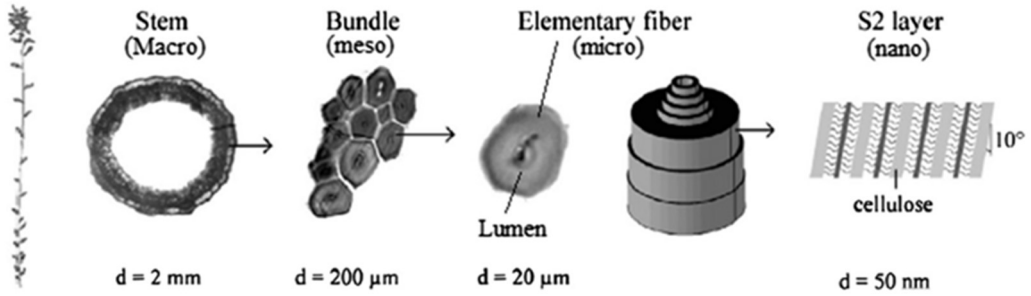

Figure 30: flax structure starting from the stem of Linum Usitatissimum until cellulose chains[63].

AUTHOR	Gauge length (mm)	Fibre diameter (µm)	Tensile strength (MPa)	Young's Modulus (GPa)
C. Baley[64]	10	21.57 (± 0.95) 23.86 (± 0.68)	1499 (± 346) 1317 (±529)	64.10 (±13.65) 51.28 (± 12.02)
K. Charlet et al.[65]	10	21.5 (± 5.3) top stem 21.3 (± 6.3) middle stem 23.5 (± 7.9) bottom stem	753 (± 353) 865 (± 413) 783 (± 347)	51 (± 22) 57 (± 29) 51 (± 26)

[63] Flax fibre and its composites- A review, Libo Yan, Nawawi Chouw, Krishnan Jayaraman, Composites Part B 56, 2014, 296-317.

[64] Influence of drying on the mechanical behaviour of flax fibres and their unidirectional composites, C. Baley et al., Composites: Part A 43, 2012

[65] Influence of an Agatha flax fibre location in a stem on its mechanical, chemical and morphological properties, K.Charlet, J.P. Jernot et al., 2009, Composite Science and Technology.

K. Charlet, C. Baley et al.[66]	10	19 (± 3.5) top stem 19.6 (± 6.7) middle stem 20.1 (± 4.1) bottom stem	1129 (± 390) 1454 (± 835) 755 (± 384)	59.1 (± 17.5) 68.2 (± 35.8) 46.9 (± 15.8)
A. Le Domigou, A Bourmau et al.[67]	10	25	1057 (± 462)	66.9 (± 16.3)

Table 4: average values of mechanical properties of flax elementary fibres as reported by different studies.

Tensile strength, also called stress (σ) is calculated dividing the force applies to the fibre for its section area.

$$\sigma = \frac{F}{A} = \frac{N}{m^2}$$

A is obtained measuring fibre diameter in different points along it by the use of an optical microscope. Starting from the average diameter and from the assumption that flax fibre has a circular section, the area has been calculated.

F is the maximum load applied to the fibre before the failure of the material.

Young's Modulus (E) is a number which expresses an object or substance resistance to being deformed elastically when a force is applied to it. It is expressed as the relation between the stress (σ) and the strain (ε). Hooke's law define this relation.

[66] Characteristics of Hermes flax fibres as a function of their location in the stem and properties of the derived unidirectional composites, K. Charlet, C. Baley, C. Morvan, J.P. Jernot, M. Gomina, J. Breard, Composites Part A 38, 2007.

[67] Improving the interfacial properties between flax fibres and PLLA by a water fibre treatment and drying cycle, A. Le Duoigou, A. Bourmaud, E. Balnois, P. Davies, C. Baley, Industrial crops and products 39, 2012, 31-39.

$$E = \frac{\sigma}{\varepsilon_m}$$

In a continuous body, deformation (ε) is the dimensionless quantity, often expressed in percentage, referred to the length variation resulting from a stress induced by applied forces. It is expressed as the ratio between the length variation and the starting length.

$$\varepsilon_m = \frac{\Delta l}{l}$$

The stress-strain curve, unique for each material, recording the amount of deformation (strain) at distinct intervals of tensile or compressive loading (stress), put in relation these parameters. From the slope of the curve it is possible to calculate the Young's Modulus.

The behavior described above is the one which occurs in standard conditions and coincides with the theoretical one. However, there are two factors which can modify this trend. The presence of mechanical damages on the fibres and the water content. About the first, it has been experimentally demonstrated that there is a correlation between the extent of damage and the Young's Modulus. Damages, as described in the previous paragraph, may accumulate in the fiber during the grow of the plant but also during the mechanical and chemical processes which flax fibres undergone to be separated from the stem. According to G. C. Davies[68], this results in a reduction of the modulus and in the increasing of the probability of failure at a given load. The author measures the extent of the damage by the use of a polarizing microscope: damaged portions of fibres result bright under polarizing light. Authors then plotted the strength of flax and nettle fibers against measured damage. In both cases there is a lower strength threshold that is almost independent from damage and an upper strength threshold that decreases with increasing damage. The explanation is that the probability of a point on the fiber having less than a given strength increases with increasing damage. Thus, maximum strength will tend to decrease with increasing damage. The lower bound of strength is, however, independent

[68] Effect of environmental relative humidityband damage on the tensile properties of flax and nettle fibres, G.C.Davies, D.M.Bruce, Textile Res. J. 68, 1998, pp.623-629.

from the amount of damage, because a fiber can contain a point sufficiently weak to allow failure without appearing extensively damaged. No such effect occurs in the static modulus measurement.

The second factor able to influence the mechanical behaviour of flax is the water content. At room temperature flax fibres contain from 6% to 10% of water by weight of fibres[69]. The high quantity of hydroxyl groups proper of pectin molecules determine the high polarity of flax fibre and, as a consequence, its highly hydrophilic nature. Water molecules are displaced both on the surface and within the fibres, inside the polymeric matrix which embeds cellulose microfibrils, mainly linked to the pectins. Water works as a cell wall plasticizer. Its removal involves an embrittlement of the material, consequent to the impairment of the interactions between microfibrils and pectic matrix, as recently demonstrated by several studies. C. Baley undergone its samples at high temperature drying (150°C for 14h) and verified a significant loss of strength (-44%) and of failure strain (-39%). Also a change in the slope of stress-strain curve was registered and, as a consequence, of Young's Modulus. It was calculated that increasing RH from 30% to 90% the reduction in static and dynamic moduli reaches 35.4% and 19.4% respectively[70]. Treatments involving high temperature couldn't modify the fibre structure (pectins are degraded by temperature above 180°C and cellulose above 230°C) but are able to modify the interfaces between the constituents[71], resulting in substantial modification of load distribution mechanisms inside the fibre cell.

Due to its highly hydrophilic nature just described above, water content are able to change constantly to find a balance with the environmental U.R. Indeed fibres are able to pick up moisture in very short time. It has been calculated that the amount rate of absorbed water by weight for an un-dried fibre is around 6.5% in 2 min[72]. This ability has been taken in consideration in planning the mechanical tensile test procedure: every sample has been

[69] Influence of drying on the mechanical behaviour of flax fibres and their unidirectional composites, C. Baley et al., Composites: Part A 43, 2012, pp. 1226.

[70] Flax fibre and its composites- A review, Libo Yan, Nawawi Chouw, Krishnan Jayaraman, Composites Part B 56, 2014, 296-317.

[71] Influence of drying on the mechanical behaviour of flax fibres and their unidirectional composites, C. Baley et al., Composites: Part A 43, 2012 .

[72] Ibidem.

previously conditioned at 50% U.R. for several days, before being tested at the tensile machine. This procedure would ensure a standard starting water content for all the samples and so a major meaningfulness of measured differences in mechanical behaviour.

Tensile behaviour of yarn

Once separated from the stem, flax fibres need to undergone drawing and spinning processes to become a yarn. Indeed, as just said above, fibres cells are long between 2 and 5 cm and thick between 10 and 25 µm. To reach dimensions useful to weave a fabric they have to be spun and twisted together producing a continuous yarn usable in textile industry. Only friction put together one fibre to another and no matrix-like material is foreseen. Thus the twisting allows to give to a fibres bundle the cohesion necessary to be applied in textile manufacturing. Twisting is obtained by rotating a bundle of parallel fibres around their axis. In this way external fibres gain an helical trend, forming an angle with the fibre axis. This angle decrease as far as proceeding to the inner yarn. This arrangement give such a cohesion to the bundle that being in vane the sliding between one fibre to another, unless reaching high tensile load.
The twisting of a fibres bundle can be characterized by three elements: twisting direction, twisting angle and number of twists per unit of length. The possible twisting directions have been traditionally described like “S” or “Z”. Considering the letters, the diagonal line which can be associated to the central segment of the symbol corresponds to the spiral incline. As a general rule, cellulosic yarns show a Z- twisting, whereas protein ones are twisted according to the “S” direction, but there are many exceptions (fig.31).

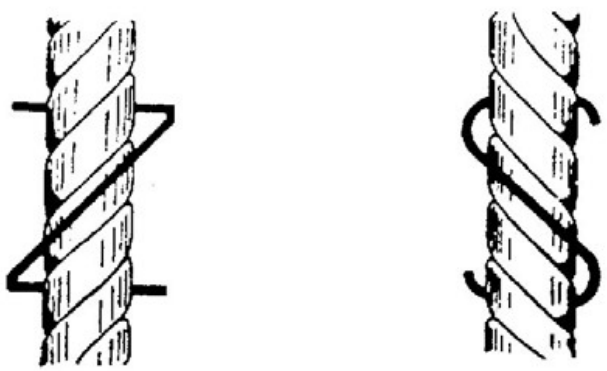

Figure 31: "Z" and "S " twisting directions.

The twisting angle is the one formed by the fibres with the yarn axis. This value involves the amplitude of the spiral and so their number for length unit. Considering short- fibre yarns, there is a relationship of direct proportionality with the number of twists per meter and the tensile strength of the yarn. As much the yarn is twisted as many the cohesion strength between fibres locks them together, hindering the sliding and increasing the strength at the same time.

Starting from that analysis about the yarn morphology, it is possible make some considerations about the tensile behaviour of yarns. Comparing the stress- strain diagram of a single fibre (fig.29) with the one of a flax yarn (fig.32), the trend is similar. Also in this case there is a non-linear part corresponding to an elasto-visco-plastic deformation followed by a linear region corresponding to the elastic response until failure. However, mechanisms involved in the tensile yarn response are different.

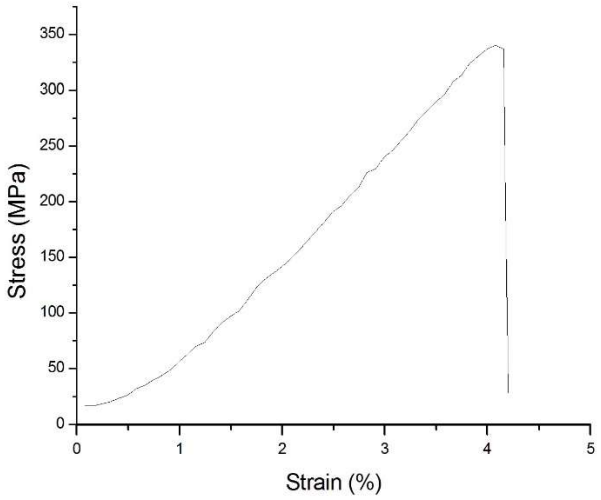

Figure 32: stress-strain curve of a flax yarn.

In the case of tensile test on a single fibre cell, the stress-strain graph (fig.29) essentially reflects the response of cellulose fibrils, before and after the stress-induced alignment of the chains along the fibre axis. The matrix, as described in previous paragraphs, have an essential role in the loading distribution, and the first part of the curve also reflects its tensile response. In the case of yarn behaviour the stress-strain graph of a flax yarn gives a curve which reflects the response of a macro system of several fibre cells, twisted together, which probably will never reach enough alignment with the fibre axis to trigger the mechanical response of the cellulose chains. Thus, in the yarn case, the tensile response is due to other mechanisms. In agreement with this position, tensile tests performed on fibre cell proportionally shows higher values of tensile strength and Young Modulus if compared to the ones resulting from tensile tests on yarns. Taking in consideration the yarn section (fig.33) it is possible obtaining an estimate of the number of fibre cells twisted together to form the yarn. By sketching out the proportion between the theoretical yarn behaviour and the real one, results as follows in table 5.

	Fiber Diameter (mm)	Area (mm^2)	Max load (N)	Tensile strength (MPa)	Young's Modulus (GPa)
Single fiber	0.021	3.46E-04	0.35	1000	57
Theoretical yarn (composed by 272 fibres)	0.346	9.42E-02	94.16	1000	57
Real Yarn (composed by 272 fibres) based on the **equivalent diameter**	0.346	9.42E-02	25.51	271	5.34
Real Yarn (composed by 272 fibres) based on the **apparent diamater**	0.367	1.06E-01	25.51	241	4.75

Table 5: mean values of tensile parameters for a standard flax fibre cell and a standard flax yarn. The values referred to the single fibre correspond to an average from values finding in literature (table 4). The theoretical yarn is a yarn composed by 272 fibres (this number has been calculated starting from section showed in fig. 33) each one with a diameter of 0.021 mm. Data referred to real yarn mechanical behaviour have been obtained from tensile tests performed on a yarn with a diameter similar to the average theoretical diameter.

Figure 33: flax yarn section obtained by embedding the yarn in epoxy resin. The value of 272 fibre composing a yarn, used in the previous table, is calculated starting from this section.

Table 5 shows that the tensile strength experimentally measured, obtained dividing the experimental maximum load with the equivalent theoretical diameter, represents only the 27% of the theoretical yarn strength. The last one has been calculated considering the yarn as a sum of fibres, supposing that the yarn failure mechanism is only related with dynamics internal to the fibres. Instead, the substantial difference observed seems to confirm that another failure mechanism have to be taken in consideration about yarn rupture: the fibre slipping. Testing a yarn with uniaxial tensile test, fibre never reached the tension values reached from the single fibre when it is tested on her own (when forces are applied at the edges of the single cell). Exceeded a certain value, the slipping of one fibre on the others takes place.
Although resulting from different mechanisms, the matching of the trends of the two stress strain curves is evident. This overlapping behaviour is given to the fact that the yarn morphology reproduce in a macro level the structure of the single fibre cell. The twisting of fibres to form the yarn reflects the orientation of cellulose micro fibrils within the secondary cell wall. So the fibre composing the yarn will response to applied loading in a similar manner described for the cellulose chains in the single fibre tensile test. The graph in figure 32 shows an initial non-linear region which corresponds to the

untwisting of the yarn, as the microfibrils in single fibre stress-strain graph. It is followed by a linear region in which fibres compact each other as much as possible in attempt to reach the alignment with the fibre axis, but likely never reaching it due to the hindrance of other fibres. Thus, as just said above, in the case of tensile test on a yarn, failure mechanism foreseen a combination of two factors: fibres breakage and fibres slipping. The first is related to an excessive stress applied to fibre cells, but in this case also the friction between single fibres contribute to it. In such a condition fibre rupture can occurred also if it is not reached the micro fibrils alignment described for the tensile tests on single fibre. About the slipping it is easy to understand that, if fibres cell length is around 2-5 cm, applying tensile stress to a yarn, load is not directly applied to fibre but to the bundle. Cohesion between fibres given from the twisting procedure succeeded to avoid slipping at low tensile stress but increasing the loading this lockage fails and fibres slip inside the bundle, involving the yarn failure.

The major tensile strength of single fiber than the yarn is related with a change in failure mechanism. Clamping the fibre crack run through the stronger cellulosic cell wall of the elementary fibre, whereas yarn failure is less related to the nano-structure response than the one of single cell fibres. The yarn mechanical response couldn't be seen as a simple multiplication of single fibre cells behaviour. Other factors must be taken into consideration. That is to say that tensile behaviour of yarn is mainly related to the macro interactions occurred at the interface between fibre cells. This mechanism must be taken into account in the identification of a yarn consolidants and in the evaluation of its consolidant efficiency. According to these arguments an interface deposition can be functional to increment the tensile resistance of fibres unless necessarily reaching a penetration of molecules into the cell walls.

CHAPTER 4

Tensile tests on single yarn

The most used way to determine the mechanical properties of textile fibres is performing tensile tests. The aim of the measurements was to evaluate the consolidation ability of funori and allyl-n-hydroxy-propyl cellulose, applied alone or together with calcium hydroxide nanoparticles. Testing yarns before and after treatments seems the better way to obtain information about their efficiency, by comparing the strength values (also called stress (σ), calculated dividing the extensional force applied to the fibre for its section area as just described in the previous chapter. σ is expressed in MPa) and the elastic modulus (Young's modulus, also measured in MPa).

Moreover, mecanical properties of treated yarns have been tested also after artificial aging, in order to verify the ability of the consolidant in restoring the mechanical strength of the not aged yarns and also its capability in preserving them from further depolimerization processes, induced by the artificial aging.

Materials and methods

Linen fabric L13/200, weight 145g/m^2, 9x9 yarns/cm, was provided by Zecchi, Florence, Italy.

Funori, sold in form of dry sheets of Gloiopeltis furcata, Gloiopeltis Complanata and Gloiopeltix Tenax, is obtained from AN.T.A.RES srl, San Lazzaro di Savena (BO), Italy.

Allyl n-hydroxy-propyl cellulose has been synthesized by the research group of Prof. Antonella Salvini, Chemistry department, via della Lastruccia 13, 50019 Sesto Fiorentino, Florence, Italy

Calcium hydroxide nanoparticles, synthesized by CSGI, Chemistry department, University of Florence, via della Lastruccia 3, 50019 Sesto Fiorentino, Florence, Italy.

Tensile tests have been performed on yarn specimens under uniaxial loading, using an Instron 5567 testing machine (fig.37) equipped with a 30 kN load cell and precision of 0.1 %, setting the gauge length at 50 mm. Yarn (10 for each category) were tested until rupture with a cross-head speed of 2.5 mm/min at constant temperature (24°C). Young's modulus (E) and stress (σ) have been calculated considering the average diameters of fibres, measured before each tensile test using an optical microscope, taking measures on three different points along ten yarns (five weft and five warp) for each group of samples. All tests were performed after conditioning at U.R. 53% and room temperature for five days, using a saturated solution of $MgNO_3$..

Yarn diameters, used to calculate the mechanical parameters, have been measured on samples before the tensile test by the use of an optical microscope equipped with an EPI 5.5 lens with an enlargement factor of 20X. A digital camera linked with the microscope and Nis- elements microscope imaging software have been used to collect images (Figure 34, left). ImageJ software allowed to take measurements in postproduction on the pictures acquired with this procedure. On each yarn, three pictures have been taken. On every picture, the fibre diameter has been measured in three points. Thus, for each fibre, nine measures have been acquired. The average value between these nine measurements has been considered as the average diameter of the yarn and has been used to calculate the average diameter value of the group of samples, by averaging it with the others nine yarns chosen as representative for the same group.

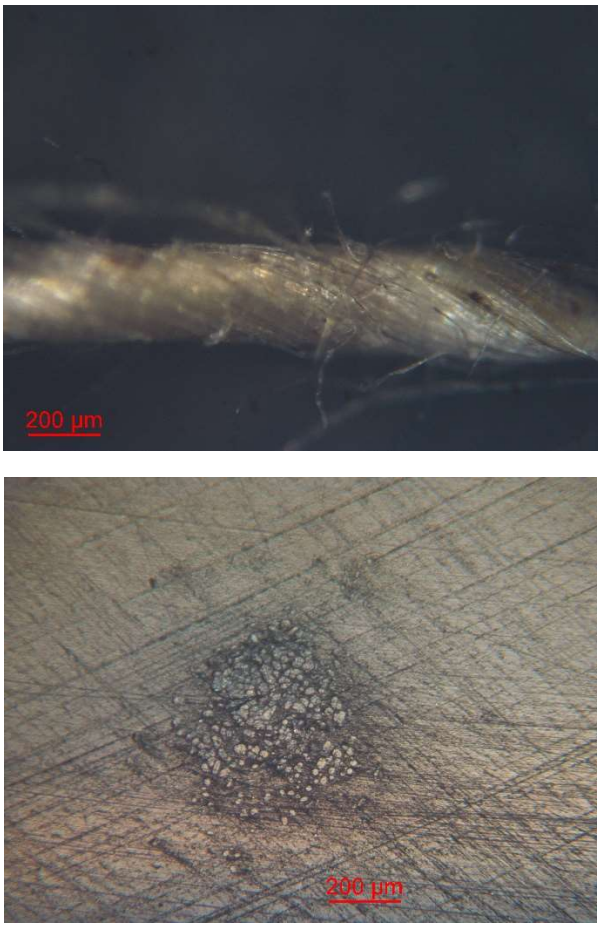

Figure 34: flax yarn image acquired using an optical microscope with a 20x enlargement. (a) free yarn; (b) cross section;

To verify the correspondence of diameters measured in such a way with the real one, some yarns have been embedded in epoxy resin. A cross section has been obtained and pictures captured with the optical microscope (Figure 34, right). The real diameter of the yarn was measured in the same way described above for the yarn samples.

ANOVA (Analysis of variance) test (table 6) was performed to compare diameter of cross section with the one previously acquired on the same yarns with the first method. This test give the possibility to evaluate if there is any evidence suggesting that the means of the populations differ[73]. The

[73] Information point: Tukey multiple comparison test, Nicola Crichton, Blackwell Science Ltd, Journal of Clinical Nursing 8, 1999, pagg. 299-304.

analysis confirmed that there is no statistically relevant differences between diameters measured following the two methods. Indeed, the value of significance was 0.78, higher than 0.05 (this meaning that the null hypothesis could be rejected at 95% confidence level). This evaluation allows to approximate yarn section to a circle and to choose the measuring on free yarn as the diameter evaluation method for the following tensile tests.

Analisi varianza: ad un fattore						
RIEPILOGO						
Gruppi	*Conteggio*	*Somma*	*Media*	*Varianza*		
diameters free yarn	9	3438810	382090	5.89E+09		
diameters cross sections	9	3339936	371104	8E+09		
ANALISI VARIANZA						
Origine della variazione	*SQ*	*gdl*	*MQ*	*F*	*Valore di significatività*	*F crit*
Tra gruppi	5.43E+08	1	5.43E+08	0.07824	0.783280011	4.493998478
In gruppi	1.11E+11	16	6.94E+09			
Totale	1.12E+11	17				

Table 6: ANOVA test to compare diameters acquired on free yarns and on yarn cross sections.

To exclude the hypothesis of slippage of the yarn samples within the clamps, during mechanical tests yarn have been photographed at regular intervals with a Canon EOS 550D placed on a tripod, together with an external calliper placed on the same plane as the tested yarn. To ensure the coupling between the displacement measured by the testing machine and the acquired images, a chronometer (which was started at the same moment as each tensile test) was also photographed in the same picture. Two pencil signs have been drown on the yarn before testing it. Measuring the variation of the segment length between A and B signs at different stages of the test it was possible verifying that no slippage occurred. This evaluation was essential to state the real correspondence between the gauge displacement registered by the tensile machine and the extension of the yarn under

loading. Once stated this correspondence, tensile test have been performed without photogrammetric measurements.

DP measurements have been verified by viscosimetric measurements at 25°C in Bis (ethylenediamine)copper(II) hydroxide solution (CED) according to the rule UNI 8282.
About artificial aging used to prepare samples in order to obtain yarns partially depolymerized on which apply treatments, two procedures have been chosen:

1. The first procedure is characterised by two steps: first samples were soaked in H_2SO_4 aqueous solution (pH=2) for 40 min. Then they were left to dry at room temperature for three days. In the second step samples, placed in a hermetic glass vessel (fig.36), were put in an oven set at 80°C for 300 hours, with a sodium chloride saturated aqueous solution to maintain U.R. value at ca. 75%. This is the procedure applied to IC-series yarns. Every group of samples identified with the prefix IC has been undergone this ageing procedure before the treatments (see Appendix 1);
2. The second ageing procedure is limited only to the first step of the aging procedure described in the point #1, that is to say the soaking in H_2SO_4 aqueous solution (pH=2) for 40 min. In the following paragraphs samples undergone this procedure are also named “acidified” samples and identified with SIN- prefix (see Appendix 1). They constitute the SIN- series.

About the additional aging procedure which half samples have been undergone (+R samples) to test the effects of aging on different treatments applied, it foreseen the same strong hydrothermal conditions described in the second step of point one: samples have been put in an oven set at 80°C for 300 hours, with a sodium chloride saturated aqueous solution to maintain U.R. value at 75%.

Samples preparation

70 mm long test wires have been cut in warp and weft direction from a linen fabric. Each wire tail was reinforced embedding it (< 20 mm) in two cardboard layers by the use of an isocyanate glue, in a sandwich manner (fig. 36a) The thickness of the cardboard allowed better clamping the specimen into the testing machine, thus avoiding its slipping within the clamps. At the same time the cardboard protected the yarn, preventing to be sheared off by the metal clamps (fig.36 b).

Samples were then subdivided into two series: IC-series and SIN-series. The first one undergone the preliminary aging described in the previous page at point one. The second has been aged with the procedure described at point two. Choosing two starting degree of depolimerization (series IC and SIN, corresponding respectively to yarns undergone complete aging procedure[74] and yarns subdued only to acidification) the aim is to simulate two possible substrate's conservation conditions on which the tested consolidants could find different applications, such as a consolidant or as antiaging treatments.

In the following step both series have been grouped eighty by eighty (forty warps and forty wefts for each group) and impregnated by five different treatments:

1. Funori (identified with –F suffix in samples ID) at 1% in demineralized water, prepared according to the extraction procedure worked out in the first step of the research;

2. Allyl n-hydroxy-propyl cellulose (shorten also as Allyl-hpc in the text below and identified with –C suffix in samples ID) dispersed in water at a concentration of 1%, synthesized by the research group of Prof. Antonella Salvini, and then put in an oven set at 60°C for four hours, to start off the cross linking of allyl groups;

3. $Ca(OH)_2$ nanoparticles dispersed in isopropanol (identified with –NP suffix in samples ID) at a concentration of 5g/L;

[74] G. Poggi, R. Giorgi, P. Baglioni et al Calcium hydroxide nanoparticles for the conservation of cultural heritage: new formulations for the deacidifications of cellulose-based artifacts, Applied Physics A 114, 2014.

4. firstly treated with the dispersion of $Ca(OH)_2$ nanoparticles in isopropanol (as described at point 3.) and, once dried, with funori (as described at point 1.). This combined treatment corresponds to –NPF suffix in samples ID;
5. firstly treated with the dispersion of $Ca(OH)_2$ nanoparticles in isopropanol (as described at point 3.) and, once dried, with allyl n-hydroxy-propyl cellulose (as described at point 2.). This combined treatment correspond to –NPC suffix in samples ID;

Forty yarns for each group (20 warps + 20 wefts) have been tested as presented. The remaining 40 yarns of each group have been put in a glass hermetic jar and undergone the additional aging (it corresponds to +R suffix in samples ID) of 300h in an oven set at 80°C, using NaCl saturated solution to keep U.R. at 75%, as described in the previous section. Then, they have been tested after aging. This procedure gave the possibility to compare the consolidant effect of the five different treatments but also to evaluate the mechanical behaviour before and after the aging and so the consolidant ability to protect the yarn from aging.

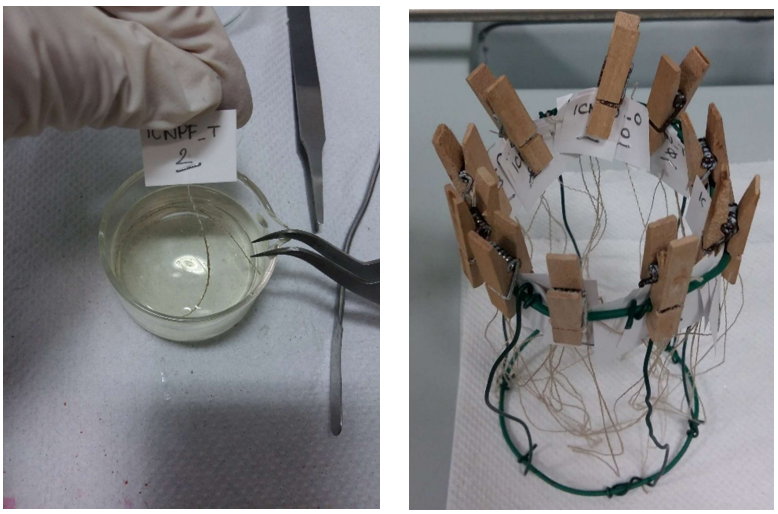

Figure 35: application of the consolidant solutions by soaking (a) and drying of the samples (b).

Funori consolidant has been prepared starting from 100g of dry seaweed as described in the second chapter. The product has been soaked in deionized water at 30°C for 2.5 hours. Then, in order to separate the insoluble fraction, the product has been purified filtering it through a strainer (mesh size 1 mm). A centrifugation with IEC CL31R multispeed centrifuge (Thermo Electron Corporation, USA) at 8000 rpm, 25°C for 5 min was performed to definitely separate insoluble fraction still dispersed in the product. Supernatants and residues were then freeze dried with a Virtis benchtop freeze dryer (SP Scientific, USA) for 48 hours. The dry consolidant obtained was used to prepare a 1% aqueous solution. Yarns have been soaked one by one in the solution by the use of tweezers.
Allyl n-hydroxy-propyl cellulose has been synthesized following the procedure[75] just described in the first chapter. An aqueous solution at 1% of concentration was prepared and yarns have been soaked in in the same way described for funori-trated samples. Treated samples, placed in a glass vessel, were put in an oven set at 60°C for 4 hours, to promote the crosslinking between the allylated cellulose ethers.
$Ca(OH)_2$ nanoparticles dispersion in isopropanol (Nanorestore ®) have been applied at a concentration of 5g/L. Then they have been applied on linen yarns by soaking the yarns in the same way described above for the application of funori and allyl n-hydroxy-propyl cellulose. Samples which have been undergone a combined treatment (ICNPF, ICNPC, SIN_NPF, SIN_NPC), have been treated before with the nanoparticles dispersion and, once dried, with the polymeric solution of funori and allyl n-hydroxy-propyl cellulose according to the series.

By following these procedures, 13 groups of samples (totally 980 specimens) have been prepared:

a) NEW: 20 yarns (10 warps + 10 wefts) from the new linen fabric;

[75] G.Cipriani, A. Salvini, P.Baglioni et al., Cellulose as a Renewable Resource for the Synthesis of Wood Consolidants, 2010.

b) ICN: 80 yarns (40 warps + 40 wefts) from the same fabric as (a) undergone strong acidic pH and hydrothermal conditions to accelerate the degradation of cellulose[76];

c) ICF: 80 yarns (40 warps + 40 wefts) as (b) treated with the Funori consolidant at 1% prepared according to the extraction procedure worked out in the first step of the research;

d) ICC: 80 yarns (40 warps + 40 wefts) as (b) treated with allyl n-hydroxy-propyl cellulose in water at a concentration of 1%, synthesized by the research group of Prof. Antonella Salvini and then put in an oven set at 60°C for four hours, to start off the cross linking of allyl groups ;

e) ICNP: 80 yarns (40 warps + 40 wefts) as (b) treated with a dispersion of CaOH nanoparticles in isopropanol at a concentration of 5g/L;

f) ICNPF: 80 yarns (40 warps + 40 wefts) as (e), additionally treated with Funori consolidant at 1% prepared according to the extraction procedure worked out in the first step of the research ;

g) ICNPC: 80 yarns (40 warps + 40 wefts) as (e), additionally treated with allyl n-hydroxy-propyl cellulose in water at a concentration of 1%, synthesized by the research group of Prof. Antonella Salvini and then put in an oven set at 60°C for four hours, to start off the cross linking of allyl groups;

h) SIN: 80 yarns (40 warps and 40 wefts) undergone strong acidic pH condition to accelerate the degradation of cellulose[4] to reach a degree of depolimerization less extreme then the one reached in case (b), which provide also strong hydrothermal conditions;

[76] G. Poggi, R. Giorgi, P. Baglioni et al Calcium hydroxide nanoparticles for the conservation of cultural heritage: new formulations for the deacidifications of cellulose-based artifacts, Applied Physics A 114, 2014.

i) SINF: 80 yarns (40 warps and 40 wefts) as (h) treated with the Funori consolidant at 1%;

j) SINC: 80 yarns (40 warps and 40 wefts) as (h) treated with allyl n-hydroxy-propyl cellulose in water at a concentration of 1%;

k) SIN_NP: 80 yarns (40 warps and 40 wefts) as (h) treated with a dispersion of CaOH nanoparticles in isopropanol at a concentration of 5g/L;

l) SIN_NPF: 80 yarns (40 warps and 40 wefts) as (k) additionally treated with Funori consolidant at 1%

m) SIN_NPC: 80 yarns (40 warps and 40 wefts) as (k) additionally treated with allyl n-hydroxy-propyl cellulose in water at a concentration of 1%;

All the 980 samples have been conditioned at U.R. 50% and room temperature for five days before performing tensile tests, using a saturated solution of $MgNO_3$.

Figure 36: (a) yarn specimens; (b) specimen positioned into the clamps;

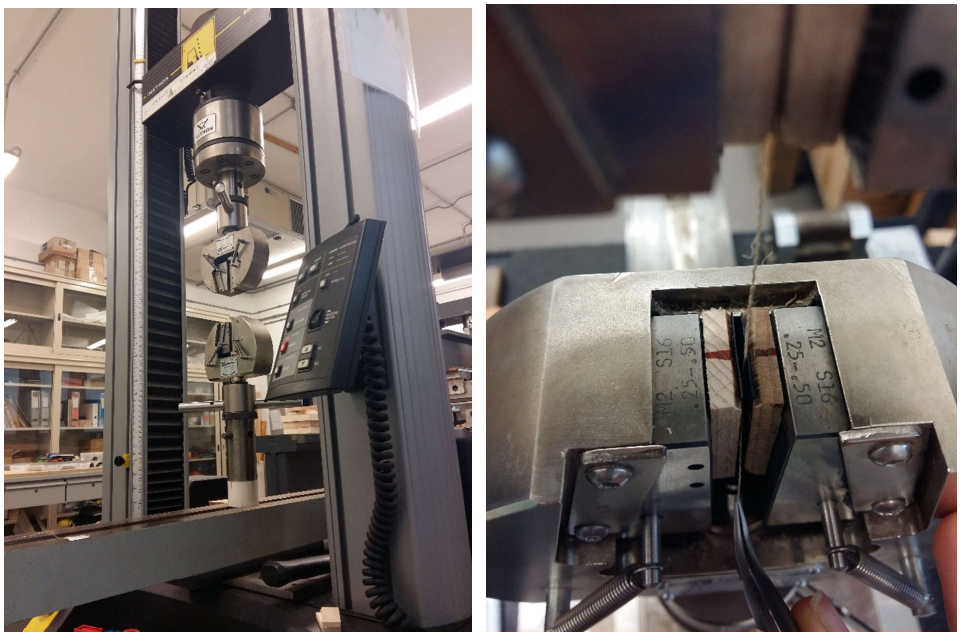

Figure 37: Instron tensile machine used to perform tensile test (a) and a focus on the positioning of the yarn into the clamps (b).

Results and discussion

Before analysing the treated samples, it is worth making some considerations about the observed differences in mechanical properties between the new flax yarns and the aged ones. As expected, tensile properties of flax yarns decreased after the ageing procedures. Measurements of the polymerization degree (DP) before and after ageing confirmed that depolymerisation took place. Starting from a DP initial value of 2727, SIN yarns, only acidified, reached a value of 2160. IC yarns, which undergone the complete hydrothermal aging, showed a DP value of 634 (corresponding to an ageing of 300-400 years[77]).

In the tensile tests this change is clearly noticeable. ANOVA (Analysis of Variance) and Tukey statistical tests confirmed the statistical significance of differences in tensile strength between new yarns (identify as NIN in the

[77] Degradazione di supporti tessili cellulosici di dipinti, A. Seves, G. Testa, C. Bozzi, A. Sardella, in *Dipinti su tela, Metodologie d'indagine per i supporti cellulosici*, A cura di Giovanna C. Scicolone, Nardini editore.

graphs below), yarns undergone only the acidifying treatment (SIN series) and those undergone the complete aging procedure (IC series). Considering also the series that undergone the additional ageing (IC+R and SIN+R groups) the graph shows an asymptotic behaviour as much as the yarns is aged. This trend is compliant with the degradation kinetics of cellulose: there is an initial high speed depolymerisation, followed by a slower one[78].The discontinuity point in literature is fixed at a value of DP = 350[79].

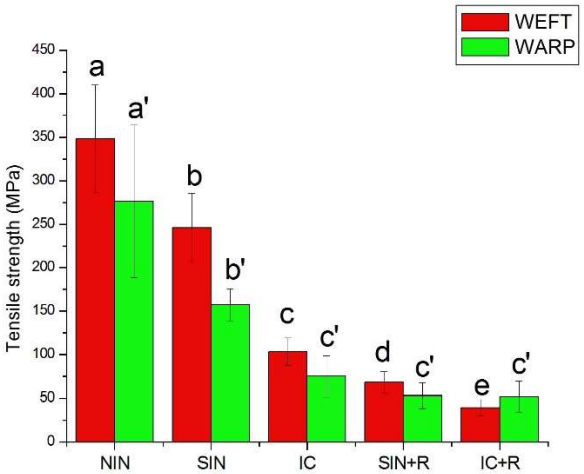

Figure 38: comparison of tensile strength between the five groups of untreated samples (see Appendix 1). Letters on top are referred to the Tukey statistical test: different letters correspond to groups between which there is a statistically significant difference. Conversely, the same letter indicates there isn't a statistically significant difference between the groups of samples.

About data referred to Young's Modulus, SIN series does not show a statistically significant difference if compared with the new yarns. Decrease in Young's Modulus value seems to require more breakages in the polymeric chains.

[78] Ibidem.
[79] Ibidem.

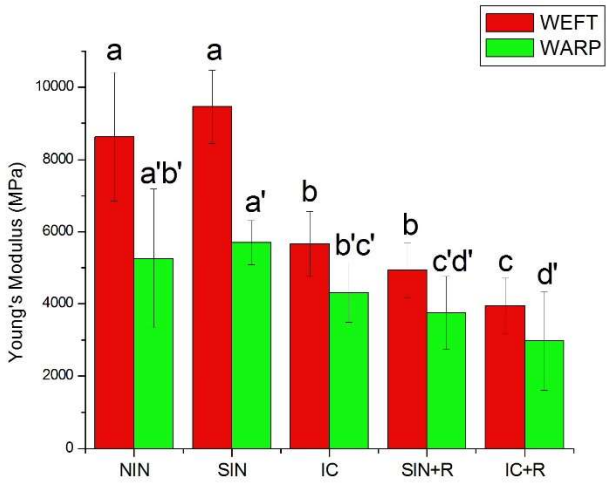

Figure 39: comparison of Young's Modulus values between the five groups of untreated samples (see Appendix 1). Letters on top are referred to the Tukey statistical test: different letters correspond to groups between which there is a statistically significant difference. Conversely, the same letter indicates there isn't a statistically significant difference between the groups of samples.

Another important consideration concerns the tensile behaviour of warps if compared to the wefts one. The general trend underline a worse mechanical behaviour in weft both in term of tensile strength and Young's modulus. The reason of that difference could be related to the different morphology of warps and wefts due to the weaving technique. Indeed, a fabric is composed by two series of yarns. The vertical ones (warp), that are preliminary stretched on the loom and which determine the length of the fabric. The horizontal ones (weft), that is throw from one side to the other side of the loom across the spaces between warp yarns which define the height of the fabric. A mechanism allows to raise warps yarns alternately, in such a way to create a straight "pass" between them in which will run the weft. The sequence of actions characterizing the weaving technique, sketched out in figures 40 and 41, determines the two different evolutions of the weft and warp yarns. Thus, warp yarns are those which wrap up the weft, being more

crimped than the second. Instead, weft yarns have a straight walk. Because of the straight evolution of weft yarns comparing with the crimped warp, the weft mechanical properties are exclusively related with the physical characteristics of the yarn and not also to the weaving technique and the greater stress they are subdued following the preliminary stretching and the constant movement, functional to create the straight “pass” for the weft.

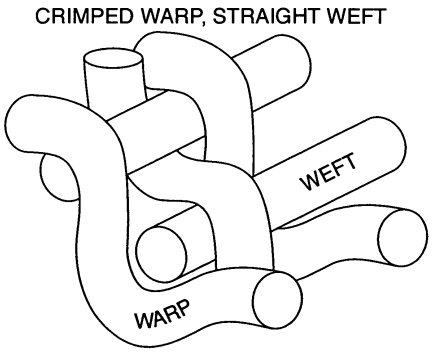

Figure 40: outline of a plane weave. Weft is characterized by a straight evolution whereas warp is crimped.

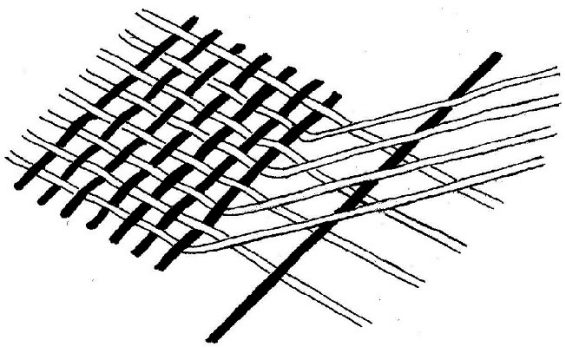

Figure 41: outline of a fabric characterized by plain weave. Warp are the white yarns, weft are the black ones.

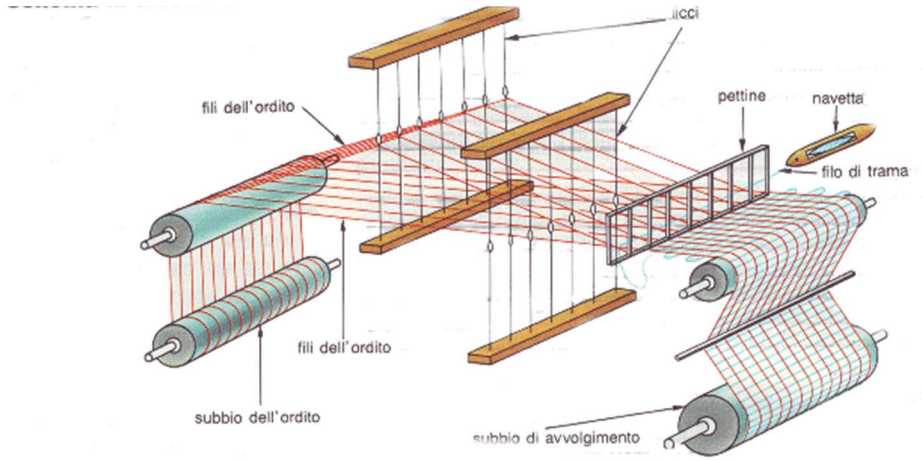

Figure 42: outline of a loom. The warp (vertical) is in red, the weft (horizontal) is in blue.

Tukey's multiple comparison test has been performed on all data obtained in tensile tests, to verify the reliability of the observed differences in mechanical characteristics. By comparing two by two the average values of each group of samples with every one other[80], this test reveals differences at 95% of significance and points out this difference by identifying the two groups with a different letter. Every table (see figures 50-51-53-54-56-57-59-60) has been subdivided in three sections by two thicker dark lines. Results from three different Tukey tests have been reported.

The first one is performed considering only two macro-groups: yarns not subjected to the aging procedure (half of the total samples) and yarns tested after aging (R). Thus, in this case the five considered treatments are not differentiated and instead samples are grouped only basing on their aging after treatment.

The second Tukey test corresponds to the comparison among the different treatments applied, regardless of their exposure to aging.

The third section of Tables compares every single group of samples considering both difference in aging and in treatments. This latter part deserves a separate description of results, which is reported below. This description takes into consideration the various considered series, by discussing firstly the results obtained in weft yarns and then in the warp ones. Moreover, the description was separated between the tensile strength (σ) and the Young's Modulus (E).

Taking in consideration weft yarns, Tukey test performed on data shows:

About tensile strength (fig. 50 and fig. 56), first of all there is a statistically significant difference between IC and IC+R groups (fig.50), It is the same between SIN and SIN+R groups (fig.56). It confirms that the second artificial aging (R), which samples have been undergone, has effectively involved a drop of tensile strength in parallel with the decrease of DP.

ICNPF treatment showed the highest values (fig.50). It increments the tensile strength from 103.2 MPa (IC untreated samples) to 180.2 MPa. Moreover,

[80]*Information point: Tukey multiple comparison test*, Nicola Crichton, Blackwell Science Ltd, Journal of Clinical Nursing, 8, 1999, pag.304.

the combined treatment of $Ca(OH)_2$ and funori has an antiaging function, maintaining unchanged the tensile strength value before and after the artificial aging (ICNPF and ICNPF+R groups are statistically equivalent, and the latter shows a tensile strength value of 167.7).

Treatments using only nanoparticles (ICNP) or funori (ICF) or allyl-n-hydroxypropyl cellulose (ICC), show not meaningful difference between each other (fig.50). They equally increase tensile strength of untreated IC (103.2 MPa) to a value included between 152 and 142.7 MPa.

The least effective treatment is represented by the association of nanoparticles and Allyl-hpc treatment, which leaves unchanged the tensile strength (fig.50). However, all the five treatments have an antiaging effect, maintaining high the strength value also after the artificial aging procedure (R). The worst tensile strength value after aging of treated yarns is 103.9 MPa (ICF+R), the one of untreated IC+R yarns is 39 MPa.

In the case of SIN group (fig.56), only the funori treatment involves an increase statistically significant in yarn tensile strength. This product increases the strength from 245.7 MPa to 321.9 MPa. Nanoparticles and combined treatment of $Ca(OH)_2$ and funori leave unchanged this mechanical property.

Also in this series the least effective treatment is the one of nanoparticles associated with allyl-hpc, and also the allyl-hpc treatment on its own doesn't change the tensile strength of treated yarns. On the other hand, as already observed in IC series, all treatments contribute in keeping unchanged (or little changed) the yarn resistance after aging. Tensile strength after aging of all treated samples is above 201.8 MPa, while the value of untreated SIN+R yarns is around 68.1 MPa.

Taking into consideration results of Tukey test for data referred to wefts Young's Modulus, also in this case there is a statistically relevant difference between unaged and aged (+R) samples, both for IC (fig.53) and SIN series (fig.59). This confirms the deleterious effect of aging also on yarns Young's Modulus.

About IC series (fig.53), the combined treatment of $Ca(OH)_2$ and funori is once again positioned on top, and the average value is the highest also after the aging treatment. As observed for tensile strength, the association of funori and $Ca(OH)_2$ nanoparticles seems to create a system little affected by further aging (ICNPF and ICNPF+R groups are identified with the same letter "a" by the Tukey test). Contrary to what happens for the tensile strength, the treatments with allyl-hpc and funori on their own belong to the same statistical group as for yarns treated with ICNPF, increasing the modulus as well. On the other hand, the test underlines a significant difference in Young's modulus average value between ICNPF treatment (group "a") and ICNP one (group "bcd"). The latter leaves unchanged the modulus of IC yarns as the ICNPC treatment (the common letter "d" means their belonging to the same set of IC untreated yarns). As also observed for tensile strength, also in the case of Young's modulus all the five treatments have an antiaging effect, maintaining the modulus after the artificial aging procedure (R) higher than the IC one. The worst modulus value of treated yarns after aging is 5856 MPa, the one of untreated IC+R yarns is 3944 MPa.

About SIN series (fig.59), funori, nanoparticles and funori+nanoparticles treatments yarns showed the highest average values (the Tukey test evidenced that there is no statistical difference among these groups). However, funori treatment (belonging to group "a" in Tukey test) seems to be the only one that really increases Young's modulus compared to the untreated (SIN) yarns (group "bcd"). In fact, after treatment with funori SIN yarns reaches a modulus of 11776 MPa from the value of 9457 MPa, which characterized SIN untreated yarns.

Also allyl-hpc treatments leave unchanged the Young's modulus, and once again the association between $Ca(OH)_2$ nanoparticles and Allyl-hpc represents the least effective treatment. In this case it even reduces the value of SIN yarns, from 9457 MPa (SIN) to 7860 MPa. On the other hand, the antiaging effect of all the five treatments is also confirmed again. Young's modulus after aging of all treated samples is over 7379 MPa, while the value of untreated SIN+R yarns is around 4931 MPa.

About warp yarns behaviour, Tukey test performed on data shows the following trends.

Tensile strength in IC series (fig. 51) increased by the use of funori and by the treatment with $Ca(OH)_2$ nanoparticles alone (156.6 MPa for ICF and 152.6 MPa for ICNP, compared with 74.7 MPa of IC untreated samples). Instead, nanoparticles used in conjunction with funori and with allyl-hpc belonged to the same group as allyl-hpc alone. However, they also significantly increase tensile strength of IC untreated samples to a value over than 104.6 MPa. In contrast to what observed about weft tensile strength, the series IC and IC+R belonged to the same statistical group, this signifying that their strength cannot be considered statistically different. By the way, also tests on warp confirmed that each treatment can be considered better than leaving untreated the samples (tensile strength after aging of all treated yarns is over 88.1 MPa, while the value of untreated IC+R is 51.9 MPa).

The trend of tensile strength in SIN series (fig.57) confirms what stated for IC series. Funori increases the strength value from 157.3 MPa to 254.1 MPa. $Ca(OH)_2$ nanoparticles dispersion and the combined treatment of funori and nanoparticles equally increase tensile strength of SIN untreated yarns in a statistically significant way. Treatments with allyl-hpc on his own and associated with $Ca(OH)_2$ nanoparticles does not modify the tensile strength of SIN yarns. However, as said for IC, all the treatments protect yarns from aging, maintaining strength values above 152.1 MPa (to be compared with the value of 52.8 MPa for SIN+R untreated samples). Contrary to IC, in the case of SIN series the decrease in warp strength due to the aging treatment is significant (Tukey test assigns SIN samples to the “de” group and SIN+R samples to “f”).

Considering the variation of Young’s Modulus (fig. 54), treatment with funori seems to be the only one able to increase the modulus of IC yarns, reaching a value of 7092 MPa from 4308 MPa. Allyl-hpc, $Ca(OH)_2$ nanoparticles, and both the combined treatments of $Ca(OH)_2$ and funori and of $Ca(OH)_2$ and allyl-hpc do not increase the modulus of IC yarns. Every treatments, unexpectedly except the combined treatment of $Ca(OH)_2$ nanoparticles and funori, protect yarns from aging. Even the worst performance of treated samples of the other remaining four series stands above 4645 MPa, while the modulus of IC+R untreated warp yarns is 2972 MPa.

In SIN series (fig.60), funori and nanoparticles used on their own belong to the same statistical group and positioned at the top. These two treatments are able to increase the warp Young's modulus up to 8231 MPa, starting from a value of 5702 MPa. Allyl-hpc and the two combined treatments (-NPC and –NPF) are not able to increase the modulus, leaving this property unchanged. Also in this case, every treatment works as an antiaging treatments, maintaining values of Young's Modulus above 5920 MPa after the aging (R).

As a general trend, the combined treatment of Funori and nanoparticles (NPF) and the one of Funori on its own (F), give the best results in terms of both tensile strength and Young's Modulus. In Tukey test tables (see figures 50-51-53-54-56-57-59-60), in which groups are presented in a decreasing efficiency order, NPF and F treatments are mainly positioned at the top.

Nanoparticles on their own improve mechanical performances of yarns. This behaviour can be justified supposing the capability of $Ca^{2+}$to create a network between cellulose chains through the formation of secondary interactions. In particular, it has been hypothesized that Ca^{2+} ions have the capability to interact with carboxylate groups of aged cellulose[81]. On the other hand, the neutralization of the acidity by alkaline earth metal hydroxide nanoparticles, which characterizes all the samples because is related both to IC and SIN artificial aging procedures, is well known in literature[82]. Thus, the increase in mechanical resistance in this case can be related both to the capability to create a network between cellulose chains and to provide a stable neutral environment, getting slower the natural degradation mechanisms due to acidic hydrolysis and so preserving the treated yarns from further degradation.

The better mechanical performance of –NPF samples is only partially related with these mechanisms. In this case, it can be hypothesized a synergic consolidant action between Funori and nanoparticles. Literature reports several studies on the capability of Ca^{2+} to create complexes with glucuronic

[81] G. Poggi, R. Giorgi, P. Baglioni et al Calcium hydroxide nanoparticles for the conservation of cultural heritage: new formulations for the deacidifications of cellulose-based artifacts, Applied Physics A 114, 2013.
[82] Ibidem.

acid[83], which is recently found in notable amount in funori extracts, especially in those extracted by cold water[84].Also the presence of sulphated groups could enhance the creation of coordination complexes with Ca^{2+} ions, since SO_4^{2-} is listed between the anionic ligands which could create such complexes. Therefore, the high tensile strength values reached from samples treated with the combination of nanoparticles and funori could hypothetically find an explanation in the capability of Ca^{2+} ions to interact with both funori polysaccharide chains and with cellulose backbone, bridging them together to form a reinforced structure.

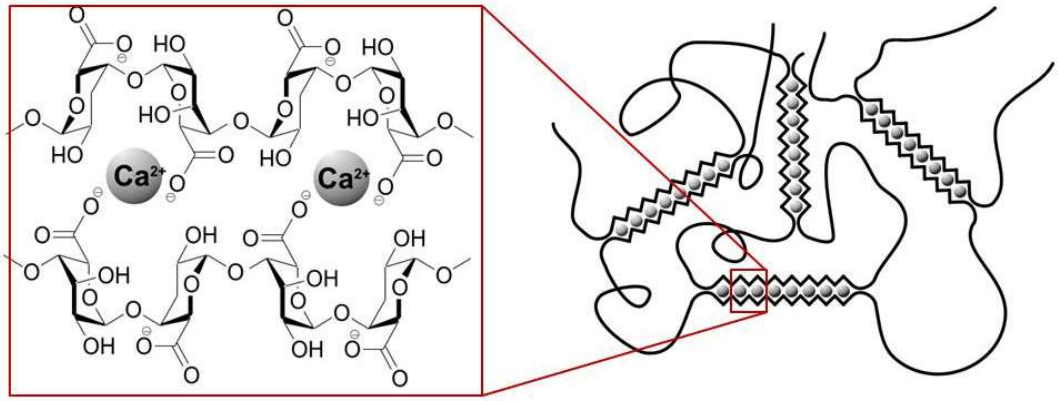

Figure 43: Ca2+ ion complexation by alginate polar functional groups (-OH and -COOH).

This is evident in the IC series, the most depolymerized one. In this case probably, the reinforcement structure described above is crucial to create a strong network between fragmented cellulose backbones.

On the other hand, the higher DPv of SIN series allows obtaining interesting results also with the funori treatment, used on its own. The better condition of the cellulose backbone undergoing only the acidification process, probably

[83] Heidar A., Tajmir R., Sugar complexes with calcium ion: infrared spectra of crystalline D-glucuronic acid and its calcium complexes, Carbohydrate research, 1983, vol.122, pag. 241-248.

[84] Rando Tuvikene et al., Funorans from Gloiopeltis species. Part I. Extraction and structural characteristics, Food Hydrocolloids, 2015, vol.43, pag. 481-432.

requires only the consolidant action related to the formation of a thin funori film on the fibre surface (fig.44) and the possible formation of secondary interactions between cellulose and funori polysaccharide chains, to increase tensile strength and modulus values in a significant manner.

About treatments based on the use of Allyl- n-hydroxy-propyl cellulose, both alone and in combination with calcium hydroxide nanoparticles, they didn't show any noticeable increase in mechanical performances of the yarns on which they have been applied. A possible explanation is related to the difficulties founded in obtaining a homogeneous dispersion of the product in water. The low substitution degree of –OH groups reached from the workup was lower than the one obtained in previous studies[85]. This probably caused limited interaction with water molecules and thus a worse solubility of the product. It necessary implies an irregular distribution of Allyl- n-hydroxy-propyl cellulose as a bulky material, unable to form the hoped interactions.

However, every treatment applied to the sample protects the yarns from the artificial aging R, thus slowing down the effects of acidic hydrolysis even in the strong hydrothermal conditions considered here (as described in the materials and methods paragraphs). As said, even the worst mechanical performance of treated samples tested after aging stands above the values obtained from untreated aged samples. In this case, there are two protection mechanisms that could explain this preservative action. The first concerns only the treatments which provide the use of calcium hydroxide nanoparticles and is related to their capacity of neutralizing the acidic pH of the yarns, slowing down the degradation mechanism due to acidic hydrolysis of cellulose chains. The second is related to the presence of polysaccharides embedding the fibres, which constitute additional material that has to be degraded before reaching the cellulose chains which constitute the yarn. Thus, it can be explained why the compresence of calcium hydroxide nanoparticles and funori gives the best performance after aging, maintaining mostly unchanged tensile strength and Young's Modulus of yarns. As just said in the previews paragraph, the highest molecular weight polysaccarides composing the funori consolidant are able to form a thin film which

[85] *G.Cipriani, A. Salvini, P.Baglioni et al., Cellulose as a Renewable Resource for the Synthesis of Wood Consolidants, 2010.*

embedded the fibre (fig. 44). On the other hand, SEM examination of fibres treated with Allyl- n-hydroxy-propyl cellulose realized in collaboration with the Ecole Superiore du Bois (Nantes) didn't show a comparable surface depositions.

The general worse mechanical performances of warp yarns compared to the weft ones is probably related to their inherent weakness due to the weaving technique, as described at the beginning of this chapter.

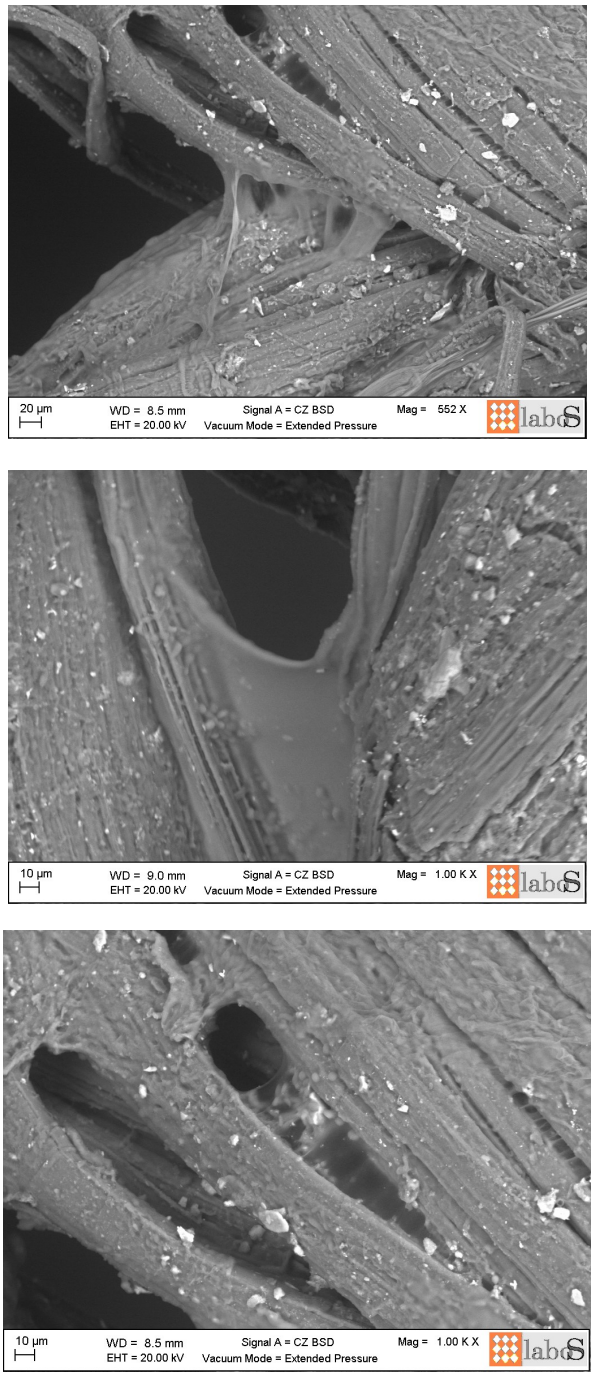

Figure 44: SEM images showing the surface deposition of funori as a thin layer embedding the fibre. SEM images have been acquired in collaboration with the scientific laboratories of Conservation and Restauration Centre of Venaria Reale (TO).

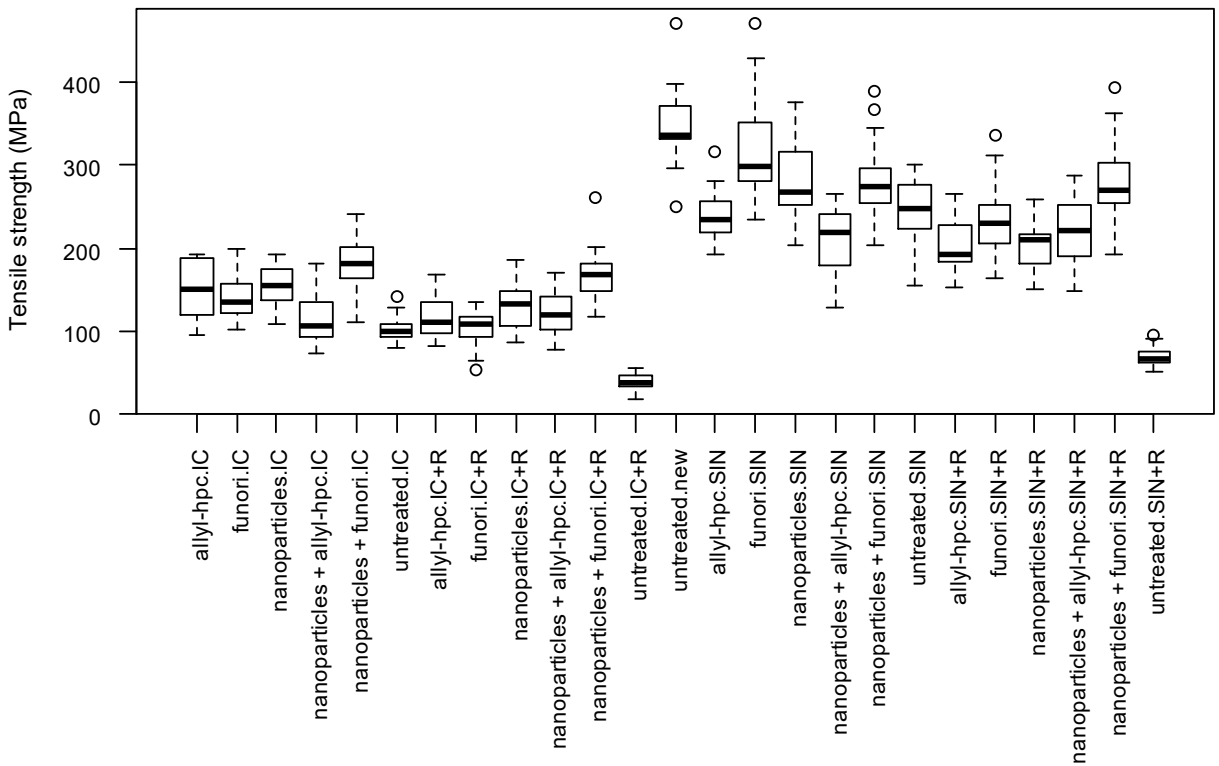

Figure 45: boxplot from weft tensile strength data (see Appendix 1).

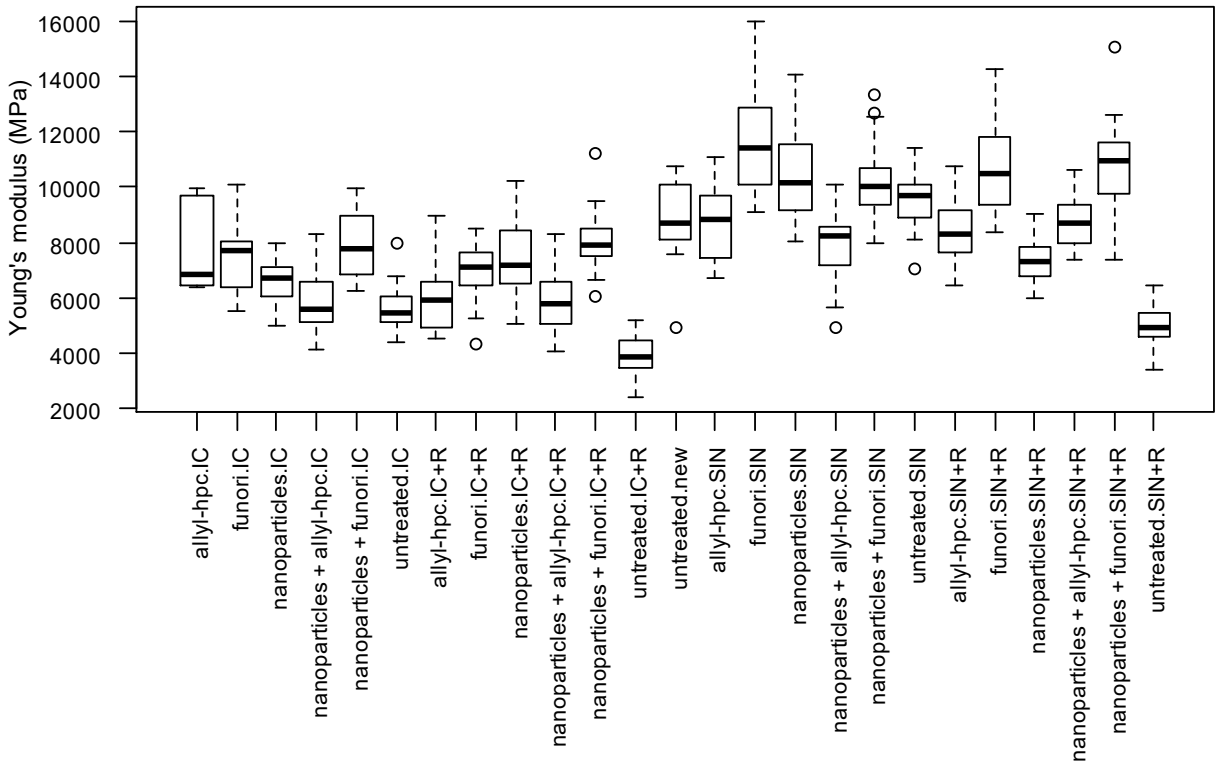

Figure 46: boxplot weft Young's modulus data (see Appendix 1).

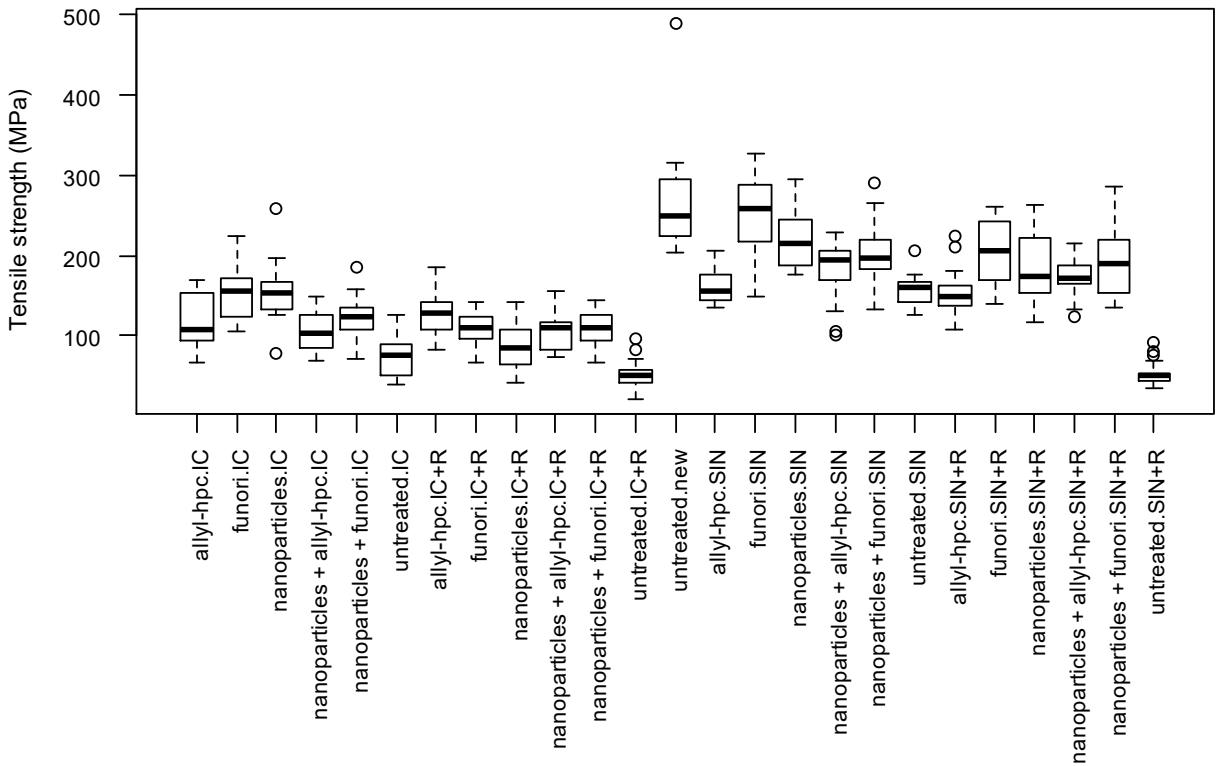

Figure 47: boxplot from warp tensile strength data (see Appendix 1).

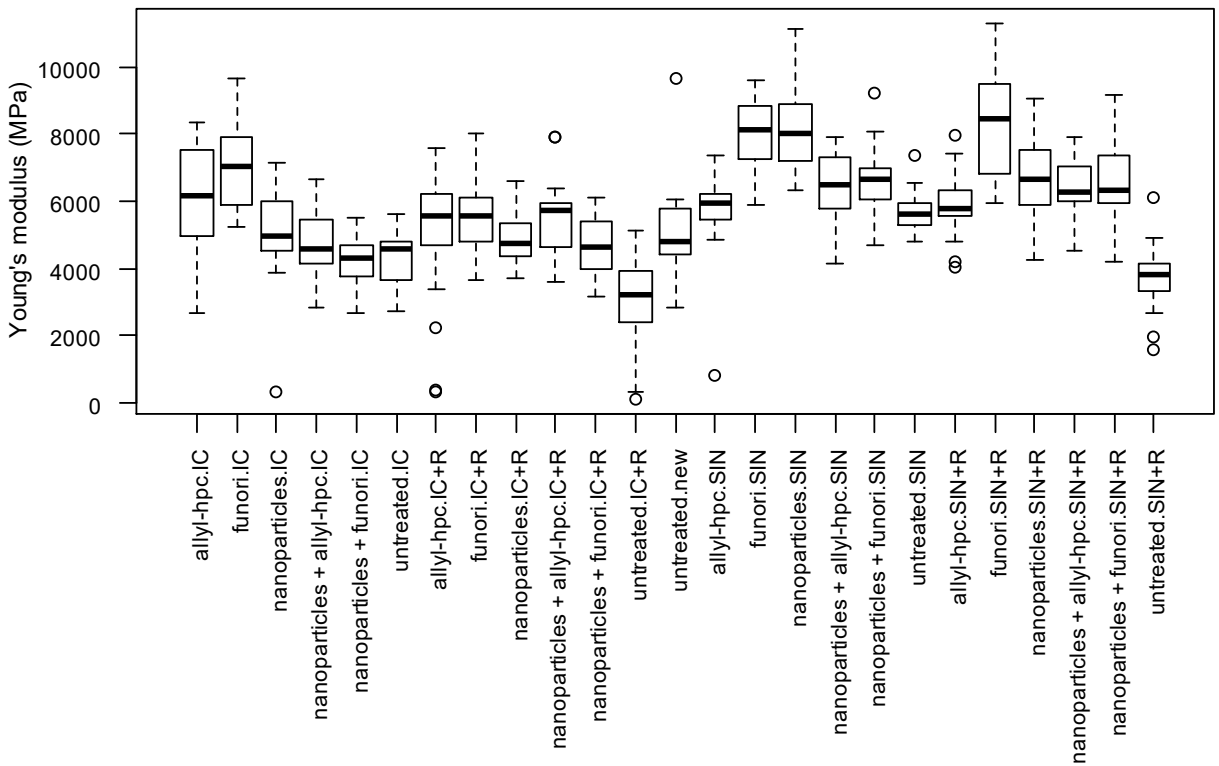

Figure 48: boxplot from warp Young's modulus data (see Appendix 1)

IC series- Tensile Strength

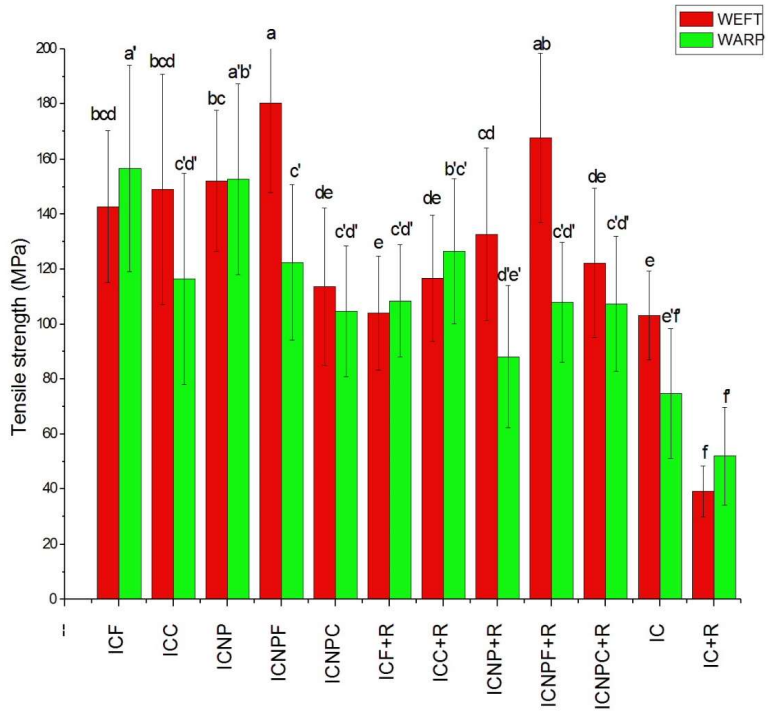

Figure 49: comparative graph between average tensile strength values of different groups of samples belonging to IC series, both warp (in green) and weft (in red) yarns. Letters upon columns correspond to the Tukey ID letter in the tables below.

SAMPLE WEFT	AVERAGE	Tukey ID
IC	139.81	a
IC+R	112	b
Nanoparticles + Funori	173.8	a
Nanoparticles	142.3	b
Funori	123.3	c
Allyl-hpc	123.1	c
Nanoparticles + Allyl-hpc	117.9	c
untreated	65.4	d

ICNPF	180.2	a
ICNPF + R	167.7	ab
ICNP	152	bc
ICC	149	bcd
ICF	142.7	bcd
ICNP + R	132.6	cd
ICNPC + R	122.3	de
ICC + R	116.7	de
ICNPC	113.7	de
ICF + R	103.9	e
IC	103.2	e
IC + R	39	f

Figure 50: data obtained from Tukey test performed on average tensile strengths from weft IC samples. Groups are listed in a decreasing efficiency order.

SAMPLE WARP	AVERAGE	Tukey ID
IC	121.9	a
IC+R	98.8	b
Funori	130.6	a
Allyl-hpc	124.4	ab
Nanoparticles	118.9	ab
Nanoparticles + Funori	115	ab
Nanoparticles + Allyl-hpc	106	b
untreated	62.7	c
ICF	156.6	a
ICNP	152.6	ab
ICC + R	126.6	bc
ICNPF	122.4	c
ICC	116.4	cd
ICF + R	108.4	cd

ICNPF + R	108	cd
ICNPC + R	107.3	cd
ICNPC	104.6	cd
ICNP + R	88.1	de
IC	74.7	ef
IC + R	51.9	f

Figure 51: data obtained from Tukey test performed on average tensile strengths values from warp IC samples. Groups are listed in a decreasing efficiency order.

IC series -Young's Modulus

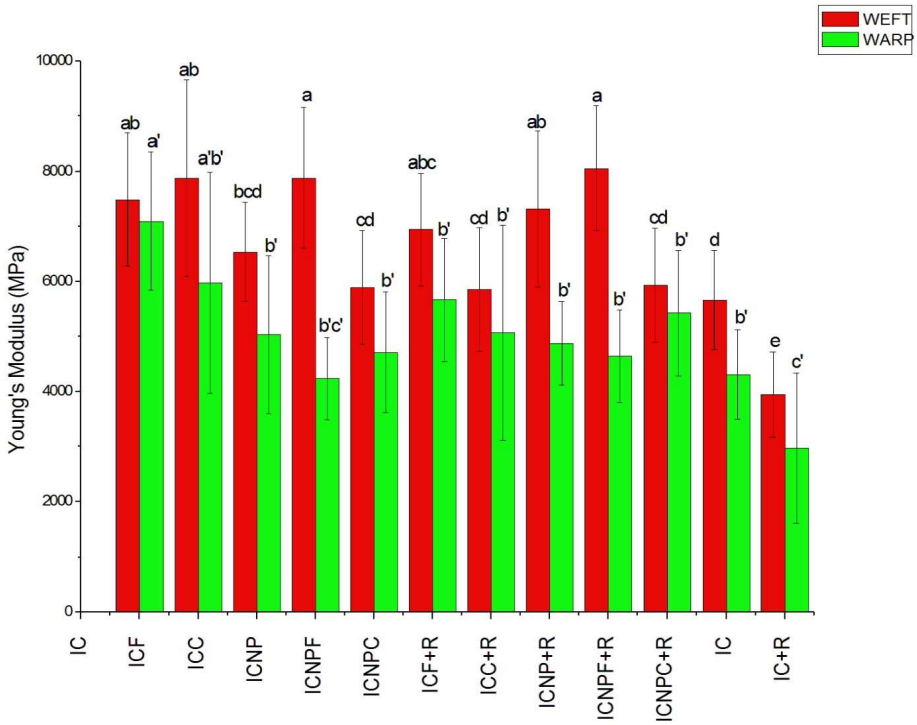

Figure 52: comparative graph between average Young's Modulus values of different groups of samples belonging to IC series, both warp (in green) and weft (in red) yarns. Letters upon columns correspond to the Tukey ID letter in the tables below.

SAMPLE WEFT	AVERAGE	Tukey ID
IC	6776	a
IC+R	6296	b
Nanoparticles + Funori	7970	a
Funori	7217	b
Nanoparticles	6926	bc
Allyl-hpc	6259	cd
Nanoparticles + Allyl-hpc	5911	d

untreated	4648	e
ICNPF + R	8054	a
ICNPF	7881	a
ICC	7874	ab
ICF	7488	ab
ICNP + R	7315	ab
ICF + R	6946	abc
ICNP	6537	bcd
ICNPC + R	5932	cd
ICNPC	5892	cd
ICC + R	5856	cd
IC	5660	d
IC + R	3944	e

Figure 53: data obtained from Tukey test performed on average Young's Modulus values from weft IC samples. Groups are listed in a decreasing efficiency order.

SAMPLE WARP	AVERAGE	Tukey ID
IC	5108	a
IC+R	4794	a
Funori	6323	a
Allyl-hpc	5263	b
Nanoparticles + Allyl-hpc	5068	b
Nanoparticles	4950	b
Nanoparticles + Funori	4445	b
untreated	3605	c
ICF	7092	a
ICC	5979	ab
ICF + R	5664	b
ICNPC + R	5427	b
ICC + R	5067	b

ICNP	5031	b
ICNP + R	4877	b
ICNPC	4709	b
ICNPF + R	4645	b
IC	4308	b
ICNPF	4234	bc
IC + R	2972	c

Figure 54: data obtained from Tukey test performed on average Young's Modulus values from warp IC samples. Groups are listed in a decreasing efficiency order.

SIN series - Tensile Strength

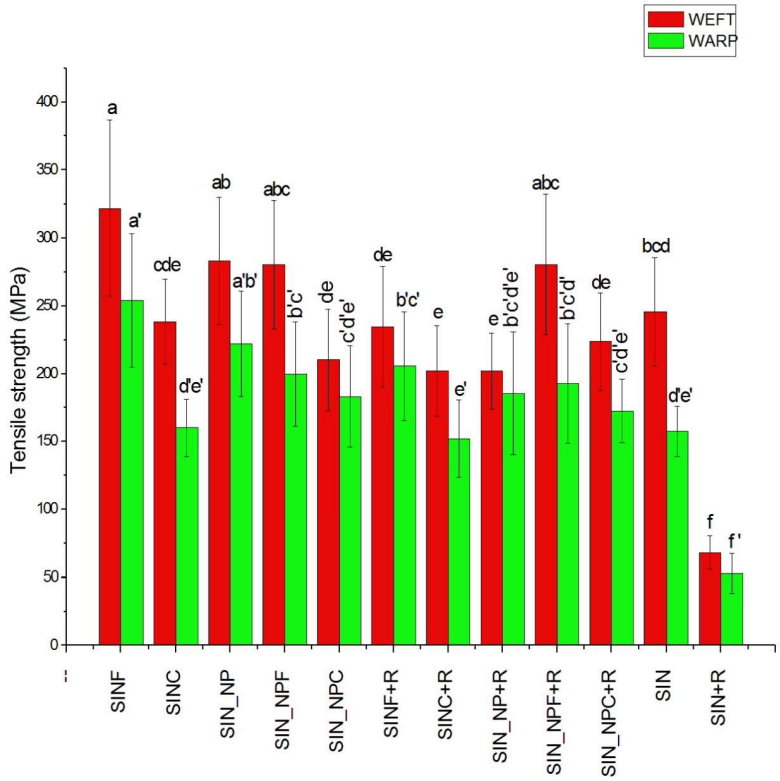

Figure 55:comparative graph between average tensile strength values of different groups of samples belonging to SIN series, both warp (in green) and weft (in red) yarns. Letters upon columns correspond to the Tukey ID letter in the tables below.

SAMPLE WEFT	AVERAGE	Tukey ID
SIN	263.1	a
SIN + R	202.7	b
Nanoparticles + Funori	280.6	a
Funori	278.3	a
Nanoparticles	244.5	b
Allyl-hpc	220.2	bc
Nanoparticles + Allyl-hpc	216.7	c

untreated	159.1	d
SINF	321.9	a
SIN_NP	283.3	ab
SIN_NPF + R	280.7	abc
SIN_NPF	280.5	abc
SIN	245.7	bcd
SINC	238.4	cde
SINF + R	234.6	de
SIN_NPC + R	223.8	de
SIN_NPC	210.3	de
SINC + R	201.9	e
SIN_NP + R	201.8	e
SIN + R	68.1	f

Figure 56: data obtained from Tukey test performed on average tensile strengths from weft SIN samples. Groups are listed in a decreasing efficiency order.

SAMPLE WARP	AVERAGE	Tukey ID
SIN	196.1	a
SIN + R	157.7	b
Funori	233.2	a
Nanoparticles	204.2	b
Nanoparticles + Funori	196.3	bc
Nanoparticles + Allyl-hpc	177.7	cd
Allyl-hpc	156	d
untreated	105.1	e
SINF	254. 1	a
SIN_NP	222.1	ab
SINF + R	205.7	bc
SIN_NPF	199.7	bc
SIN_NPF + R	192.8	bcd

SIN_NP + R	185.4	bcde
SIN_NPC	183.2	cde
SIN_NPC + R	172.4	cde
SINC	160	de
SIN	157.3	de
SINC + R	152.1	e
SIN + R	52.8	f

Figure 57: data obtained from Tukey test performed on average tensile strengths from warp SIN samples. Groups are listed in a decreasing efficiency order.

SIN series -Young's Modulus

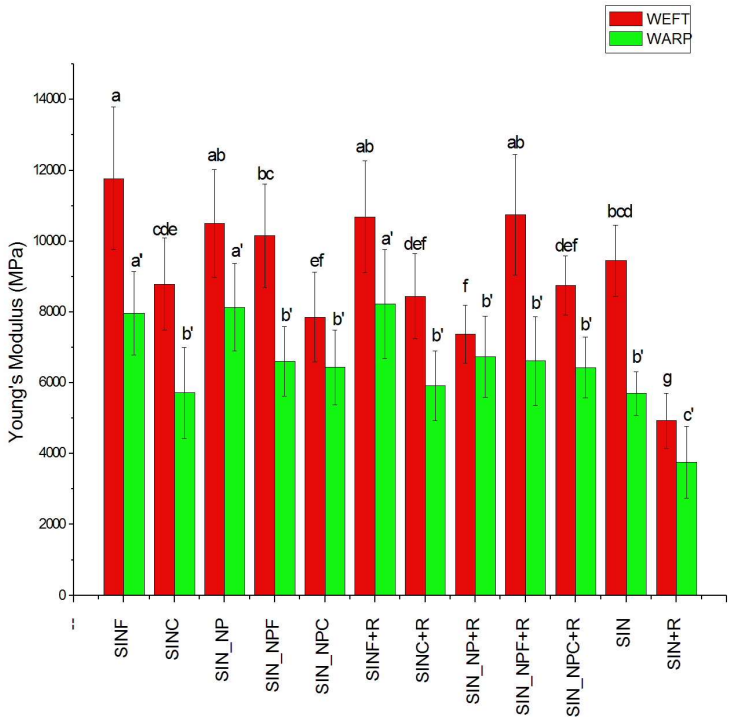

Figure 58: comparative graph between average Young's Modulus values of different groups of samples belonging to SIN series, both warp (in green) and weft (in red) yarns. Letters upon columns correspond to the Tukey ID letter in the tables below.

SAMPLE WEFT	AVERAGE	Tukey ID
SIN	9748	a
SIN + R	8526	b
Funori	11228	a
Nanoparticles + Funori	10450	a
Nanoparticles	9016	b
Allyl-hpc	8620	b
Nanoparticles + Allyl-hpc	8288	b
untreated	7249	c

SINF	11776	a
SIN_NPF + R	10745	ab
SINF + R	10681	ab
SIN_NP	10504	ab
SIN_NPF	10155	bc
SIN	9457	bcd
SINC	8792	cde
SIN_NPC + R	8759	def
SINC + R	8448	def
SIN_NPC	7860	ef
SIN_NP + R	7379	f
SIN + R	4931	g

Figure 59: data obtained from Tukey test performed on average Young's Modulus values from weft SIN samples. Groups are listed in a decreasing efficiency order.

SAMPLE WARP	AVERAGE	Tukey ID
SIN	6755	a
SIN + R	6190	b
Funori	8081	a
Nanoparticles	7457	a
Nanoparticles + Funori	6613	b
Nanoparticles + Allyl-hpc	6439	bc
Allyl-hpc	5821	c
untreated	4728	d
SINF + R	8231	a
SIN_NP	8136	a
SINF	7966	a
SIN_NP + R	6742	b
SIN_NPF + R	6620	b
SIN_NPF	6606	b

SIN_NPC	6445	b
SIN_NPC + R	6434	b
SINC + R	5920	b
SINC	5716	b
SIN	5702	b
SIN + R	3754	c

Figure 60: data obtained from Tukey test performed on average Young's Modulus values from warp SIN samples. Groups are listed in a decreasing efficiency order.

Conclusions

The research underlined the applicability in the flax canvas restoration field of a product obtained from natural sources, never applied before for this purpose. The optimization of the funori extraction procedure has been reached, developing a four steps procedure to obtain a more standardized product. Differential Scanning Calorimetry (DSC) and Thermogravimetric Analysis (TGA) revealed that the product, obtained with the extraction procedure developed, contains only water molecules tightly bound with the polymer chains. Thus, these molecules are inactive about degradation processes. Data obtained on samples undergone at different U.R. condition assessed that funori extract is not affected by U.R. values around 50- 60% (corresponding to the standard value established for museum's rooms[86]). So, the product obtained is suitable for treating works allocated to museums.

To verify the consolidation ability of funori compared to allyl-n-hydroxipropil-cellulose on linen yarns, both alone and in a combined treatment with calcium hydroxide nanoparticles, tensile tests on treated yarns have been performed in order to evaluate the effect on the average tensile strength and Young's Modulus. Considering the variability of natural materials, an experimentation based on nearly 1000 samples has been carried out. To analyse data, Anova and Tukey statistical tests have been performed. They show clearly that one of the most effective treatments results from the association of calcium hydroxide nanoparticles and funori as two subsequent treatments (-NPF samples).

Nanoparticles on their own improve mechanical performances of yarns. The supposed explanation can results from the capability of Ca2+ to create a network between cellulose chains through the formation of secondary interactions. In particular, it has been hypothesized that Ca^{2+} ions have the capability to interact with carboxylate groups of aged cellulose[87]. The

[86] Atto di indirizzo sui criteri tecnico-scientifici e sugli standard di funzionamento e sviluppo dei musei (D.M. 10 may 2001).

[87] G. Poggi, R. Giorgi, P. Baglioni et al Calcium hydroxide nanoparticles for the conservation of cultural heritage: new formulations for the deacidifications of cellulose-based artifacts, Applied Physics A 114, 2013.

neutralizing action against fibre acidity, proper of alkaline earth metal hydroxide nanoparticles, must be also taken in consideration as a mechanism able to preserve yarn from degradation, finally resulting in a major resistance and Young's modulus of yarns after aging.

Also funori treatments alone give important results in increasing mechanical performances of depolymerized yarns. The supposed consolidation mechanism in this case is related to the formation of a thin funori film (fig.61) on the fibre surface and the possible establishment of secondary interactions between cellulose and funori polysaccharide chains.

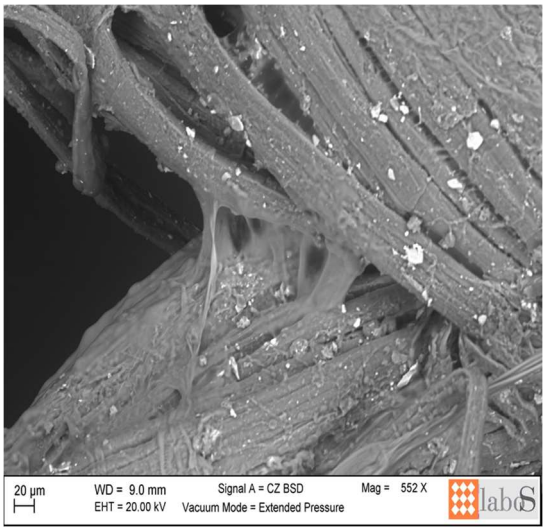

Figure 61: SEM images showing the surface morphology of yarns treated with funori. captured by SEM-EDX microscope of Scientific laboratories at Conservation and Restoration Centre "La Venaria Reale".

There is probably a synergic consolidant action between Funori and nanoparticles, due to the capacity of $Ca2^{+}$ ions to interact with both funori *β*-d-galactose-6-sulfate – 3,6-anhydro-*α*-l-galactose chains and cellulose backbone, bridging them together to form a reinforced structure (fig.43), that enhances yarn mechanical performances if compared with the untreated yarns. In particular, the sulphated groups characterizing the main polysaccharides, together with the presence of notable amount of glucuronic acid in funori extracts, could enhance the creation of coordination complexes with Ca^{2+} ions.

The further hydrothermal aging performed on treated samples, to verify the efficiency of the consolidant over time, confirms that funori and the combined treatment of $Ca(OH)_2$ and funori are the best ones, able to maintain, in many cases, almost the same value of tensile strength and Young's modulus before and after aging.

For the three more efficient treatments just mentioned above, a reiterative comparison between averages values of both tensile strength and Young's modulus is presented in table 7.

In conclusion, funori, alone and in association with calcium hydroxide nanoparticles, could be considered an interesting product in the field of flax fibres consolidation. Further investigation will be required to thoroughly understand its consolidation mechanism and the other aspects connected to its broad applicability as a consolidant for depolymerized canvas support of paintings and archaeological textiles, as suggested from the beginning of this work.

	warp		weft	
	Tensile strength (MPa)	Young's modulus (MPa)	Tensile strength (MPa)	Young's modulus (MPa)
NIN	276.6 (± 88)	5258 (±1929)	348.2 (±62.11)	8631 (±1744)
ICN_R	52.0 (± 17.7)	2972 (± 1362)	39.1 (±9.2)	3945 (± 773)
ICN	74.8(± 23.6)	4309(±814)	103.2(±16.2)	5660(±901)
ICF_R	108.5 (±20.5)	5664 (1118)	104.0 (20.7)	6947 (±1022)
ICF	156.6 (±37.4)	7092 (±1252)	142.7 (±27.5)	7488 (±1210)
ICNP_R	152.7 (±34.6)	5032 (±1142)	152.1 (±25.6)	6537 (±899)

ICNP	88.2 (± 25.8)	4877 (± 762)	132.6 (±31.2)	7315 (±1412)
ICNPF_R	108.0 (21.9)	4645 (±840)	167.7 (±30.6)	8055 (± 1131)
ICNPF	122.5 (±28.2)	4235 (±752)	180.3 (±32.4)	7882 (±1269)
SINb	52.8 (±14.7)	3754 (±1014)	68.2 (±12.3)	4931 (±772)
SIN	157.4 (±18.6)	5703 (±615)	245.8 (±39.8)	9458 (±1008)
SINF	254.2 (± 49.1)	7967 (±1180)	322.0 (±64.7)	11776 (±2003)
SINF_R	205.7 (±40.2)	8232 (±1536)	234.6 (±44.5)	10681 (±1572)
SIN_NP	222.2 (±39)	8136 (±1234)	283.4 (±47)	10505 (±1525)
SIN_NPR	185.4 (±45.3)	6743 (±1151)	201.9 (±28.2)	7379 (±823)
SIN_NPF	199.7 (±38.4)	6606 (±985)	280.5 (±47.4)	10156 (±1469)
SIN_NPFR	192.9 (±44.2)	6620 (±1253)	280.7 (±51.9)	10745 (±1698)

Table 7: comparative table of average values of both tensile strength and Young's modulus for treatments -NP, -F and -NPF (the ones that lead to an increasing of mechanical performances) in relation with values obtained from untreated samples (see Appendix 1).

Appendix 1

	BOXPLOT ID	
ID	**TREATMENT**	**AGING**
NIN	untreated	new
ICN	untreated	IC
ICN_R	untreated	IC+R
ICC	allyl-hpc	IC
ICC_R	allyl-hpc	IC+R
ICF	funori	IC
ICF_R	funori	IC+R
ICNP	nanoparticles	IC
ICNP_R	nanoparticles	IC+R
ICNPC	nanoparticles + allyl-hpc	IC
ICNPC_R	nanoparticles + allyl-hpc	IC+R
ICNPF	nanoparticles + funori	IC
ICNPF_R	nanoparticles + funori	IC+R
SIN	untreated	SIN
SINb	untreated	SIN+R
SINF	funori	SIN
SINF_R	funori	SIN+R
SINC	allyl-hpc	SIN
SINC_R	allyl-hpc	SIN+R
SIN_NP	nanoparticles	SIN
SIN_NPR	nanoparticles	SIN+R
SIN_NPF	nanoparticles + funori	SIN
SIN_NPF_R	nanoparticles + funori	SIN+R
SIN_NPC	nanoparticles + allyl-hpc	SIN
SIN_NPC_R	nanoparticles + allyl-hpc	SIN+R

Appendix 2

During the Phd I have been partially involved in the development of a new method for the removal of gypsum degradation layers from carbonatic matrices in cultural heritage conservation, based on the application of aqueous Highly Viscous Polymeric Dispersions (HVPDs) embedded with chelators.

CHELATORS CONFINED INTO 80PVAC-BORAX HIGHLY VISCOUS DISPERSIONS FOR THE REMOVAL OF GYPSUM DEGRADATION LAYERS

Chiara Berlangieri[1], Elisabetta Andrina[1], Caterina Matarrese[1], Emiliano Carretti[1], Rita Traversi[2], Mirko Severi[2], David Chelazzi[1], Luigi Dei[1,*], Piero Baglioni[1]

[1]Department of Chemistry "Ugo Schiff" & CSGI Consortium, University of Florence, via della Lastruccia, 3 - 50019 Sesto Fiorentino (Florence), Italy
[2]Department of Chemistry "Ugo Schiff", University of Florence, via della Lastruccia, 3 - 50019 Sesto Fiorentino (Florence), Italy

* Corresponding author, luigi.dei@unifi.it; Phone: +39 055 4573045 Fax: +39 055 4574913

E-mail addresses: berlangieri@csgi.unifi.it (C. Berlangieri), elisabetta.andrina@gmail.com (E. Andrina), matarrese@csgi.unifi.it (C. Matarrese), carretti@csgi.unifi.it (E. Carretti), rita.traversi@unifi.it (R. Traversi), mirko.severi@unifi.it (M. Severi), baglioni@csgi.unifi.it (P. Baglioni)

Abstract

In this paper a new method for the removal of gypsum degradation layers from carbonatic matrices in cultural heritage conservation, using aqueous Highly Viscous Polymeric Dispersions (HVPDs) based on partially hydrolyzed poly(vinyl acetate) and borax, embedded with chelators, is presented. Due to

their interesting viscoelasticity, these systems guarantee a good adhesion to the treated surface and easiness of removal in one step, minimizing the residues. Thus, they can potentially overcome the “residue question” limit associated to traditional methodologies that use thickened solutions of chelators. Here the rheological properties of HVPDs containing different amounts of selected chelating agents are explored and their efficacy in the extraction of gypsum is verified through cleaning tests onto artificially sulfated travertine tiles. The homogeneous removal of gypsum across the surface was checked non-invasively via Fourier Transform Infrared Spectroscopy (FTIR) 2D Imaging. An analytical protocol for the pre-treatment and the analysis of HVPD samples by means of Ion Cromatography (IC) and Inductively Coupled Plasma Atomic Emission Spectroscopy (ICP-AES) was set up and the approximate amount of calcium sulfate removed was determined.

Keywords: **chelates, poly vinyl alcohol-borax, viscoelasticity, gypsum layers, desulphatisation**

Introduction

Since ancient times, limestones have been used as base material for artworks, statues and mural paintings, constituting the larger part of our cultural heritage for many centuries.

A common degradation that affects artifacts made of natural or artificial carbonatic materials is the sulphatisation, the transformation of calcium carbonate in calcium sulfate bihydrate (gypsum) due mainly to the interaction with the atmospheric sulfur dioxide in the presence of humidity and oxidation catalysts.[1] The elementary cell of gypsum occupies almost a double volume compared to that of calcium carbonate. In the case of carbonatic supports, when this reaction takes place and new crystals of gypsum form inside the porous structure, the consequent volume expansion determine mechanical stresses that cause cracking, fissuring and pulverization of the carbonatic matrix.[2] In particular, for frescoes, when the phenomenon is particularly severe, we observe lifting and detachment of the paint layer, with loss of decoration and pigments.[3]

One of the most effective traditional treatments for the gypsum removal from carbonatic supports is the Ferroni-Dini method,[4] developed in 1966 by Enzo Ferroni, chemistry professor at the University of Florence, and Dino Dini, headmaster in the restoration of frescoes. It's a two-phases treatment consisting in the solubilization of gypsum with a water solution of ammonium carbonate followed by the application of barium hydroxide that ensures the consolidation of the degraded matrix and at the same time makes the sulfate unreactive and insoluble.[5-7]

An alternative, widely used technique for the removal of soluble salts and, in particular, of calcium sulfate from frescoes, mural paintings and plasters consists in the use of ion-exchanger resins.[8-9] Generally they are synthetic resins that swell when in contact with water and are completely insoluble in it.[10] Due to this feature, when ion-exchangers are in contact with an artwork contaminated by salts, their action is limited to the surface up to a depth of about 70-100 μm, without penetrating into the porosity of the object, thus avoiding the interaction with the original materials to preserve.[11]

Other substances used by restorers to treat the efflorescences are chelators. The most diffused are disodium EDTA, Rochelle salt (especially for the cleaning of gilded bronzes because of its mild action that preserve the original gilded foil[12]), citrate salts and benzotriazole.[13-17] Usually they are applied in aqueous solution (1-5% of additive).[18] The solution pH has a fundamental role for the dissociation equilibria of the chelator and its selectivity towards different ions.

A potential risk in the use of these substances is that calcium ions coming from the carbonate matrix could be solubilized as well. To limit the penetration of the cleaning agent into the inner layers and to avoid the solubilization of the original material constituting the plaster and the paint layer, chelators aqueous solutions are usually adsorbed into poultices of carboxymethylcellulose or gelled with a thickener as Klucel G[19-20] or Carbopol.[6]

The main drawback of these applicative methods is the "residue question"[21], as the thickened systems release residues onto the treated surface. The necessity of a clearance step with a neat liquid (generally water)

and/or extra mechanical action can be critical in presence of fragile or hydrophilic surfaces/materials.

At the Chemistry Department of the University of Florence and CSGI Consortium, innovative peelable poly(vinyl) acetate (PVAc)-borax based Highly Viscous Polymeric Dispersions (HVPDs) for cleaning artistic surfaces were developed and studied.[22]

The viscoelastic and cleaning/removing properties of the HVPDs can be modulated by varying the entanglements density of the network[23-24] and/or the polarity of the continuous phase by incorporating different organic solvents.[25-27] Their high elastic modulus and viscosity allow the minimization of the residues left onto the treated surface and of the penetration of the cleaning agent into the porous matrix of the artwork. The first applicative tests on canvas and wood paintings[22,28] resulted in a controllable, gradual, selective cleaning action.

Recently, considering the great versatility of these HVPDs, the capability of embedding chelators was explored. This achievement could extend the application field of these systems to mural paintings and metal surfaces, both frequently affected by the presence of foreign patinas like salt efflorescences and corrosions/oxidation deposits respectively. In fact, it must be noted that this class of HVPDs has a broad range of potential applications that include the cleaning of both classic and modern artifacts (easel/mural paintings, graffiti, metallic and plastic objects), therefore their current implementation will highly benefit from studies concerning their characterization and effectiveness.

In this work three chelating species were selected: disodium EDTA, ammonium carbonate and sodium/potassium tartrate. The maximum loadable amount of each, before observing phase separation, was determined. The viscoelastic properties of HVPDs containing different amounts of chelator were investigated to study how the additive influence their elastic response.

To evaluate the efficacy in the removal of calcium sulfate, these HVPDs embedded with chelators were tested onto artificially sulfated travertine tiles. The qualitative, non-invasive evaluation of the cleaning treatment was carried out through FTIR 2D Imaging, in order to estimate the homogeneousness of the removal of gypsum across the treated surface.

HVPD samples collected after the cleaning tests were analyzed through Ion Cromatography and Inductively Coupled Plasma techniques. The quantification of the gypsum extracted was possible thank to the set-up of an analytical protocol for the pre-treatment and the analysis of samples that was suitable for IC/ICP.

Materials and methods

80% hydrolyzed poly(vinyl acetate) was supplied by Kuraray Co., Ltd. as random copolymer (M_W = 47300) and was used as received. Sodium tetraborate decahydrate (99,5-100%, Sigma-Aldrich), ammonium carbonate (Sigma-Aldrich), disodium EDTA dihydrate (99-100%, ACS reagent, Sigma-Aldrich), potassium sodium tartrate tetrahydrate (99%, ACS reagent, Sigma-Aldrich), ammonium hydroxide (Sigma, NH_3 content 28-30%), hydrochloric acid 37% (CARLO ERBA, min. assay 36.5%) and sulphuric acid 96% (96±1%, CARLO ERBA) were used as received. Water was purified by a Millipore Elix3 apparatus (R ≥ 15 MΩ cm).

Preparation of the polymeric dispersions

The PVAc was dissolved in a water solution of the chelating agent; then a solution of borax was added and the system was stirred with a VORTEX apparatus until it became rigid in few minutes. The polymer/borax weight ratio was kept to 4:1. The pH of all the systems was adjusted in order to warrantee the maximum complexation ability. All the measurements and cleaning tests were carried out one week after the samples preparation to ensure their equilibration.

Travertine samples sulfation

The sulfation of the travertine tiles was inducted by soaking one of their surface (4.8 x 4.8 cm) into a 5M H_2SO_4 solution for 1h. Then they were let dry until a constant weight was reached.

Gravimetric determination of the calcium sulfate dihydrate formed onto the travertine samples

The average amount (g) of gypsum formed ($W_{CaSO4\cdot 2H2O}$) onto the travertine tiles was determined gravimetrically, according to the stoichiometric equilibrium of the sulfation reaction (1), using the formula (2):

$$CaCO_3 + H_2SO_4 + H_2O \rightarrow CaSO_4 \cdot 2H_2O + CO_2 \qquad (1)$$

$$W_{\mathrm{CaSO4\cdot 2H2O}} = \frac{\Delta W \cdot Mw_{\mathrm{CaSO4\cdot 2H2O}}}{Mw_{\mathrm{CaSO4\cdot 2H2O}} - Mw_{CaCO3}} \qquad (2)$$

where ΔW (g) is the difference between the final weight W_f (g) and the initial weight W_i (g) of the travertine tile after the sulfation, $MW_{CaSO4\cdot 2H2O}$ and MW_{CaCO3} are the molecular weights of $CaSO_4\cdot 2H_2O$ and $CaCO_3$ respectively. The total average amount of $CaSO_4\cdot 2H_2O$ formed onto the travertine surface was 6.7 mg/cm^2.

Application of HVPDs embedded with chelators onto the sulfated travertine tiles

A weighed amount (1 g) of an HVPD containing the chelator was applied onto a confined area (2.28 cm^2) of a sulfated travertine tile using a plastic ring, for different contact times: 5, 10, 20, 30, 60 min (Fig. 1). Each test was repeated four times. HVPD samples were weighed before and after each application to determine the weight loss. For samples containing ammonium carbonate or Rochelle salt, additional applications lasting 1080 and 1380 min were performed.

Figure 1: Exemplifying images showing the four “60 min-long” applications of the HVPD containing EDTA onto the sulfated travertine tile (left) and the ease removal step (right) achieved by confining the HVPD into a plastic ring.

Rheological Measurements

Oscillatory shear measurements were performed with a Paar Physica UDS200 rheometer working at 25 ± 0.1°C (Peltier temperature control system) using cone-plate geometry (25 mm diameter and 1° cone angle). The gap between the plates was 0.5 mm. After being loaded, samples were equilibrated for 30 min at 25°C prior to start the experiments. Frequency sweep measurements were done in the linear viscoelastic region (2-3% strain) based on an amplitude sweep test. The storage modulus *G'* (Pa) and the loss modulus *G''* (Pa) were measured over the frequency range 0.001-100 Hz. The intrinsic elastic modulus G_0 (Pa), represented by the asymptotic value of the elastic shear modulus *G'* was calculated as the average value of the last five *G'* points in the *plateau* region of the flow curves.

Ion Cromatography (IC)

IC analyses were performed with a Dionex ICS-90 Ion Cromatography System, using a Dionex AG4A guard-column (4 mm diameter, 5 cm length) and a Dionex AS4A column (4 mm diameter, 20 cm length). The eluent was a buffer solution with Na_2CO_3 (1.8 mM) and $NaHCO_3$ (1.8 mM) in MilliQ water (1.65 mL/min flow). A 10 mM H_2SO_4 solution was used as the regeneration fluid for the conductivity suppressor (3.36 mL/min flow). The injection loop was 25 µL.

Inductively Coupled Plasma Optical Emission Spectrometry (ICP-OES)

ICP analyses were performed using a Varian 720-ES ICP-OES spectrometer with an optical detector. The external, auxiliary, and nebulizer flows were 16.5, 1.50, and 0.75 L/min, respectively. A 50 ppm solution of Germanium was used as the internal standard to quantify the analyte of interest.

2D imaging-Fourier transform infrared (FTIR)

The 2D imaging-Fourier transform infrared (FTIR) analysis of the travertine tiles was carried out on a Cary 620-670 FTIR microscope, equipped with an FPA (Focal Plane Array) 128x128 detector (Agilent Technologies). The spectra were recorded directly on the surface of the samples (or of the Au background) in Reflectance mode, with a spectral resolution of 4 cm^{-1}, acquiring 128 scans for each spectrum. The spatial resolution of each Imaging map is 5.5 µm (i.e. each pixel has dimensions of 5.5 x 5.5 μm^2). Five measurements were carried out on each type of travertine sample

(untreated, sulfated, sulfated and cleaned with a HVPD containing 0.5 wt% of ammonium carbonate; four consecutive applications with a contact time of 60' each were carried out), and the representative spectra for each sample are shown in this contribution. In order to improve the readability of the spectra, the background noise was reduced using the "smooth" tool (set at 10) of the Igor Pro software, taking care not to alter any diagnostic information deemed useful to this qualitative investigation. In each 2D map, the intensity of the gypsum absorption at 3570 cm^{-1} (OH stretching of water) was imaged as the area of the absorption peak between 3692 and 3542 cm^{-1}. The chromatic scale of the maps shows increasing absorbance of the band as follows: green < yellow < red.

Results and Discussion

Being the use of monophasic systems an essential condition to control the cleaning action of the HVPDs, the maximum amount of EDTA, Rochelle salt and ammonium carbonate loadable in the 80PVAc-borax systems before observing phase separation was determined. The obtained values were 0.5 wt%, 1 wt% and 0.5 wt% respectively.

In a previous paper it was observed that to warrantee an adequate performance in terms of ease of application and complete removal through a peeling action[27], the HVPDs should preserve adequate elastic properties even upon addition of additives active against the foreign patinas of the artifacts. In particular their intrinsic elastic modulus G_0 values should be always higher than 400 Pa. To verify if these features were preserved after the addition of chelators, the mechanical properties of the HVPDs set up were explored. Fig. 2 shows that upon the addition of ammonium carbonate (A) or Rochelle salt (B), the mechanical behavior of the HVPDs is invariant for chelator concentrations respectively up to 0.5 and 0.9 wt%. Fig. 3 displays that a further increase of Rochelle salt concentration up to 1 wt% determines the formation of a gel (the shear elastic modulus G' is higher than the shear viscous modulus G'' over the entire range of frequencies explored).[29]

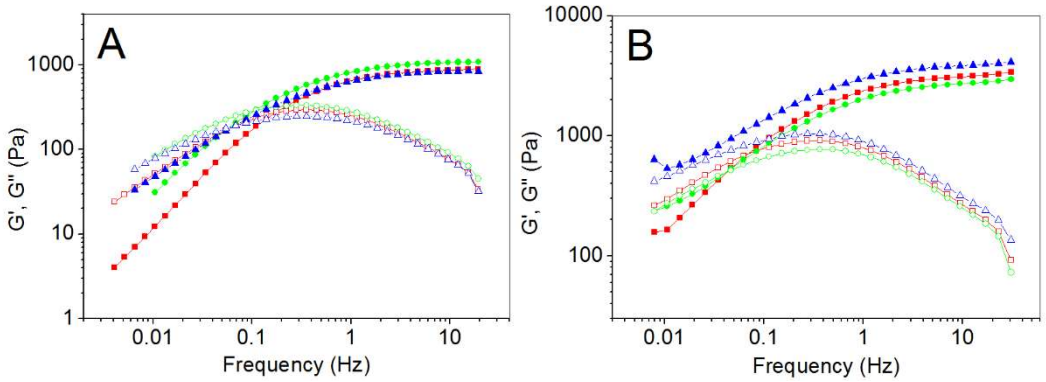

Figure 2: Flow curves of the *G'* (closed symbols) and *G''* moduli (open symbols) for the HVPDs containing: (A) 0.1 wt% (squares), 0.3 wt% (circles), 0.5 wt% (triangles) of ammonium carbonate; (B) 0.5 wt% (squares), 0.7 wt% (circles), 0.9 wt% (triangles) of Rochelle salt.

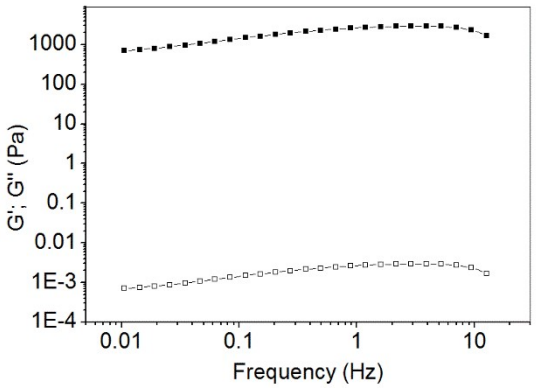

Figure 3: Flow curves of the G' (closed symbols) and G'' moduli (open symbols) for the HVPD sample with 1 wt% Rochelle salt, showing the rheological behavior typical of a gel (G' >> G'').

The frequency sweeps of the HVPDs containing different amounts of ammonium carbonate or Rochelle salt normalized to the crossover point between the *G'* and the *G''* curves (Fig. 4) indicate that even if changes occur in the timescale of the relaxation process when the concentration of the chelator is increased, the mechanism associated with the relaxation remains almost the same.

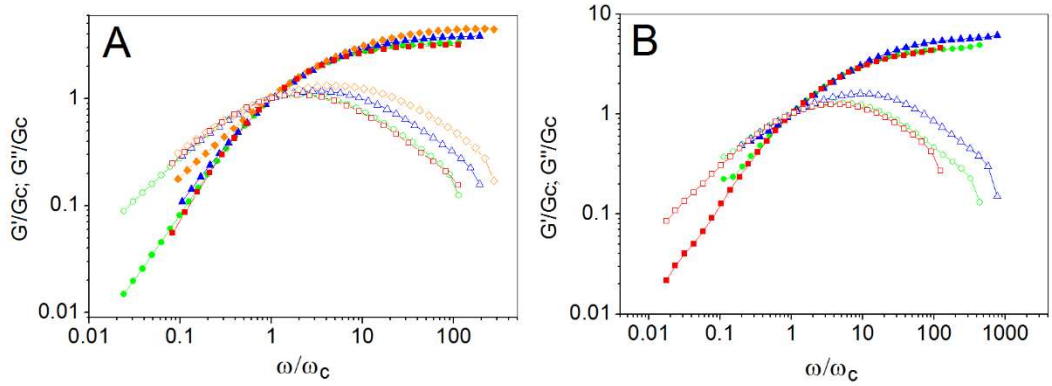

Figure 4: Normalized mechanical histograms for the 80PVAc-borax with: (A) 0 wt% (red squares), 0.1 wt% (green circles), 0.3 wt% (blue triangles) and 0.5 wt% (orange diamonds) of ammonium carbonate; (B) 0 wt% (red squares), 0.5 wt% (green circles) and 0.7 wt% (blue triangles) of Rochelle salt. Closed symbols indicate the G'/G_c ratios; open symbols indicate the G''/G_c ratios. G_c (Pa) and ω_c (Hz) are the coordinates of the crossover point.

Fig. 5 shows the trends of the G_0 values as a function of $(NH_4)_2CO_3$ (A) and Rochelle salt (B) content; for concentrations around 0.3 wt% and 0.9 wt% respectively, the salts addition has a structuring effect on the systems as indicated by the increase of their elasticity. In presence of a higher amount of additive, the lowering of G_0 indicates a reduction of the entanglements density of the PVA network.

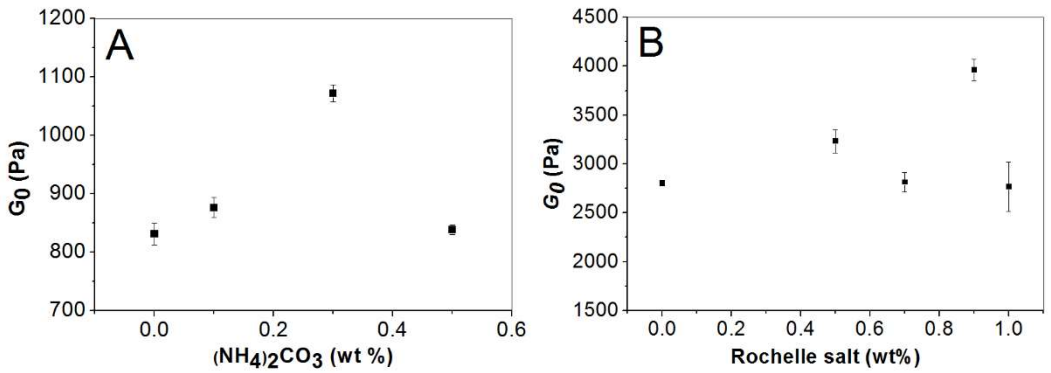

Figure 5: Intrinsic elastic modulus *G_0* of 80PVAc-borax HVPDs as a function of ammonium carbonate (A) and Rochelle salt (B) concentrations (wt%).

Finally, the addition of EDTA determines a significant increase in the intrinsic elasticity (G_0) due to a structuring role of the salt. This behavior was ascribed to a combination of salt and pH effect, assuming that the EDTA tetra-anionic species Y^{4-} [30] (~50% at pH ~11 as that of our EDTA-containing systems), mediates some cross-links between the hydroxyl groups of 80PVAc chains (Matarrese et al., paper submitted).

Even if traditional gel systems used for the conservation of artistic surfaces contain higher concentrations of chelators (1-5 wt%), the ones achievable with the 80PVAc-borax HVPDs, although significantly lower, were expected to be still adequate for cleaning purposes. An auxiliary benefit of the lower chelator concentrations is that the cleaning action is more gradual and controllable, favoring the preservation of the original layers of the artifacts.

The HVPDs selected for the application tests on sulfated travertine tiles, contained 0.25 wt% EDTA (pH = 11), 0.5 wt% ammonium carbonate and 1 wt% Rochelle salt, respectively (Table 1). The aim was to evaluate their efficacy in the gypsum patina removal as a function of both the additive type and the application time. To better confine the cleaning action, the systems were applied into plastic rings that ensured also a quick and easy removal step (Experimental Section, Fig. 1).

HVPD	**PVAc (wt%)**	**Borax (wt%)**	**Additive (wt%)**		**H_2O (wt%)**
System A	3%	0.75%	**Disodium EDTA**	0.25%	95.55%
			NH_3	0.45%	
System B	3%	0.75%	**Ammonium carbonate**	0.5%	95.75%
System C	4%	1%	**Rochelle salt**	1%	94%

Table 1: Composition of the HVPDs used for the cleaning tests on sulfated travertine tiles.

To verify the retentive capability of the HVPDs towards the liquid fraction confined into them once in contact with the porous matrixes, the HVPDs weight was monitored before and after each test. To eliminate the

contribution due to the water evaporation, a “blank” adsorption was recorded by weighing a HVPD kept close to the samples on which the cleaning tests were carried out without being in contact with the porous matrix. The weight loss of the blank was subtracted to the one registered for the HVPDs applied onto the tiles.[31] The ratio between the water content before and after the test gives the Absorption Index (A.I. %):

$$A.I.\% = \frac{W_{Abs} - W_{\mathrm{Re}f}}{W_i - W_{\mathrm{Re}f}} \times 100 \qquad (3)$$

where W_{Abs} is the weight of the absorbed water, W_{Ref} is the weight of the evaporated water, W_i is the initial weight of the water in the HVPDs in contact with the travertine surface. Fig. 6 shows the A.I. % as a function of the application times of the HVPDs containing the different chelators.

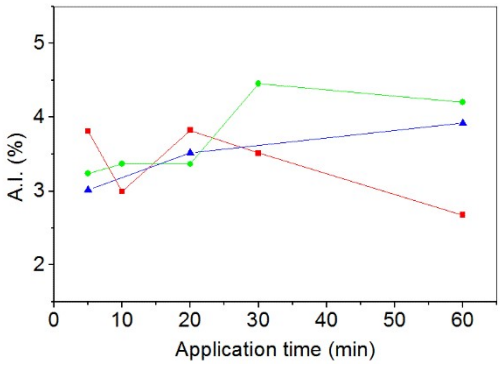

Figure 6: Absorption Index (%) as a function of the application time for the system containing 0.25 wt% EDTA (squares), 0.5 wt% ammonium carbonate (circles) and 1 wt% Rochelle salt (triangles).

The weight loss undergone by the system due to the migration of the liquid fraction (water solution) into the porous structure of the stone resulted very low: around 4% after 60 min of application for samples containing ammonium carbonate and Rochelle salt and around 3% for those with EDTA. These data confirmed the very good retentive properties of the HVPDs, even when embedded with chelators.

Optical micrographs (Fig. 7) of the sulfated travertine surfaces before (B) and after (C) the application of the HVPDs loaded with $(NH_4)_2CO_3$ 0.5 wt%

(contact time 60') indicate that the system is effective in the superficial removal of the gypsum patina.

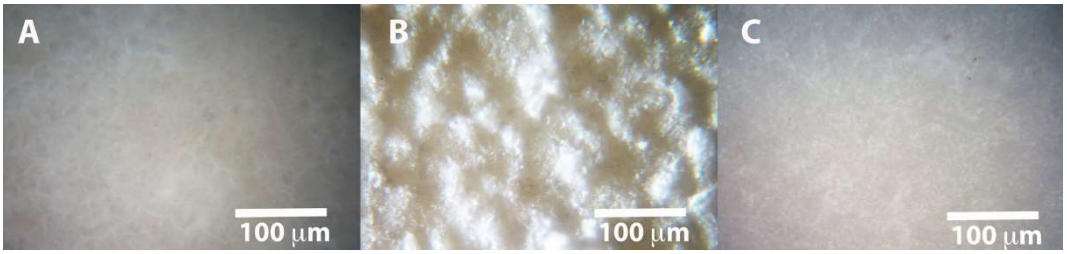

Figure 7: Optical micrographs (20x magnification) of the travertine surface before the sulfation treatment (A), the sulfated surface before (B) and after (C) the cleaning test with the HVPD containing 0.5 wt% ammonium carbonate.

To quantitatively evaluate the amount of sulfates removed, IC analyses were performed and a measuring protocol for the preparation and the analyses of the samples was developed as follow.

Standard solutions for calibrations were freshly prepared in precleaned polyethylene vials by diluting a stock standard solution (1000 mg L^{-1}) purchased from Merck (Darmstadt, Germany). To take into account the matrix effect, a "blank" HVPD sample without the analyte of interest (the sulfate ion) was dissolved with HCl (37% mol), diluted 1:100 in MilliQ ultrapure water and added in each standard solution. The sample had previously been applied for 5 min onto a no-sulfated travertine tile, so that the standard solutions contained all the components present in the unknown samples except for the analyte of interest. Before being analyzed, the HVPD samples containing the extracted calcium sulfate dihydrate (~1 g) were solubilized with 50 µL of HCl 37% and diluted 1:100 using MilliQ ultrapure water. The sulfate concentration was determined from the calibration curve based on the signal intensity (µS) of the analyte. Considering that the retention time of the sulfate ion and, thus, the instrument sensitivity can slightly change due to measurement conditions or to the matrix complexity, the calibration curve was constructed for each measuring session.

Fig. 8 shows the IC chromatograms of the HVPD samples embedded with EDTA after the different cleaning tests. Sulfate shows a retention time of

4,30 min while the ionic species responsible for the peak at 4,70 min could not be identified but did not represent a drawback for the reliable measurement of sulfate peak.

Sulfate peak increased with the contact time between the sulfated surface and the HVPD, whatever was the chelator supported by the system (Table 2).

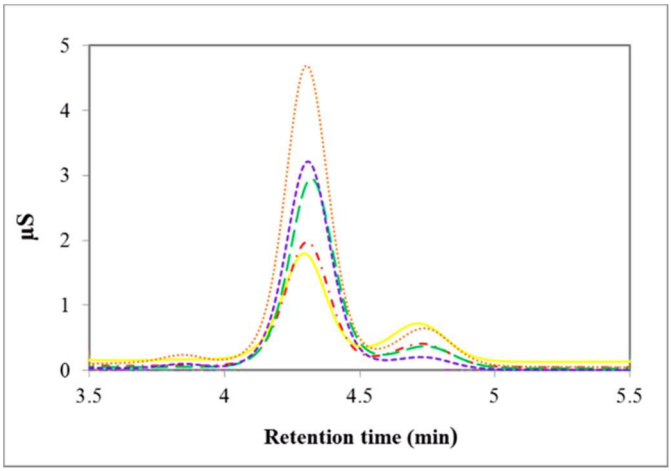

Figure 8: IC chromatograms for the EDTA-containing samples after being applied onto the travertine tile for 5‘ (yellow solid), 10‘ (red dash-dot), 20‘ (green dashed), 30‘ (purple short dashed) and 60‘ (orange dotted). The peak coming from the sulfate ions is at ~ 4,30 min.

	EDTA		**Ammonium carbonate**		**Rochelle salt**	
Contact time	**ppm**	**St. dev.**	**ppm**	**St. dev.**	**ppm**	**St. dev.***
5'	2.76	0.21	4.30	0.26	1.96	/
10'	3.51	0.15	5.13	0.35	/	/
20'	5.19	0.16	8.52	1.14	2.69	/
30'	6.03	0.30	9.55	1.30	/	/
60'	8.92	0.30	25.11	3.62	27.97	/

* the experimental error is not reported because tests were carried on only once.

Table 2 IC results displaying the amount of sulfates extracted (ppm) at different contact times for the HVPD containing 0.25 wt% EDTA, 0.5 wt% ammonium carbonate and 1 wt% Rochelle salt.

As regard samples containing Rochelle salt, IC technique wasn't suitable for the sulfates detection. The peak at 4,35 min due to the tartrate ions significantly overlapped with the sulfate peak at around 4,15 min (Fig. 9); thus, the quantification of the sulfates extracted was affected by a big error.

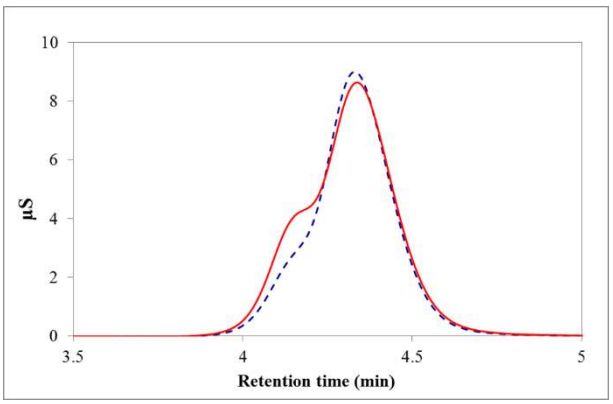

Figure 9: IC chromatograms for the Rochelle salt-containing samples after being applied onto the travertine tile for 5' (blue dashed) and 60' (red solid). The peak coming from the sulfate ions is at ~ 4,15 min while the peak at 4,35 min comes from the tartrate ions.

Taking into account the experimental uncertainty on Rochelle salt-containing samples, the percent of sulfates removed by each additive was determined and compared (Table 3). Ammonium carbonate resulted more effective for the thinning of the gypsum patina (the values relative to the systems functionalized with Rochelle salt were considered affected by a 50% error).

Contact time	% of sulfates removed per unit area (2.28 cm^2)		
	EDTA	Ammonium Carbonate	Rochelle salt
5'	1.91	3.04	1.36
10'	2.45	3.68	/
20'	3.81	6.04	2
30'	4.45	6.81	/
60'	6.67	18.43	21.29

Table 3 Sulfates extracted per unit area (%) at different contact times for the HVPDs containing 0.25 wt% EDTA, 0.5 wt% ammonium carbonate and 1 wt% Rochelle salt.

A more accurate quantification of the sulfates extracted by the HVPDs containing 1 wt% Rochelle salt was achieved via ICP analyses by measuring the sulfur contained in samples collected after being applied for 60‘, 1080‘ and 1380‘. To make a comparison, cleaning tests of the same duration were carried out using the HVPD with 0.5 wt% ammonium carbonate (that had resulted the most performing according to the previous tests) and the samples were analyzed through ICP technique as well. Also for ICP analyses a measuring protocol was developed. Before being analyzed, the HVPD samples (~1 g) were solubilized with 50 µL of HCl (37%) and diluted 1:100 using MilliQ ultrapure water. A standard solution with 1000 ppm of SO_4^{2-} was used to obtain standard solutions with different SO_4^{2-} concentrations in which 100 µL of a solution containing Ge as internal standard was then added. For each sample, a triplicate measurement was carried on. The sulfur concentrations (ppb) were determined as the average in ppb recorded at two different detection wavelengths (180.669 nm and 181.972 nm). The concentration of sulfate anions SO_4^{2-} present in the diluted HVPD samples was determined from the sulfur concentration given by the instrument, based on stoichiometric calculations (assuming that the detected sulfur came exclusively from the sulfates extracted by HVPD). Considering the

1:100 dilution, the effective concentration C_e (ppm) of sulfur removed resulted from equation (4):

$$C_e = \frac{C_d \cdot P_i}{P_e} \cdot 100 \qquad (4)$$

where P_i is the initial amount of HVPD sample used for the cleaning test (mg), C_d is the amount of sulfate anion (ppm) measured in the diluted HVPD sample, P_e is the effective amount (mg) of the HVPD sample collected after the cleaning test and actually used for the ICP analysis.

ICP results led to believe that, as expected, IC data regarding Rochelle salt-containing HVPDs were affected by a significant error and the values were overestimated. In fact, according to ICP analyses, only 6.58% of sulfates were extracted after a 60 minutes-long treatment against the 21.29% calculated on the basis of IC analyses.

Comparing both IC and ICP analyses, the most performing additive for the extraction of gypsum still resulted ammonium carbonate, removing 37% of sulfates after an application of 1380‘ (Fig. 10). Regardless of the additive, the extraction power increased with the contact time. Systems containing ammonium carbonate and Rochelle salt gave significantly better performances when applied for 60‘ or more.

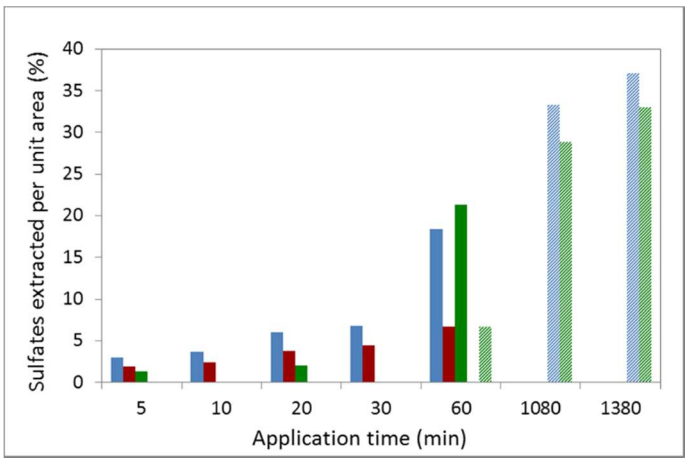

Figure 10: Sulfates extracted per unit area (%) at different contact times based on IC (filled histograms) and ICP (striped histograms) results for the HVPD containing 0.5 wt% ammonium carbonate (light blue), 0.25 wt% EDTA (dark red) and 1 wt% Rochelle salt (green).

In order to evaluate the homogeneousness of the gypsum removal across the surface, 2D FTIR Imaging was carried out on travertine samples before sulfation, after sulfation, and after sulfation and application of the HVPDs loaded with ammonium carbonate 0.5 wt% (four consecutive applications were carried out with a contact time of 60 mins each). Figure 11 shows the obtained results. The intense absorption bands in the spectrum of the sulfated travertine tile, respectively at 3572, 3437 (ν_3 and ν_1 H_2O of gypsum) [32], and 1152 cm^{-1} (ν_3 SO_4, which looks inverted in the reflectance spectrum), are no longer clearly observable in the spectra of both the untreated and the cleaned tiles. It must be noted that, according to the literature, the FPA detector allows enhanced sensitivity as compared to attenuated total reflection (ATR) measurements, as for instance in cases where the lowest detectable concentration of drugs passed from 0.35% (ATR) down to 0.075% (FPA) [33]. The intensity of the gypsum band at 3572 cm^{-1} (imaged as the area of the peak between 3692 and 3542 cm^{-1}) decreases dramatically upon cleaning, becoming comparable to that of untreated travertine. Namely, the gypsum peak absorbance is evenly decreased all across the surface, indicating the homogeneous removal of gypsum after the application of the HVPDs.

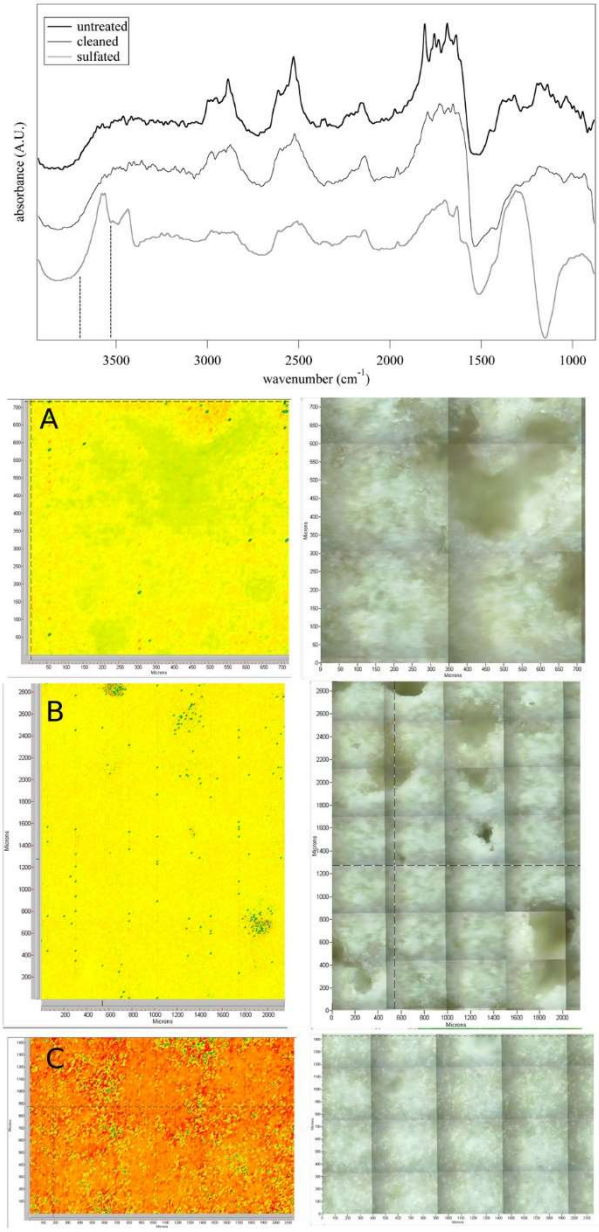

Figure 11: FTIR spectra of travertine tiles. The top panel shows the comparison between the Reflectance spectra of tiles that were: (i) untreated; (ii) sulfated and then cleaned with the HVPDs; (iii) sulfated. Each spectrum relates to a single pixel (5.5 x 5.5 μm^2) of the corresponding 2D Imaging maps shown in the bottom panels (A-C). The intensity of the gypsum absorption at 3570 cm^{-1} (OH stretching of water) was imaged in the chromatic maps as the area of the peak between 3692 and 3542 cm^{-1}. The

chromatic scale of the maps qualitatively shows the increasing intensity of the band as follows: green < yellow < red. Beside each chromatic map, the corresponding image under visible light is shown. Map A (700 x 700 μm^2): untreated travertine; Map B (2800 x 2000 μm^2): travertine sulfated and then cleaned with the HVPDs; Map C (1400 x 2100 μm^2): travertine sulfated.

Conclusions

In the present work, the effectiveness of 80PVAc-borax HVPDs embedded with three different chelators (EDTA, ammonium carbonate and Rochelle salt) in the removal of gypsum from a carbonatic matrix was explored.

As confirmed by the rheological measurements, upon the addition of the chelating agents the mechanical properties of the HVPDs resulted still adequate for their removal from the treated surface in one step by a simple peeling action, minimizing the potential residues. As concern the systems containing ammonium carbonate or Rochelle salt, the viscoelastic behavior was invariant for chelator concentrations respectively up to 0.5 and 0.9 wt%. However, a further increase of Rochelle salt concentration to 1 wt% determined the formation of a true gel. At concentrations around 0.3 wt% and 0.9 wt%, for ammonium carbonate and Rochelle salt respectively, the addition of these salts had a structuring effect on the HVPDs as indicated by the increase of their intrinsic elasticity (G_0). For higher amounts of additive, a lowering of G_0 was recorded, indicating a reduction of the entanglements density of the PVA network.

The cleaning efficacy and the easiness of removal of the systems embedded with 0.25 wt% disodium EDTA, 0.5 wt% ammonium carbonate, 1 wt% Rochelle salt were tested through several applications on artificially sulfated travertine tiles: they were removed easily in one step (with the aim of plastic rings) without leaving any visible residue. Optical micrographs of the sulfated surfaces before and after the cleaning tests revealed their effectiveness in the thinning of the gypsum patina. The quantification of the sulfates extracted was achieved through IC and ICP techniques by setting up suitable measuring protocols for the pre-treatment and the analysis of samples. Regardless of the additive, the extracting power increased with the contact time between the surface and the cleaning systems, confirming their

gradual, gentle action. The ammonium carbonate resulted the most effective, removing 37% of sulfates after an application of 1380'.

Acknowledgements

Financial support from the University of Florence, from Consorzio Interuniversitario per lo Sviluppo dei Sistemi a Grande Interfase (CSGI), Florence, and SICAMOR Project PAR-FAS (Tuscany Region, Action Line 1.1.a.3) is gratefully acknowledged. This project has received funding from the European Union's Horizon 2020 research and innovation programme under grant agreement No 646063.

References

1. R. Steudel, *Angew. Chem.* **34** (1995) 1313-1315.

2. L. Borgioli, *Polimeri di sintesi per la conservazione della pietra*, Collana I Talenti, Il Prato (2002).

3. E. Ferroni, P. Baglioni, In *Proceedings of the Symposium on Scientific Methodologies Applied to Works of Art*, Firenze (1984), Montedison Progetto Cultura, Milano, (1986) p.108.

4. M. Ciatti, *Appunti per un manuale di storia e di teoria del restauro. Dispense per gli studenti*, Edifir (2009).

5. M. Matteini, S. Scuto, *Consolidamento di manufatti lapidei con idrossido di bario*, Arkos **1** (2001).

6. L. Campanella et al., *Chimica per l'arte*, Zanichelli Editore **(**2007).

7. P. Baglioni, E. Carretti, L. Dei, R. Giorgi, *Self-Assembly* (Ed.: B.H. Robinson), IOS, Amsterdam (2003), pp.32-41.

8. A. Giovagnoli, C. Meucci, M. Tabasso Laurenzi. In: *Deterioration and preservation of stones, Proceedings of the 3rd International Congress*, Venezia, October 24-27, 1979, Università degli Studi—Istituto di Chimica Industriale, Padova (1982), pp. 499-510.

9. M. Matteini, A. Moles, M. Oeter, I. Tosini. In: *The cleaning of architectural surfaces, Proceedings of a symposium*, Bressanone, July 3-6, 1995, Libreria Progetto, Padova (1995), pp. 283-292.

10. P. Fiorentino, M. Marabelli, M. Matteini, A. Moles. In *Studies in Conservation* **27** (1982) pp.145-153.

11. N. Berlucchi, R. G. Corradini, R. Bonomi, E. Bemporad, M. Tisato. In: *Proceedings of the 9th International Congress on Deterioration and conservation of stone*, Venezia (2000), pp. 23-31.
12. G. Carbonara, *Trattato di Restauro Architettonico,* Torino (1996).
13. H. Burgess, *The Paper Conservator* **15** (1991) pp.36-44.
14. A. Phenix, A. Burnstock. In *The Conservator* **16** (1992) pp.28-38.
[15] J. Heuman. In *The Conservator* **16** (1992) pp.12-17.
16. I.D. MacLeod. In *Studies in conservation* **32** (1987) pp.25-40.
17. L. Carlyle, J.H. Townsend, S. Hackney. In *Dirt and Pictures Separated*, United Kingdom Institute for Conservation, London (1990), pp. 44-48.
18. R. Wolbers, *Cleaning painted surfaces: aqueous methods*, Archetype Publications, London (2000).
19. Materiali tradizionali ed innovativi nella pulitura dei dipinti e delle opere policrome mobili, in: *Proceedings of Primo Congresso Internazionale - Colore e conservazione: materiali e metodi nel restauro delle opere policrome mobili*, Piazzola sul Brenta, October 25-26, 2002, Il prato, 2003.
20. A. Onesti, *CAB newsletter* **2** (1993) pp.10-13.
21. D. Stulik, V. Dorge, *Solvent gels for the cleaning of works of art: the residue question*, Getty Publications, Los Angeles, USA (2004).
22. E. Carretti, I. Natali, C. Matarrese, P. Bracco, R.G. Weiss, P. Baglioni, A. Salvini, L. Dei, *J. Cult. Herit.* **11** (2010) pp.373-380.
23. C.Y. Chen, T.L. Yu, *Polymer* **38** (1997) pp.2019-2025.
24. A. Koike, N. Nemoto, T. Inoue, K. Osaki, *Macromolecules* **28** (1995) pp.2339-2344.
25. L.V. Angelova, P. Terech, I. Natali, L. Dei, E. Carretti, R.G. Weiss, *Langmuir* **27** (2011) pp.11671-11682.
26. E. Carretti, M. Bonini, L. Dei, B.H. Berrie, L.V. Angelova, P. Baglioni, R.G. Weiss, *Acc. Chem. Res.* **43** (2010) pp.751-760.
27. E. Carretti, C. Matarrese, E. Fratini, P. Baglioni, L. Dei, *Soft Matter* **10** (2014) pp.4443-4450.
28. I. Natali, E. Carretti, L. Angelova, P. Baglioni, R.G Weiss., L. Dei, *Langmuir* **27** (2011) pp.13226-13235.
29. L. Piculell, M. Egermayer, J. Sjostrom, *Langmuir* **19** (2003) pp.3643-3649.
30. M. Chen, R. Stephen Reid, *Can. J. of Chem*. **71** (1993) pp.763-768.

31. S. Grassi, E. Carretti, P. Pecorelli, F. Iacopini, P. Baglioni, L. Dei, *J. Cult. Herit.* **8** (2007) pp.119-125.
32. G. Anbalagan, S. Mukundakumari, K. Sakthi Murugesan, S. Gunasekaran, *Vibrational Spectroscopy* **50** (2009) pp.226-230.
33. K. L. Andrew Chan and Sergei G. Kazarian, *Analyst* **131** (2006) pp.126-131